TECHNISCHE UNIVERSITÄT
ILMENAU

Technische Universität Ilmenau
Fakultät für Informatik und Automatisierung
Institut für Automatisierungs- und Systemtechnik
Fachgebiet Prozessoptimierung

Real-Time Optimization of Energy Networks with Battery Storage Systems under Uncertain Wind Power Penetration

Dissertation Zur Erlangung des akademischen Grades Doktoringenieur (Dr.-Ing.)

Erfan Mohagheghi

Gutachter:

1. Prof. Dr.-Ing. habil. Pu Li (Technische Universität Ilmenau, Germany)
2. Prof. Dr. Frede Blaabjerg (Aalborg University, Denmark)
3. Prof. Dr.-Ing. Steven Liu (Technische Universität Kaiserslautern, Germany)

Tag der Einreichung : 05.11.2018
Tag der wissenschaftlichen Aussprache: 24.04.2019

urn:nbn:de:gbv:ilm1-2019000126

Erklärung

Ich versichere, dass ich die vorliegende Arbeit ohne unzulässige Hilfe Dritter und ohne Benutzung anderer als der angegebenen Hilfsmittel angefertigt habe. Die aus anderen Quellen direkt oder indirekt übernommenen Daten und Konzepte sind unter Angabe der Quelle gekennzeichnet.

Weitere Personen waren an der inhaltlich-materiellen Erstellung der vorliegenden Arbeit nicht beteiligt. Insbesondere habe ich hierfür nicht die entgeltliche Hilfe von Vermittlungsbzw. Beratungsdiensten (Promotionsberater oder anderer Personen) in Anspruch genommen. Niemand hat von mir unmittelbar oder mittelbar geldwerte Leistungen für Arbeiten erhalten, die im Zusammenhang mit dem Inhalt der vorgelegten Dissertation stehen.

Die Arbeit wurde bisher weder im In- noch im Ausland in gleicher oder ähnlicher Form einer Prüfungsbehörde vorgelegt.

Ich bin darauf hingewiesen worden, dass die Unrichtigkeit der vorstehenden Erklärung als Täuschungsversuch bewertet wird und gemäß § 7 Abs. 10 der Promotionsordnung den Abbruch des Promotionsverfahrens zur Folge hat.

Ilmenau, 05.11.2018

Acknowledgments

First and foremost I would like to express my sincere gratitude to my advisor Prof. Pu Li for the continuous support of my research, for his patience, guidance and encouragements.

My sincere thanks also go to Prof. Frede Blaabjerg from Aalborg University and Prof. Steven Liu from Technische Universität Kaiserslautern for their precious time reviewing my thesis and their insightful comments.

I would like to express my deepest appreciation to my colleagues in Process Optimization Group of Technische Universität Ilmenau. In particular, I am very much thankful to Prof. Horst Puta, Dr. Siegbert Hopfgarten, Dr. Abebe Geletu, and Dr. Aouss Gabash for their help and support. Sincere thanks to Mr. Alramlawi, Mr. Björn Töpper, Mr. Jens Hollandmoritz, Dr. Duc Dai Pham, Dr. Quoc Dong Vu, Mr. Kibru Teka Nida, Mr. Evgeny Lazutkin, Mr. Xujiang Huang, Miss Mei-chen Yuan, Mr. Shih-Jan Lin, for their friendship and sharing beautiful memories in Ilmenau.

Moreover, I gratefully acknowledge the Carl-Zeiss-Stiftung for funding this work, and DAAD for funding my research stay at Zhejiang University.

Last but by no means least, I would like to thank my family from the bottom of my heart: my wife *Sajedeh* and my parents for their love, endurance, and continuous support.

Abstract

There has been a huge trend to penetrate renewable energies into distribution networks (DNs). However, a considerable amount of this generation may need to be curtailed due to technical constraints in the network. Battery storage systems (BSSs) can be optimally used to store the energy, decrease the curtailment and consequently increase economic benefits. However, BSSs introduce dynamic terms to the problem of optimal power flow (OPF). In addition, considering both active and reactive power of the BSSs with flexible operation strategies, as well as maximizing the lifetime of the batteries further increase the complexity of the problem. Furthermore, wind power is intermittent, and therefore the network operator has to fast update the operation strategies correspondingly. This task should be carried out by an online optimization aiming at determining huge number of mixed-integer decision variables leading to a real-time dynamic active-reactive OPF (RT-DAR-OPF) problem. Therefore, developing a suitable framework for RT-DAR-OPF is of utmost importance for ensuring both optimality and feasibility in the operation of DNs with BSSs under intermittent wind energy penetration. The most challenging issue hereby is that a large-scale dynamic mixed-integer nonlinear programming (MINLP) problem has to be solved in real-time. To solve this problem, a multi-phase multi-time-scale RT-DAR-OPF framework is developed in this dissertation to optimally deal with the spontaneous changes of wind power in DNs with BSSs.

In the first phase, a huge number of mixed-integer decision variables are simultaneously optimized to compute operation strategies of BSSs on a day-to-day basis. The variables of BSSs computed in the first phase will be used as fixed input parameters for the second phase. Note that in the next phase, other decision variables will be recomputed. In the second phase, based on the forecasted wind power values for short prediction horizons, the most probable wind power scenarios are generated to describe uncertain wind power with a non-Gaussian distribution. Then MINLP active-reactive OPF problems corresponding to the scenarios are solved in parallel in advance of each prediction horizon resulting in a lookup table. A new reconciliation algorithm is proposed to ensure both the feasibility and optimality of the solutions in the lookup table. In the third phase, based on the measured actual values of wind power, one of the solutions is selected, modified and finally realized to the network for very short intervals. The applicability of the proposed RT-DAR-OPF framework is demonstrated using a medium-voltage DN.

Zusammenfassung

Es gibt einen starken Trend, erneuerbare Energien in Verteilungsnetze (VNs) der Elektroenergieversorgung einzuspeisen. Jedoch muss wegen technischer Beschränkungen dieser Anteil um eine beträchtliche Menge gekürzt werden. Batteriespeichersysteme (BSSs) können optimal genutzt werden, um die Energie zu speichern, den gekürzten Anteil der zu senken somit den ökonomischen Vorteil zu erhöhen. Allerdings werden durch die BSSs dynamische Terme in das Problem des optimalen Lastflusses (engl.: optimal power flow (OPF)) eingeführt. Weiterhin tritt die Windeneergie intermittierend auf, weshalb der Netzbetreiber die Betriebsstrategie schnell entsprechend aktualisieren muss. Diese Aufgabe sollte durch eine Online-Optimierung durchgeführt werden, die auf die Bestimmung einer enormen Anzahl von gemischt-ganzzahligen Entscheidungsvariablen abzielt und auf ein dynamisches Echtzeit Wirk-/Blindleistungs-OPF-Problem (engl.: real-time dynamic active-reactive optimal power flow problem (RT-DAR-OPF problem)) führt. Deshalb ist die Entwicklung eines geeigneten Rahmens für das RT-DAR-OPF-Problem von größter Bedeutung für die Gewährleistung von sowohl Optimalität als auch Umsetzbarkeit in der Betriebsführung von VNs mit BSSs unter intermittierender Windenergieeinspeisung. Das herausforderndste Merkmal dabei ist, dass ein hochdimensionales, dynamisches, gemischt-ganzzahliges nichtlineares Optimierungsproblem (engl.: mixed-integer nonlinear programming problem (MINLP)) in Echtzeit gelöst werden muss. Zusätzlich wird die Problemkomplexität sowohl durch die Betrachtung der Wirk- als auch der Blindleistung des BSSs mit flexiblen Betriebsstrategien genauso wie durch die Minimierung der aufgewendeten Lebensdauerkosten der BSSs erhöht. Um dieses Problem zu lösen, wird ein Mehrphasen- und Mehrfachzeitskalen-RT-DAR-OPF-Rahmen in dieser Dissertation entwickelt, der sich mit der optimalen Behandlung spontaner Änderungen bei der Windenergie in VNs und BSSs beschäftigt.

In der ersten Phase werden eine enorme Anzahl an gemischt-ganzzahligen Entscheidungsvariablen simultan optimiert und damit wird die Betriebsstrategie für den kommenden Tag berechnet. Die Variablen der BSSs, die in der ersten Phase berechnet wurden, werden in der anderen Phasen als feste Eingangsparameter verwendet. Zu vermerken ist, dass in der nächsten Phase andere Entscheidungsvariablen erneut berechnet werden. In der zweiten Phase werden basierend auf den vorhergesagten Windenergiewerten für kurze Vorhersagehorizonte die wahrscheinlichsten Windenergieszenarios generiert, um die Unsicherheiten bei der Windenergie mit einer Nicht-Gaußschen Verteilung zu beschreiben. Dann werden die MINLP-AR-OPF-Probleme entsprechend der Szenarios parallel im Vorfeld des Vorhersagehorizonts gelöst und in einer Lookup-Tabelle gespeichert. Ein neuer

Abgleichsalgorithmus wird vorgeschlagen, um sowohl die Optimalität als auch die Umsetzbarkeit der Lösungen in der Lookup-Tabelle zu garantieren. In der dritten Phase wird basierend auf den Messungen der aktuellen Werte der Windenergie eine der Lösungen ausgewählt, modifiziert und schließlich am Netz für kurze Zeitintervalle realisiert. Die Demonstration der Anwendbarkeit des vorgeschlagenen RT-DAR-OPF-Ansatzes erfolgt unter Verwendung eines Mittelspannung-VN.

Contents

Nomenclature

a, b	Constant parameters of a BSS
C_{PP}	Active energy price
C_{PQ}	Reactive energy price
DoD_{ave}	Average depth of discharge of a BSS
E_b	Energy level in a BSS
$E_{b.\max}$	Upper limit of energy level in a BSS
$E_{b.\min}$	Lower limit of energy level in a BSS
ELC	Expended life cost of a BSS
f	Objective function
f_1	Total revenue from wind power
F_1	Total cost of active energy imported from an upstream network
f_2	Total cost of active energy losses in the grid
F_2	Total cost of reactive energy imported from an upstream network
f_3	Total cost of active energy at slack bus
F_3	Total expended life costs of BSSs
f_4	Total cost of reactive energy at slack bus
f_P	Network active power function
F_{PDF}	Probability distribution function
f_Q	Network reactive power function
F_T	Total objective function for one day (proposed approach)
F_{TD}	Total objective function for one day (deterministic approach)
$\mathbf{g}$	Model equations
i, j	Indices for buses, i.e., $i, j = 1,...,N_{bus}$
k	Index for prediction horizons
$\mathbf{l}$	Vector of discrete decision variables
L	Upper bound on integer variables
m	Index for sampling intervals T_S, i.e., $m = 1,...,M$
M	Total number of sampling intervals in each prediction horizon

n	Index for prediction horizon T_{P2}, i.e., $n=1,...,N$
N_{bus}	Total number of buses
n_c	Index for wind power scenario combinations, i.e., $n_c=1,...,N_c$
N_c	Total number of wind power scenario combination
n_{cyc}	Index for charge-discharge cycles of a BSS, i.e., $n_{cyc}=1,...,N_{cyc.\max}$
N_{cyc}	Number of charge-discharge cycles of a BSS in each prediction horizon T_{P1}
$N_{cyc.\max}$	Maximum number of charge-discharge cycles of a BSS in each prediction horizon T_{P1}
$N_{cyc.T}$	Battery total number of cycles
N_{pr}	Total number of processors
n_s	Index for wind power scenarios for each individual wind farm (WF), i.e., $n_s=1,...,N_s$
N_s	Total number of wind power scenario for each WF
n_w	Index for WFs, i.e., $n_w=1,...,N_w$
N_w	Total number of WFs
P_{ch}	Active power charge of a BSS
P_d	Active power demand
P_{dis}	Active power discharge of a BSS
PF_w	Power factor of a WF
$PF_{w.\max}$	Upper limit of a WF power factor
$PF_{w.\min}$	Lower limit of a WF power factor
P_{loss}	Active power losses
P_s	Active power at the slack bus
P_w	Wind power of a WF
$\mathbf{P}_w$	Vector of active power of WFs
$P_{w.A}$	Actual wind power
$P_{w.M}$	Mean (forecasted) wind power
$P_{w.R}$	Rated installed wind power
$P_{w.s}$	Active power of a WF for a selected scenario

Q_b	Reactive power dispatch of a BSS
Q_d	Reactive power demand
Q_{loss}	Reactive power losses
Q_s	Reactive power at the slack bus
Q_w	Reactive power dispatch of a WF
$Q_{w.s}$	Reactive power of a WF for a selected scenario
S	Apparent power in a feeder
S_b	Set of buses
S_{BSS}	Set of BSS buses
$s_{l.\max}$	Upper limit of apparent power in a feeder
S_{PCS}	Apparent power of a power conditioning system (PCS) in a BSS
$S_{PCS.\max}$	Maximum capability of a PCS in a BSS
$S_{s.\max}$	Upper limit of apparent power at slack bus
SUC_T	Total operation cost of storage units
SUC_u	Per unit cost of storage units
S_w	Set of WF buses
t	Time
t_0	Initial time
T_{ch}	Charge periods of a BSS
T_{cyc}	Length of charge-discharge cycles of a BSS
t_d	Duration of time steps for BSSs
T_{dis}	Discharge periods of a BSS
T_{D-OPF}	Computation time for dynamic OPF in Phase 1 of the RT-DAR-OPF framework
t_f	Final time
T_{OPF}	Reserved time for computing OPF problems
$T_{OPF.ave}$	Average computation time
$T_{OPF.\max}$	Highest computation time
$T_{OPF.\min}$	Lowest computation time
T_P	Prediction horizon

T_{P1}	Prediction horizon in Phase 1 of the RT-DAR-OPF framework
T_{P2}	Prediction horizon in Phase 2 of the RT-DAR-OPF framework
T_r	Reserved time for data management
T_S	Sampling interval
$\mathbf{u}$	Vector of continuous decision variables
$\mathbf{u_{max}}$	Upper limits on continuous decision variables
$\mathbf{u_{min}}$	Lower limits on continuous decision variables
V	Voltage at a PQ bus
$V_{lo.in}$	Lower boundary of voltage for inner tube
$V_{lo.out}$	Lower boundary of voltage for outer tube
$V_{\max}$	Upper limit of voltage at a PQ bus
$V_{\min}$	Lower limit of voltage at a PQ bus
V_s	Voltage at slack bus
$V_{s.\max}$	Upper limit of voltage at slack bus
$V_{s.\min}$	Lower limit of voltage at slack bus
VSS	Value of stochastic solution
$V_{up.in}$	Upper boundary of voltage for inner tube
$V_{up.out}$	Upper boundary of voltage for outer tube
$\mathbf{y}$	Vector of binary decision variables
$\mathbf{x}$	Vector of state variables
$\mathbf{x}_0$	Initial states
$\mathbf{x_{max}}$	Upper limits on state variables
$\mathbf{x_{min}}$	Lower limits on state variables
α	Binary variable for charge/discharge of a BSS
α_b	First shape parameter of Beta distribution
β_b	First shape parameter of Beta distribution
β_w	Wind power curtailment of a WF
$\boldsymbol{\beta}_w$	Vector of curtailment factors
γ_{Ps}	Coefficient for active power limit at the slack bus
γ_{Qs}	Coefficient for reactive power limit at the slack bus
ΔV_s	Step change of voltage at slack bus

μ_d	Mean value for demand
ξ	Vector of random variables
ρ	Density function
σ_d	Standard deviation for demand
σ_w	Standard deviation for wind power
φ	Phase angle
$\varphi_{\max}$	Upper limit of phase angle
$\varphi_{\min}$	Lower limit of phase angle
Ω	Set of random variables

Acronyms

AC	Alternating current
AR-OPF	Active-reactive optimal power flow
BSS	Battery storage system
DC	Direct current
DN	Distribution network
DoD	Depth of discharge
EMS	Energy management system
ESS	Energy storage system
GA	Genetic algorithm
GPU	Graphics processing unit
HV	High-voltage
LP	Linear programming
LV	Low-voltage
MAPE	Mean absolute percentage error
MILP	Mixed-integer linear programming
MINLP	Mixed-integer nonlinear programming
MIP	Mixed-integer programming
MPC	Model predictive control
MV	Medium-voltage
NLP	Nonlinear programming
OLTC	On-load tap changer
OPF	Optimal power flow
PCS	Power conditioning system
PDF	Probability density function
PF	Power factor
PSO	Particle swarm optimization
REG	Renewable energy generation
RT-AR-OPF	Real-time active-reactive optimal power flow
RT-DAR-OPF	Real-time dynamic active-reactive optimal power flow
RT-EMS	Real-time energy management system
RT-OPF	Real-time optimal power flow
SQP	Sequential quadratic programming
VSS	Value-of-stochastic-solution
WF	Wind farm

1 Literature Review

1.1 Introduction

Optimal power flow (OPF) plays a significant role in the operation of power systems. In general, OPF schedules the decision variables of the power system in an optimal way which simultaneously satisfies power flow balance equations and power system constraints (e.g., nodal voltages and apparent power in the feeders). The resulting optimization problem is usually large-scale non-convex and with mixed-integer variables. Various approaches have been put forward to solve the OPF problem for different types of network topologies, voltage levels, with/without renewable energy generations (REGs) and embedded battery storage systems (BSSs). These approaches were assessed in detail in a number of review papers on OPF, published over the past decades [1-14].

Renewable energies are considered to be the main source of energy to cover demand in the near future. This is mostly due to the increasingly strict emission policies and the shrinking price of their technology. The integration of REGs into energy networks leads to a transformation from passive to active energy networks. However, this transformation brings new challenges to the network operators. Since REGs are fluctuating, some amount of generated power cannot be accommodated in the network. This amount of power will be curtailed [15] due to technical reasons, meaning that not all the potentials of the REGs are utilized. Therefore, many studies have been carried out to decrease the curtailment levels in energy networks [16-21]. A promising solution to reduce the curtailments is to use BSSs to store the surplus amount of the energy and provide it back to the grid in a proper time. However, the incorporation of BSSs into the network leads to dynamic state operations and thus introduces dynamic model equations to the OPF which makes the problem more complex to solve.

Another issue is that the REGs are uncertain. It means their output cannot be forecasted accurately and there may be discrepancies between the forecasted and actually realized values. The uncertainties can lead to constraint violations and thus safety problems if they are not handled properly. Therefore, deterministic OPF methods are not suitable for real operation of the networks, or their solutions need further modifications before realization. Besides, owing to fast fluctuating REG, in particular wind power, the network operators need to fast update, i.e., in real-time, the operation strategies correspondingly in order for the

network to operate economically and in its feasible region. Therefore, the real-time energy management systems (RT-EMSs) have attracted increasing interest of many researchers. One can classify the RT-EMSs into two main categories: 1) constraint-satisfaction-based RT-EMSs, and 2) OPF-based RT-EMSs. The former can satisfy the technical constraints of the network in real-time but the solutions may not be optimal. The latter provides optimal solutions in real-time while satisfying related technical constraints.

In this chapter, first we formulate OPF problem with embedded BSSs under uncertainty. Then the studies on offline and real-time EMSs are reviewed and finally the contributions of this thesis are highlighted.

1.2 Problem Formulation

Conventional power flow analysis [22-24] aims at determining state variables (e.g., voltage and phase angle at PQ buses, and power flow in the feeders) in a network based on given input parameters (e.g., active and reactive power at PQ buses and phase angle at the slack bus). In such analysis there is no free variable and therefore it is carried out based on simulation. In contrast, OPF aims to optimize an objective function by finding optimal free variables while keeping the network constraints in their acceptable limits. The OPF problem is, in general, a large-scale non-convex optimization problem which may also have uncertain, continuous and discrete variables (leading to a mixed-integer nonlinear programming (MINLP) problem under uncertainty). In addition, the incorporation of BSSs in the network adds dynamic model equations to the OPF problem. Therefore, the OPF problem can be in general defined as a stochastic dynamic MINLP optimization problem as follows:

$$
\begin{aligned}
\min_{\mathbf{u}(t),\mathbf{l}(t),\mathbf{y}(t)} \quad & f\left(\mathbf{x}(t),\mathbf{u}(t),\mathbf{l}(t),\mathbf{y}(t),\boldsymbol{\xi}(t)\right) \\
s.t. \quad & \dot{\mathbf{x}}(t)=\mathbf{g}\left(\mathbf{x}(t),\mathbf{u}(t),\mathbf{l}(t),\mathbf{y}(t),\boldsymbol{\xi}(t)\right), \quad \mathbf{x}(t_0)=\mathbf{x}_0 \\
& \mathbf{x}_{\min}(t)\le\mathbf{x}(t)\le\mathbf{x}_{\max}(t) \\
& \mathbf{u}_{\min}(t)\le\mathbf{u}(t)\le\mathbf{u}_{\max}(t) \\
& \mathbf{l}(t)\in\{0,1,2,...,L\} \\
& \mathbf{y}(t)\in\{0,1\} \\
& \boldsymbol{\xi}(t)\in\Omega \\
& t_0\le t\le t_f .
\end{aligned}
\tag{1.1}
$$

In Equation 1.1, f is the objective function to be minimized, $\mathbf{x}$ is the vector of state variables, $\mathbf{u}$ is the vector of continuous decision variables, $\mathbf{l}$ is the vector of integer decision variables, $\mathbf{y}$ is the vector of binary decision variables, and $\boldsymbol{\xi}$ is the vector of random variables. Here, $\mathbf{g}$ denotes dynamic model equations with initial states of $\mathbf{x}_0$ at t_0, $\mathbf{x}_{\min/\max}$

are the lower/upper limits of state variables, $\mathbf{u}_{\min/\max}$ are the lower/upper limits of continuous decision variables, and t_f is the final time.

There could be many different objective functions when formulating an OPF. The most common ones are the minimization of total generation costs [25, 26], total network losses [17], and/or the maximization of total yield from the network [18] and environmental benefits [27, 28]. The vector of state variables $\mathbf{x}$ could consist of voltages of the PQ buses [29-33], active and reactive power at slack bus, and power flows in feeders [34]. The vector of continuous control variables $\mathbf{u}$ could include active and reactive power generation of generators [29] (conventional and/or renewable generations) and charge and discharge flow of the storage units [17, 18]. The vector of discrete control variables $\mathbf{l}$ could consist of reference values of slack bus voltage [35, 36] (for the sake of simplicity some studies consider the slack bus voltage as a continuous variable e.g., [37, 38]) , and the vector of binary control variables could consist of charge/discharge status of BSSs. The vector of random variables ξ could consist of REGs and/or load demand [39-41]. The random variables are the generated amounts of REGs usually regarded as being stochastically distributed with a known probability density function $\rho(\xi)$. The time step t could also be considered as an integer variable to be optimized in the optimization problem, for instance it could be the number of charge/discharge hours of BSSs per day [18]. The dynamic model equations $\mathbf{g}$ is generally consist of active and reactive power flow equations at the buses [35] and the energy balance equations for batteries [17]. The inequality constraints could include lower and upper boundary of state and control variables.

The optimization problem expressed in Equation 1.1 is a large-scale dynamic MINLP problem under uncertainty. This problem is difficult to be readily treated and therefore a numerous number of studies either focused on specific instances of the problem or simplified the OPF problem by using various assumptions. For instance, OPF has been solved by linear programming (LP) [42, 43], nonlinear programming (NLP) [26, 44], quadratic programming [25, 45, 46], mixed-integer linear programming (MILP) [47, 48], and MINLP [35, 49-51]. For a detailed review on these methods we refer the reader to the survey in [10].

1.3 Offline EMSs

Different methods have been proposed and used for offline energy management of energy networks. The methods are broadly classified into two main categories:

1) Deterministic EMSs by which the outputs are determined using forecasted parameter values. In other words, uncertainties are not considered when computing the solutions.

2) Stochastic EMSs which consider the uncertainties and inaccuracies of the forecasted values when computing the solutions. It means the control strategies obtained in this way are more likely to be feasible for practical applications under uncertainty.

1.3.1 Deterministic EMSs

Deterministic EMSs do not take into account the uncertainties in the energy networks. Therefore, it is based on the assumption that the forecasted values are accurate neglecting the probable deviations from the actually realized values. For this, here we adapt the general OPF problem formulation in Equation 1.1 for a deterministic OPF as follows:

$$\begin{aligned} \min_{\mathbf{u}(t),\mathbf{l}(t),\mathbf{y}(t)} \quad & f\left(\mathbf{x}(t),\mathbf{u}(t),\mathbf{l}(t),\mathbf{y}(t)\right) \\ s.t. \quad & \dot{\mathbf{x}}(t) = \mathbf{g}\left(\mathbf{x}(t),\mathbf{u}(t),\mathbf{l}(t),\mathbf{y}(t)\right), \quad \mathbf{x}(t_0) = \mathbf{x}_0 \\ & \mathbf{x}_{\min}(t) \le \mathbf{x}(t) \le \mathbf{x}_{\max}(t) \\ & \mathbf{u}_{\min}(t) \le \mathbf{u}(t) \le \mathbf{u}_{\max}(t) \\ & \mathbf{l}(t) \in \{0,1,2,...,L\} \\ & \mathbf{y}(t) \in \{0,1\} \\ & t_0 \le t \le t_f \end{aligned} \tag{1.2}$$

where, comparing to Equation 1.1, $\boldsymbol{\xi}(t)$ has been removed from the objective function f and model equations $\mathbf{g}$ (usually they are replaced by their nominal or expected values), meaning that there is no randomness in the problem formulation. Focusing on different aspects of Equation 1.2, a vast number of studies have been made on OPF for offline operation planning of energy networks since it was proposed by Carpentier in 1962 [44]. Indeed, from 1962 to late 90s, most of the studies focused on OPF without REGs. For instance, a reactive-volt-ampere control method was proposed in [52] to minimize the losses of a power transmission network. Based on [44], the general problem of minimizing the operation cost of a power system was formulated in [53] as a NLP problem. The study in [53] was later extended in [26] where an approach was proposed to solve OPF considering active and reactive power and the tap ratios of transformers as decision variables to minimize losses or costs in a network. Besides, a unified approach based on the Carpentier's formulation [44] was proposed in [54] to solve the OPF problem.

Several studies have been conducted on the incorporation of security constraints in power flow formulations. For instance, the outage-contingency constraints [55] was incorporated in [56] extending the OPF problem formulation in [26]. Using a sequential LP [57], Refs. [58, 59] solved a security constrained economic dispatch problem. Ref. [60] proposed an approach for economic dispatch and security control using the combined

quadratic-separable programming methods. Using sequential quadratic programming (SQP) [61-63], the authors in [64] presented a procedure for solving the problem of security constrained economic dispatch.

Optimal reactive power flow has attracted the attention of many research studies. For instance, [65, 66] presented methodologies for the optimal scheduling of reactive power sources in a power system. A method for optimal dispatch of active and reactive power flow in large-scale networks was presented in [25, 46]. A dual augmented Lagrangian approach was proposed in [67] for solving optimal active and reactive power flow. Using a heuristic method, [68] developed an optimization tool to find the optimal location and size of reactive power sources while considering security constraints for a transmission network. Extending the interior point method introduced in [69], the authors in [70] solved an economic dispatch and a reactive power scheduling problems. A full alternating current (AC) OPF to determine the reactive power margins from the point of voltage collapse was formulated in [71]. Based on the Newton's method, [72] proposed an approach for the problem of optimal reactive power dispatch. Ref. [73] proposed a LP-based trade-off methodology to solve reactive power compensation problem considering both technical and economic aspects. Ref. [30] incorporated the costs of adjusting control devices into an optimal reactive power flow problem while minimizing energy losses. A planning approach for optimal capacitor allocation was proposed in [74] aiming at minimizing energy losses while reducing installation costs. Incorporating the expected lifetime of devices in the optimization formulation, the optimal number and location of the capacitors were obtained in [74]. Ref. [75] proposed an approach for OPF to manage voltages in interconnected networks through switching of the reactive power compensators, tap positions of transformers, etc.

A number of studies have incorporated discrete decision variables into the optimization problem formulation, leading to MINLP problems in which special methods to address integer variables are required. For instance, [76] proposed a distributed algorithm to solve OPF for large-scale systems with discrete decision variables. Ref. [77] proposed an iterative approach based on the Lagrangian multiplier to treat discrete variables in OPF computations. Ref. [78] proposed an enhanced genetic algorithm (GA) [79, 80] for solving OPF with both continuous and discrete decision variables. The continuous decision variables in [78] included active power of generators and bus voltage magnitudes. The discrete decision variables in [78] were the tap positions of transformers and switchable shunt devices.

From another perspective, many studies have focused on numerical approaches to solving OPF for different purposes. For instance, for the sake of fast and reliable computations, [81-83] applied a LP method to power systems security control calculations. Ref. [84] presented a LP-based approach for OPF to reschedule active power controls and satisfy voltage constraints. Using LP, [85] presented a method to find an optimal solution for

both planning and operation of large-scale systems. In [86], the authors extended the reduced gradient method [87] to solve OPF problems for large-scale networks. An OPF problem was solved in [88] using a Hessian method. Ref. [89] proposed an approach to identify binding inequality constraints in OPF problems solved by the Newton method. A nonlinear interior point method to find the maximum loadability of a power system was proposed in [90]. Based on the Lagrangian relaxation decomposition procedure, [91] developed a framework for multi-area OPF aiming at independent dispatch of each area while achieving the economic optimum of the whole system. Ref. [92] proposed a method to solve dynamic constrained OPF as a semi-infinite programming problem with infinite constraints. A method for non-convex OPF problems was proposed in [93], which is based on the derivation of OPF dual as a convex linear matrix inequality optimization. Under specific conditions, the duality gap is zero leading to recovering the global optimal solutions of the OPF from a dual optimal solution [93].

Since late 90s, there has been a strong increase of penetration of REGs into energy networks. The optimal location of REGs was initially considered in [94] where the objective was to find the optimal location of distributed generation units which could result in minimization of energy losses, feeders power, and reactive power requirements. Afterward, many studies focused on the different aspects of renewable energy penetration into the networks. For instance, [95] developed an OPF framework to maximize the penetration of wind generation by optimally determining different control variables, e.g., generation curtailment, reactive power absorption, and tap position of on-load tap changers (OLTCs). Ref. [96] presented OPF-based techniques to evaluate DN capacity for the connection of renewable energy sources.

More recently, BSSs have been used with REGs to decrease their curtailment levels and absorb their fluctuations. For this reason, many studies have been published on optimal allocation and sizing of BSSs in the energy networks. For instance, [97, 98] proposed a method for optimal sizing and allocation of BSSs in a DN to decrease the wind power curtailment. Ref. [99] developed an optimization method for the sitting and sizing of BSSs in DNs. Using GA, [100] proposed an approach for the optimal allocation and economic analysis of BSSs in microgrids. Optimal sizing and control methodologies for a zinc-bromine BSSs was proposed in [101]. Ref. [102] developed a tool to be used in a decision-making process to install BSSs. The tool in [102] is based on a multi-objective optimization to determine the trade-off between annual cost, peak power reduction, and voltage regulation.

A growing number of studies have investigated the optimal operation of BSSs in energy networks. For instance, [103] proposed an approach to optimally control BSSs in microgrids aiming at minimizing the total cost of energy import at the point of common coupling. An OPF with simple charge-discharge dynamics for large-scale BSSs was formulated in [104].

Considering REG curtailments, BSSs, and flexible demand, [105] developed a dynamic OPF framework for an active network management. Using a linear lossless direct current (DC) OPF, [106] proposed a method to decrease REG curtailments in presence of storage devices. An OPF problem was formulated in [17] employing both active and reactive power capabilities of BSSs [107, 108] to increase the total yield of a DN. It is worth mentioning that utilizing the reactive power capability of distributed energy resources leads to significant economic [109] and technical benefits [110, 111]. In addition, the BSSs in [17] operate based on a fixed length of charge and discharge periods, which was later extended in [18] for flexible charge and discharge periods, but still fixed length of charge-discharge cycles. It is noted the work in [18] provides identical operation strategies for different BSSs which was later improved in [112, 113] by determining optimal decision variables for each individual BSS, resulting in more complex and larger optimization problem.

1.3.2 Stochastic EMSs

Deterministic EMSs require predicted values of network variables (e.g., REG, demand, prices, etc.). However, it is impossible to precisely forecast the values of these variables. In addition, there exist many other uncertainties (e.g., REG [27, 114-119], power demand [40, 112, 120, 121], line outage [122-124], generator outage [122], plug-in electric vehicles [125, 126], fuel price [122, 127, 128], and grid blackouts [129-132]) in the operation of energy networks. This poses numerous challenges for network operators when ensuring reliability of the optimal operation strategies. The OPF could be a stochastic dynamic MINLP optimization problem, but in contrast to Equation 1.1, here the OPF problem is solved offline.

In general, many mathematical models have been developed for optimization under uncertainty [133], each of which could be suitable for a specific type of application. For instance, robust optimization or worst-case scenario optimization [134] is used when an application does not tolerate any constraint violation. In the problem formulation of robust optimization, the uncertain variables are described as random values in defined intervals [134]. Robust optimization has attracted the interest of many researchers dealing with uncertainties in power systems [135-141]. For instance, using a DC model, [142] developed an OPF algorithm to achieve robust operation when there exist uncertainties associated with REG and demand.

In power systems, however, there are some types of constraints (e.g., lines currents) which are allowed to be out of their permissible limits but only to some degree and/or for a limited time. For this reason, the chance constrained optimization method [143-148] can be used to formulate the OPF problem under uncertainty. In the problem formulation of chance constrained optimization, the uncertain variables are described as random variables with

defined stochastic distributions. In particular, the distributions of the generation of renewable energy are non-Gaussian, e.g. wind energy is usually described by the beta-distribution [149-151]. Based on the distribution function of the random penetration, chance constrained OPF [40, 41, 152-154] aims at minimizing/maximizing an objective function while satisfying certain constraints with a predefined probability level. For a chance constrained OPF, if the model is linear and random variables are normally distributed, there exists an equivalent deterministic representation. Otherwise, the problem should be solved using an approximation method, e.g., sample-average approximation [155], back-mapping [40, 156], and inner-outer approximation [157, 158].

1.4 Real-Time EMSs

In recent years, the penetration of REGs has been increased significantly leading to increasing the complexity of energy networks. Therefore, in addition to the uncertainty of load demand, the REG introduces further randomness and fluctuations to the network which pose new challenges for system operators. The main difference between these two sources of uncertainty is that the load demand is more predictable than the REGs (in particular wind power) for very short-term forecasting [159-162]. Moreover, the fluctuations of the REGs, in particular wind power, are more considerable. To react to these fluctuations, the system operators need to update operation strategies in real-time. To this end, different approaches have been proposed for the online management of the networks. Here we classify those approaches into two main categories as follows:

1) Constraint-satisfaction-based RT-EMSs which provide solutions to satisfy technical constraints. The solutions obtained in this way may not be optimal.
2) OPF-based RT-EMSs which provide '(sub)optimal' solutions in real-time while satisfying technical constraints.

1.4.1 Constraint-Satisfaction-Based RT-EMSs

Constraint-satisfaction-based RT-EMSs do not 'optimize' the decision variables of the networks. Therefore, the main focus is to find feasible (but not optimal) decision variables which, in real-time, satisfy the network constraints, e.g., nodal voltages, apparent power in feeders, etc. For this, the general OPF problem formulation in Equation 1.1 is adapted as follows:

$$
\begin{aligned}
&\dot{\mathbf{x}}(t) = \mathbf{g}\big(\mathbf{x}(t), \mathbf{u}(t), \mathbf{l}(t), \mathbf{y}(t), \boldsymbol{\xi}(t)\big), \quad \mathbf{x}(t_0) = \mathbf{x}_0 \\
&\mathbf{x}_{\min}(t) \le \mathbf{x}(t) \le \mathbf{x}_{\max}(t) \\
&\mathbf{u}_{\min}(t) \le \mathbf{u}(t) \le \mathbf{u}_{\max}(t) \\
&\mathbf{l}(t) \in \{0,1,2,...,L\} \\
&\mathbf{y}(t) \in \{0,1\} \\
&\boldsymbol{\xi}(t) \in \Omega \\
&t_0 \le t \le t_f
\end{aligned}
\tag{1.3}
$$

where there is no objective function to be minimized/maximized, but the model equations and inequality constraints must be satisfied. There is a vast amount of literature on such RT-EMSs each of which focusing on a particular aspect in power systems. For instance, a real-time energy management algorithm for mitigating of pulse loads in hybrid AC/DC microgrids with REG and energy storage systems (ESSs) was developed in [163]. The main objective of the RT-EMS in [163] is to manage the energy in the network in a way that the impacts of short duration loads on the network stability are minimized. Another RT-EMS was introduced in [164] for grid-connected plug-in hybrid electric vehicle charging parks with REGs. The developed method in [164] mainly aims at reducing the overall daily costs of charging plug-in hybrid electric vehicles as well as the effects of the charging park on the main network.

A real-time control approach was proposed in [165] to dynamically balance electric demand and generation while considering REGs and ESSs in the network. The method in [165] is based on model predictive control (MPC) [166-169] by which the set points for traditional generation units and the ESSs are continuously updated regarding the state of the charge of BSSs and forecasted REGs and demand. The MPC-based approach in [165] was extended in [170] to enable the day-ahead power reference tracking functionality for efficient operation of the network while ensuring feasible operation of ESSs. The main objective in [170] was controlling and smoothing of the net power profile exchanged in the high-voltage/medium-voltage (HV/MV) substation when high REGs are penetrated to the MV network.

Using intelligent systems techniques, an autonomous regional active network management system was developed in [171] aiming at voltage control, automatic restoration, and power flow management. The use of constraint programming for autonomous management of power flows was reported in [172]. The method in [172] utilized artificial intelligence technique of constraint programming to determine the decision variables. The studies in [171, 172] were extended in [19] to investigate the effects of the methods on reducing REG curtailments. In [19], a number of scenarios are provided to the closed-loop energy management algorithm to detect and mitigate of thermal constraint violations.

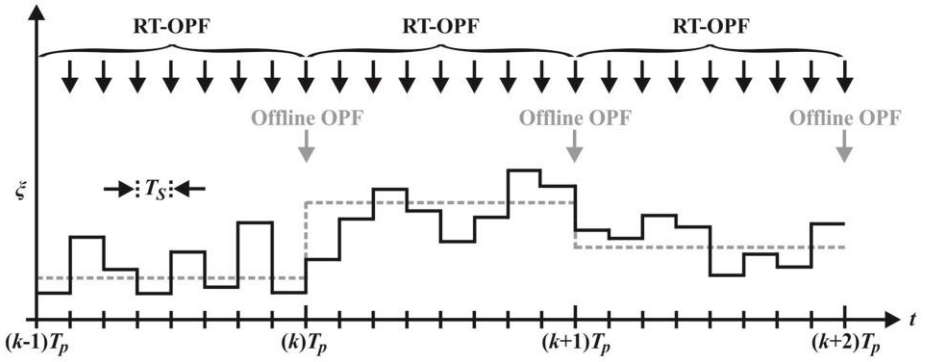

Figure 1.1. Illustration of offline OPF (denoted by gray) and RT-OPF (denoted by black).

1.4.2 OPF-Based RT-EMSs

Aiming at replacing classical real-time economic dispatch, optimization-based RT-EMS represents the most advanced and challenging version of Equation 1.1, in which a large-scale stochastic dynamic MINLP problem should be solved in real-time. As illustrated in Figure 1.1, the main idea of real-time optimal power flow (RT-OPF) is to react to the fluctuation of uncertain parameters ξ in the energy network at every sampling time T_S. These reactions could be either optimal or suboptimal. This is in contrast to offline OPF (deterministic and stochastic) where the optimal operation strategies are calculated only once for each prediction horizon T_P. A general RT-OPF method is illustrated in Figure 1.2. The optimal set points of the controller are obtained by OPF in each T_P, which are later corrected in real-time based on actual measurements. A feedback control system measures, monitors and controls the variables to ensure the desired response of the network.

In 1988 [173] Bacher and Van Meeteren presented the concept, mathematical formulation and solution of a RT-OPF. Their work was based on a linear model and a quadratic optimization method. A real-time implementation of optimal reactive power flow was presented in [174]. The main objectives of the study in [174] are to avoid voltage violation and excessive adjustment of transformer tap settings and var source switches while minimizing energy losses in the network. It is noted that the networks in [173, 174] included

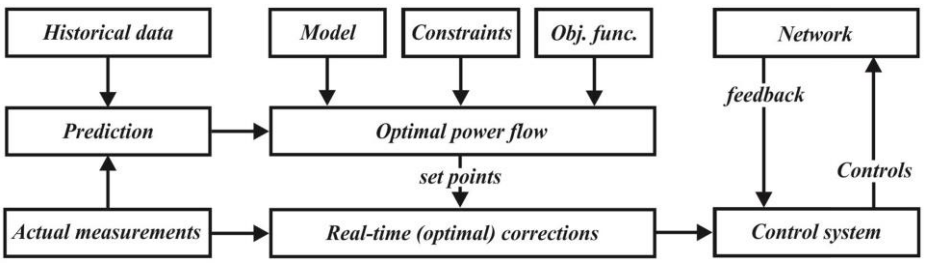

Figure 1.2. Illustration of a general RT-OPF method.

only traditional power generation units, i.e., REGs were not taken into account.

Considering REGs and using learning architecture based on fully connected neuron networks, the authors in [175] proposed a RT-OPF approach to achieve a short sampling time (e.g., less than three minutes). The neural networks are trained on several scenarios of the uncertainties (i.e., REG and load demand) in the network. The method in [175] was verified by using a 23-bus radial distribution network (DN) including two wind generators. A risk-based RT-OPF approach was proposed in [16] aiming at maximizing wind energy harvesting while satisfying network constraints with a pre-specified risk level. Using multi-minute control cycles while considering uncertainty of wind power, the management system in [16] reduces the number of control actions of OLTCs and REGs.

An online gradient-based algorithm for OPF on radial DNs was proposed in [176]. The method is based on a quasi-sequential approach proposed in [177] and improved in [178]. The problem is decomposed into two stages: simulation and optimization. In the simulation stage, model equations are solved to determine the values of state variables. In the optimization stage the control strategies are obtained by a NLP solver. Barrier terms are used in the objective function to penalize the violations of inequality constraints. However, this requires feasible guess points which could be difficult to determine for the OPF. The key feature of the method in [176] is that the intermediate iterates of the OPF can be realized to the network in real-time. Although the intermediate solutions are not optimal, they satisfy power flow equations and network constraints.

In [179], the authors extended the work carried out in [171, 172] to focus on the application and real-time testing of the OPF to the distribution energy management problem. For this, [179] demonstrates the practical applicability of the OPF to operate in an online closed-loop operation mode. The study in [179] was further extended in [19] to reduce REG curtailment. The results in [19] show that using the OPF-based RT-EMS leads to a lower REG curtailment comparing to the constraint-satisfaction-based RT-EMS.

To decrease the REG curtailment, [180] proposed a data-driven hourly real-time power dispatch. The method in [180] uses a linear model and a probabilistic optimization approach under uncertain penetration of REG. The dispatchable ranges of REG outputs are determined to cover the most possible scenarios. Based on the dispatchable ranges, the operating base points for the conventional generators are obtained for the next hour. The operations are corrected when the observations of the actual REG are available. Furthermore, using the same computational framework developed in [181-183], the authors in [184] adopted a multi-period AC OPF method to minimize energy losses by real-time control of REGs.

A real-time strategy for OPF in presence of BSSs and wind farms (WFs) was proposed in [185]. Considering uncertain wind power, the method in [185] uses linear MPC to continuously update the planned wind power profiles. The method was tested on a 14-bus

transmission network with the sampling period of 5 minutes. A real-time algorithm was proposed in [186] to automatically alleviate contingencies (e.g., feeder overloads and voltage constraint violations). A multi-stage stochastic optimization for real-time economic dispatch of pumped hydro storage was developed in [187]. A feedback-based RT-OPF methodology was proposed in [188] to satisfy system constraints in real-time. A distributed MPC-based RT-OPF approach was proposed in [189] for the operation of a network of smart microgrids.

Taking into account variable demand and REG during the period between two consecutive schedules, [190] proposed a RT-OPF strategy to decrease the computation burden. The scheduling intervals (e.g., 10 minutes) are divided into a certain number of subintervals (e.g., 1 minute). The forecasted values of REG and load demand are assumed to be available for the subintervals. The participation factors of conventional generators in the network are determined by solving an OPF problem. The OPF is performed only at the beginning of each scheduling interval but also satisfying all the constraints of the subintervals by incorporating the generating costs of the subintervals. The obtained operation strategies in this way are named 'best-fit' participation factors [191, 192]. They are then utilized to correct the decision variables of subintervals based on forecasted values of REG and demand. The RT-OPF approach in [190] is only applicable when the total demand and losses in the network is greater than the REG. Otherwise, the approach needs to be adopted to incorporate REG curtailment and/or bidirectional power exchange with an upstream network and/or BSSs (like in [193, 194]) in the formulation.

Hierarchical control methods are widely used to control the frequency in the network and keeping the active power of generators near to the optimal operating point when there exist disturbances in the network. Recently, a distributed RT-OPF control strategy for smart grids was proposed in [195] using a feedback mechanism to achieve the same objective as hierarchical controls without the need of load forecast. Based on a dual ascent method and real-time measurements, a distributed feedback control approach for optimal reactive power flow problem was proposed in [196]. The reactive power capability of micro-generators is utilized in [196] to minimize losses while satisfying voltage constraints in low-voltage (LV) or HV networks.

A feedback controller for photovoltaic inverters was developed in [197] to seek inverter set points corresponding to AC OPF solutions. The study in [197] was recently extended in [198] by improving convergence properties of the feedback controllers for the case of time-varying network and ambient conditions. The development of a RT-OPF on a hybrid AC/DC smart grid test-bed was reported in [199]. When the AC OPF fails to converge, a DC optimization (i.e., using a linearized model) is used to facilitate the convergence. Based on a gradient-projection method and a linearized distribution system flow model, a local reactive

power control framework was developed in [200] to fast respond to voltage mismatch in the networks with high penetration of REG.

1.5 Contributions

In the previous sections, we have given an account of various real-time approaches which have been applied to power system operation and planning. The applications of these methods on different aspects of the power systems were investigated confirming that the developed methods are very promising for power systems decision makers. However, the most important limitation of the available literature lies in the fact that only few studies considered optimal operation of BSSs in their networks [201], which could be of high interest of network operators in next years. It is also noted that all the above studies on RT-OPF have not considered optimal operations of BSSs when optimizing mixed-integer decision variables of the network. Therefore, in this study we propose a real-time dynamic active-reactive OPF (RT-DAR-OPF) framework to address the above issues. The contributions of this dissertation are summarized as follows:

- A multi-time-scale dynamic active-reactive optimal power flow (AR-OPF) framework is developed to optimally react to the spontaneous changes in wind power and ensure the feasibility of operations in real-time.
- The framework offers the possibility of simultaneous optimization of all following mixed-integer variables in a prediction horizon:
  - Wind power curtailment of each WF (continuous)
  - Active power charge/discharge of each BSS (continuous)
  - Reactive power dispatch of each WF and BSS (continuous)
  - Length of charge and discharge periods of each BSS (discrete)
  - Length of charge-discharge cycles of each BSS (discrete)
  - Number of charge-discharge cycles of each BSS in the prediction horizon (discrete)
  - Status of charge/discharge of each BSS (binary)
  - Slack bus voltage (discrete)
  - Active-reactive reverse power flow to an upstream network (continuous)
- A scenario generation method is integrated in the RT-OPF framework to represent uncertain wind power for the prediction horizon, which leads to a set of uncoupled MINLP problems solved by parallel computing.

- A novel reconciliation algorithm is proposed, which allows for online solving the problem of non-convergence of the MINLP OPF by providing sub-optimal and feasible control strategies to be realized to the network in real-time.
- Based on the operating mode of the WFs, a power factor modification scheme is introduced to ensure a feasible operation in the realization phase of the framework.
- Fully flexible optimal operation strategies for BSSs are determined for the dynamic AR-OPF while minimizing the expended life costs of the BSSs.

2 A Framework for Real-Time Optimal Power Flow

Developing a suitable framework for RT-OPF is of utmost importance for ensuring both optimality and feasibility in the operation of energy DNs under intermittent wind energy penetration. The most challenging issue thereby is that a large-scale complex optimization problem has to be solved in real-time. Online simultaneous optimization of the wind power curtailments of WFs and the discrete reference values of the slack bus voltage which leads to a MINLP problem, in addition to considering variable reverse power flow, make the optimization problem even much more complicated. To address these difficulties, a two-phase solution approach to RT-OPF is proposed in this chapter. In the prediction phase, a number of MINLP OPF problems corresponding to the most probable scenarios of the wind energy penetration in the prediction horizon, by taking its forecasted value and stochastic distribution into account, are solved in parallel. The solution provides a lookup table for optional control strategies for the current prediction horizon which is further divided into a certain number of short time intervals. In the realization phase, one of the control strategies is selected from the lookup table based on the actual wind power and realized to the grid in the current time interval, which will proceed from one interval to the next, till the end of the current prediction horizon. Then, the prediction phase for the next prediction horizon will be activated. A 41-bus medium-voltage DN is taken as a case study to demonstrate the proposed RT-OPF approach.

2.1 Problem Formulation

The ultimate goal of the RT-OPF framework proposed in this study is to compute optimal operation strategies for DNs which will autonomously be updated according to spontaneous changes of energy penetrated from WFs. Thus, the updating time interval (sampling time) T_S should be kept as short as possible. However, due to its high complexity, the computation time T_{OPF} needed to solve the optimization problem can be much higher than the sampling time. To address this conflict, we employ the forecasted data of wind energy which are available in advance of a future time horizon T_P. In this study, this forecasted time

horizon is called a prediction horizon. Since the prediction horizon T_P is usually higher than the sampling time T_S, we can divide the prediction horizon into *M* sampling times, i.e.,:

$$T_P = M\ T_S. \tag{2.1}$$

In this study, we assume that the total computation time T_{OPF} is smaller than the prediction horizon T_P. Under this assumption, a prediction-realization approach for RT-OPF will be developed in this study. In the prediction phase, the optimization problem is solved in advance for a number of probable wind energy scenarios, based on the forecasted data in the prediction horizon and its probability density function (PDF), leading to a lookup table for optional optimal operation strategies. In the realization phase, the actual wind energy data are successively available from one sampling time to the next. In each sampling time, the actual data will be compared with the predefined wind energy scenarios and an optimal operation strategy corresponding to the nearest higher scenario will be selected from the lookup table and realized in the network. In this way, an online update of the operation strategy according to the spontaneously changing wind energy generation is carried out.

In this section, the optimization problem to be solved for each prediction horizon, during the prediction phase, is defined. To explain the complex problem in a clear way, we define at first a general optimization problem for OPF. A detailed and concrete problem definition of the RT-OPF is given in Section 2.3. For a prediction horizon, i.e., $t \in [kT_P, (k+1)T_P]$, the OPF problem of a DN with wind energy penetration is defined as:

$$\begin{aligned} \max_{\mathbf{u}(t),\mathbf{l}(t)} \quad & f\left(\mathbf{x}(t),\mathbf{u}(t),\mathbf{l}(t),\boldsymbol{\xi}(t)\right) \\ s.t. \quad & \mathbf{g}\left(\mathbf{x}(t),\mathbf{u}(t),\mathbf{l}(t),\boldsymbol{\xi}(t)\right) = \mathbf{0} \\ & \mathbf{x}_{\min} \le \mathbf{x}(t) \le \mathbf{x}_{\max} \\ & \mathbf{u}_{\min} \le \mathbf{u}(t) \le \mathbf{u}_{\max} \\ & \mathbf{l}(t) \in \{0,1,2,\cdots,L\} \end{aligned} \tag{2.2}$$

where $\mathbf{x}$ is the vector of state variables, $\mathbf{u}$ and $\mathbf{l}$ are the vectors of continuous and integer decision variables, respectively. Relating to the OPF under consideration, the state vector $\mathbf{x}$ comprises voltages of the PQ buses, active and reactive power at slack bus, and power flows in the feeders, the continuous control vector $\mathbf{u}$ consists of curtailment factors of each WF, and the discrete control vector $\mathbf{l}$ denotes the reference values of slack bus voltage. The vector $\boldsymbol{\xi}$ represents random variables of wind energy of each WF which will be generated in the prediction horizon. In this study, these random variables are regarded as being stochastically distributed with a known PDF $\rho(\xi)$. Therefore, the optimization problem expressed in Equation 2.2 is a MINLP problem under uncertainty.

In fact, power demand also needs to be considered as an uncertain parameter, but in comparison to the wind power, its value is more predictable in the application of online optimization. Many approaches have been developed for very short-term load forecasting aiming at prediction ranges of a few minutes to an hour [159-162]. In [159], it is shown that the mean absolute percentage error (MAPE) can be less than 0.2% for a 120-s prediction horizon. Furthermore, MAPE values of 3.23% and 2.44% were obtained in [162] for the prediction of 30-min ahead individual household load and aggregation load, respectively. Considering the accuracy of the forecasts in the abovementioned studies, the variation of demand in short time slots (e.g., 120 s) is not considered in this study. Thus the forecasted demand for each prediction horizon is used in our RT-OPF framework, but it may change from horizon to horizon.

2.2 Scenario Generation

It is necessary to describe the uncertain vector ξ in Equation 2.2 in advance of each prediction horizon. To do this, a set of wind power scenarios for the prediction horizon representing the stochastic behaviors of the wind power need to be generated, for which we need the PDF. The wind power scenarios are generated within the range [0, 1] pu where 1 pu corresponds to the rated power value $P_{w.R}(n_w)$. N_s scenarios are generated for each WF. We define $N_s - 1$ intervals for the wind power $P_w(n_w, n_s), n_s = 1, \cdots, N_s$, such that:

$$\Pr\{P_w(n_w, n_s) - P_w(n_w, (n_s - 1))\} = \frac{1}{N_s - 1}, \quad \text{for } n_s \geq 2 \tag{2.3}$$

where Pr is the probability operator. In this way, an equal probability between two adjacent scenarios is ensured. It is noted that Equation 2.3 can be applied to any type of continuous bounded distribution as far as the area under its PDF curve equals one. Beta distribution is suggested to be highly suitable to represent the forecast errors of wind power ([149-151]). Although Beta distribution cannot model the fat tail of the forecast errors perfectly [151], due to its variable kurtosis [151], it is still more suitable than the Gaussian distribution and gives reasonably accurate results [151, 202]. Beta PDF has been used in many recent studies [203-205] and therefore is chosen in this study to represent wind power forecast errors. The PDF of the Beta distribution is defined as [149]:

$$\rho(y, \alpha_b(n_w), \beta_b(n_w)) = y^{\alpha_b(n_w)-1}(1-y)^{\beta_b(n_w)-1}, \quad 0 \leq y \leq 1 \tag{2.4}$$

where $\alpha_b(n_w), \beta_b(n_w)$ are the first and second shape parameters of the Beta distribution. The corresponding probability distribution function is expressed as:

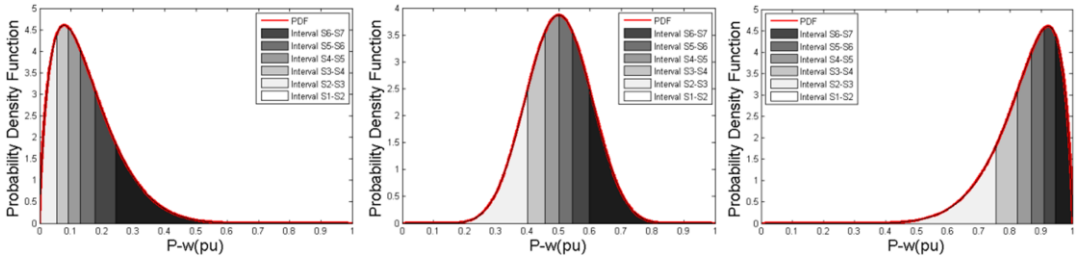

Figure 2.1. Illustration of wind power scenarios (i.e., S_1, …, S_7), for a WF with $\sigma_w = 0.1$ $P_{w.M} = 0.15$ (left), $P_{w.M} = 0.5$ (middle), and $P_{w.M} = 0.85$ (right).

$$F_{PDF}\left(P_w(n_w,n_s),\alpha_b(n_w),\beta_b(n_w)\right) = \int_0^{P_w(n_w,n_s)} \rho\left(y,\alpha_b(n_w),\beta_b(n_w)\right)dy. \tag{2.5}$$

As a result, the probability in the interval between 0 and scenario n_s is $\frac{n_s-1}{N_s-1}$ and then the scenarios can be generated by:

$$P_w(n_w,n_s) = F_{PDF}^{-1}\left(\frac{n_s-1}{N_s-1}\right), \quad \text{for } n_s = 1,\cdots,N_s; \quad N_s \geq 2. \tag{2.6}$$

The parameters $\alpha_b(n_w)$, $\beta_b(n_w)$ can be determined by [151]:

$$\alpha_b(n_w) = \left(\frac{1-P_{w.M}(n_w)}{\left(\sigma_w(n_w)\right)^2} - \frac{1}{P_{w.M}(n_w)}\right)\left(P_{w.M}(n_w)\right)^2 \tag{2.7}$$

$$\beta_b(n_w) = \alpha_b(n_w)\left(\frac{1}{P_{w.M}(n_w)} - 1\right) \tag{2.8}$$

where $P_{w.M}(n_w)$ and $\sigma_w(n_w)$ are the values of the mean and standard deviation of the wind power generation, respectively. For the RT-OPF, we take the forecasted values available before each prediction horizon, as $P_{w.M}(n_w)$. It is noted that the value of $\sigma_w(n_w)$ cannot be forecasted, but it can be evaluated from historical data.

Figure 2.1 illustrates the generated scenarios for three forecasted wind power values when $N_s = 7$ and $\sigma_w = 0.1$. It can be seen that this scenario generation method leads to more scenarios near the mean value. The scenarios generated are the boundaries of intervals. In this way, the scenarios cover the whole range [0, 1] (i.e., from zero to the rated power). Consequently, our RT-OPF can deal with any actual wind power generation (also see Section 2.3). It is noted that the scenarios here are not those from the Latin hypercube sampling method where the scenarios are randomly generated inside each interval [206]. In addition, it is noted that this scenario generation method is a significant improvement to that used in [28, 207] where the scenarios were generated based on a constant width of intervals which cannot

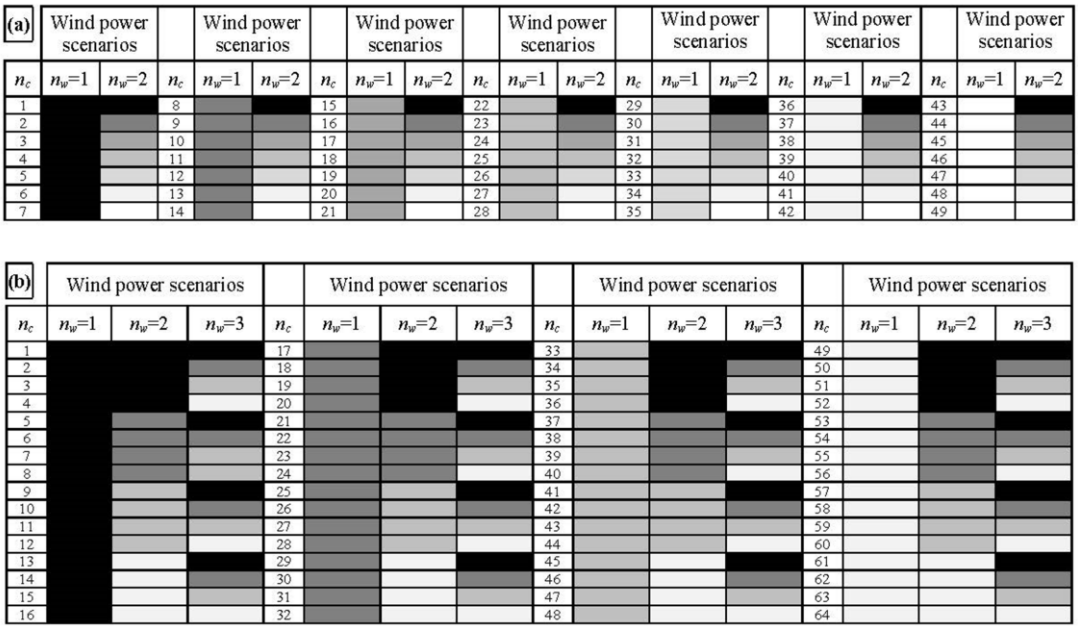

Figure 2.2. Graphical examples of wind power scenario combinations for (**a**) $N_w = 2$, $N_s = 7$ and (**b**) $N_w = 3$, $N_s = 4$. Here, dark to light colors denote high to low wind power scenarios, respectively.

cover the whole range when a limited number of scenarios is chosen. For a power system with N_w WFs, the total number of scenario combinations N_c is:

$$N_c = (N_s)^{N_w}. \tag{2.9}$$

Thus, we need to define the power scenarios for individual WFs $P_w(n_w, n_s), n_s = 1, \cdots, N_s$, and the combinations of the scenarios for all WFs, $\mathbf{P}_w(n_c), n_c = 1, \cdots, N_c$ (i.e., each combination is a vector), respectively. According to Equation 2.9, when the number of WFs increases, the number of scenario combinations increases exponentially. In this case, parallel computing seems not reasonable to address the computational problem which is expectedly solved by the next generation of hardware and software, considering the rapid advancement of the computer technology. All scenarios finally generated for the power system is given in Table 2.1. The rules based on which the scenario combinations are sorted from the first row to row N_c is further cleared by graphical examples in Figure 2.2. It is noted that the scenarios are listed from the highest to the least wind power values, due to the reason described in Section 2.3. To the best of the authors' knowledge, the integration of such a scenario generation method into a RT-OPF framework has not yet been considered.

Table 2.1. The list of wind power scenario combinations for all WFs.

	Scenario Combination				
n_c	$P_w(n_w,n_s)$ $n_w = 1$	$P_w(n_w,n_s)$ $n_w = 2$	…	$P_w(n_w,n_s)$ $n_w = N_w - 1$	$P_w(n_w,n_s)$ $n_w = N_w$
1	$P_w(1,N_s)$	$P_w(2,N_s)$	…	$P_w((N_w-1),N_s)$	$P_w(N_w,N_s)$
2	$P_w(1,N_s)$	$P_w(2,N_s)$	...	$P_w((N_w-1),N_s)$	$P_w(N_w,(N_s-1))$
⋮	⋮	⋮	⋮	⋮	⋮
$N_c - 1$	$P_w(1,1)$	$P_w(2,1)$	…	$P_w((N_w-1),1)$	$P_w(N_w,2)$
N_c	$P_w(1,1)$	$P_w(2,1)$	…	$P_w((N_w-1),1)$	$P_w(N_w,1)$

2.3 Solution Framework

2.3.1 Prediction Phase

The task of the prediction phase is to solve the OPF problems corresponding to the N_c scenario combinations of wind power (see Table 2.1) for each prediction horizon. The active and reactive power demand at bus i, denoted as $(P_d(i),Q_d(i))$ as well as the active and reactive energy prices (C_{PP},C_{PQ}) are assumed to be constant in the short prediction horizon. But they may change from horizon to horizon. In addition, the power system model/structure is considered to be as in [17, 208] and fixed in the prediction phase. The OPF problem defined in Equation 2.2 is formulated here in more detail for each scenario combination $n_c,(n_c=1,\cdots,N_c)$:

$$\max_{\beta_w(i,n_c),V_S(n_c)} f(n_c) = f_1(n_c) - f_2(n_c) - f_3(n_c) - f_4(n_c) \tag{2.10}$$

where:

$$f_1(n_c) = C_{PP} \sum_{i=1}^{N_{bus}} P_w(i,n_c)\beta_w(i,n_c) \tag{2.11}$$

$$f_2(n_c) = C_{PP}\, P_{loss}(n_c) \tag{2.12}$$

$$f_3(n_c) = C_{PP}\, P_s(n_c) \tag{2.13}$$

$$f_4(n_c) = C_{PQ}\, Q_s(n_c). \tag{2.14}$$

The objective function in Equation 2.10 aims to maximize the total revenue from the wind power $f_1(n_c)$, and meanwhile to minimize the total cost of the active energy losses in the grid $f_2(n_c)$, the cost of the active energy at slack bus $f_3(n_c)$, and the cost of the reactive energy at slack bus $f_4(n_c)$. Here, $P_{loss}(n_c)$ is the grid total active power losses [17] for

scenario combination n_c. $P_w(i,n_c)$ is the active power of WF located at bus i for scenario combination n_c. $P_s(n_c)$ and $Q_s(n_c)$ are the active and reactive power injected at slack bus, respectively (i.e., the imported active and reactive energy from an upstream HV network). The vector of discrete decision variables $\mathbf{l}$, in Equation 2.2, consists of slack bus voltage $V_s(n_c)$, representing the controller reference of tap positions of the OLTC. The vector of continuous decision variables $\mathbf{u}$ includes the curtailment factors of wind power for each WF, $\beta_w(i,n_c)$. Here, $(0 \le \beta_w(i,n_c) \le 1)$, where $\beta_w = 1$ when no curtailment and $\beta_w < 1$ otherwise [17].

The objective function of Equation 2.10 is subject to the active and reactive power flow equations at the buses:

$$f_P(n_c) + P_d(i) - P_w(i,n_c)\,\beta_w(i,n_c) - P_s(n_c) = 0, \qquad i \in S_b \tag{2.15}$$

$$f_Q(n_c) + Q_d(i) - Q_s(n_c) = 0, \qquad i \in S_b \tag{2.16}$$

where $f_P(n_c)$ and $f_Q(n_c)$ are the network active and reactive power functions [17] for scenario combination n_c, respectively. $P_s(n_c)$ and $Q_s(n_c)$ are the active and reactive power terms included only for slack bus, respectively. In addition, the following inequality constraints should be held:

Bounds of active and reactive power at slack bus:

$$\left(P_s(n_c)\right)^2 + \left(Q_s(n_c)\right)^2 \le \left(S_{s.\max}\right)^2 \tag{2.17}$$

$$-\gamma_{Ps} S_{s.\max} \le P_s(n_c) \le S_{s.\max}, \qquad 0 \le \gamma_{Ps} \le 1 \tag{2.18}$$

$$-\gamma_{Qs} S_{s.\max} \le Q_s(n_c) \le S_{s.\max}, \qquad 0 \le \gamma_{Qs} \le 1 \tag{2.19}$$

voltage bounds of buses:

$$V_{\min}(i) \le V(i,n_c) \le V_{\max}(i), \qquad i \in S_b; \quad i \ne 1 \tag{2.20}$$

$$V_{s.\min} \le V_s(n_c) \le V_{s.\max} \tag{2.21}$$

$$V_s(n_c) = 1 + \Delta V_s(n_c), \qquad \Delta V_s(n_c) = \{-0.1, -0.09, \cdots, 0.09, 0.1\} \tag{2.22}$$

feeder sections limits:

$$S(i,j,n_c) \le S_{l.\max}(i,j), \qquad i,j \in S_b; \quad i \ne j \tag{2.23}$$

and the limits of the curtailment factors:

$$0 \le \beta_w(i,n_c) \le 1. \tag{2.24}$$

In Equations 2.18 and 2.19, the parameters γ_{Ps} and γ_{Qs} define the percentage of the allowable reverse active and reactive power to an upstream HV network. For instance, if $\gamma_{Ps}=1$, active power exported to the HV network is fully allowed and if $\gamma_{Ps}=0$, no active power export is allowed. In addition, based on Equations 2.21 and 2.22, for scenario combination n_c, an optimal value of slack bus voltage $V_s(n_c)$ is obtained by selecting the best $\Delta V_s(n_c)$ which is a *discrete* variable. Therefore, the formulation of Equations 2.10–2.24 leads to a high-dimensional, MINLP problem for each scenario combination n_c. The solution of this problem is obtained by using a MINLP solver. Parallel computing can be easily carried out because each scenario is independent of the other scenarios, i.e., multiple processors can be used each of which are responsible for a number of the MINLP OPF problems. The solutions of the MINLP OPF problems lead to a lookup table providing options of operation strategies, one of which will be selected for the grid operation in the realization phase.

2.3.2 Realization Phase

The lookup table provides N_c solutions corresponding to the scenario combinations generated based on forecasted wind power $P_{w.M}(n_w)$. The actually generated wind power values of the WFs are available at each sampling interval m. For each sampling interval, one of the solutions in the lookup table will be selected and the corresponding control values realized to the network. The selection is made by comparing the actual wind power $P_{w.A}(n_w,m)$ with the wind power scenarios of each WF $P_w(n_w,n_s)$, based on the following

Algorithm 2.1. Selection algorithm

for each WF $n_w=1,\cdots,N_w$ and $n_s\geq 2$
If $P_w(n_w,(n_s-1))<P_{w.A}(n_w,m)\leq P_w(n_w,n_s)$
then consider $P_{w.A}(n_w,m)$ as $P_w(n_w,n_s)$
end
Achieve $\mathbf{P}_w(n_c)$
Based on n_c, set $\boldsymbol{\beta}_w(m)=\boldsymbol{\beta}_w(n_c)$ and $V_s(m)=V_s(n_c)$

This means, for each WF n_w, if $P_{w.A}(n_w,m)$ is not equal to $P_w(n_w,(n_s-1))$, then consider it to be *the nearest higher* scenario. This is because a higher wind power associates with a lower curtailment factor, leading to a feasible operation strategy. Since the scenarios generated in the prediction phase cover the whole range [0, 1], for any actual value of wind power, there is a higher or equal scenario corresponding to an optimal operation strategy. It should be noted that the decision made in this way also has a certain degree of built-in

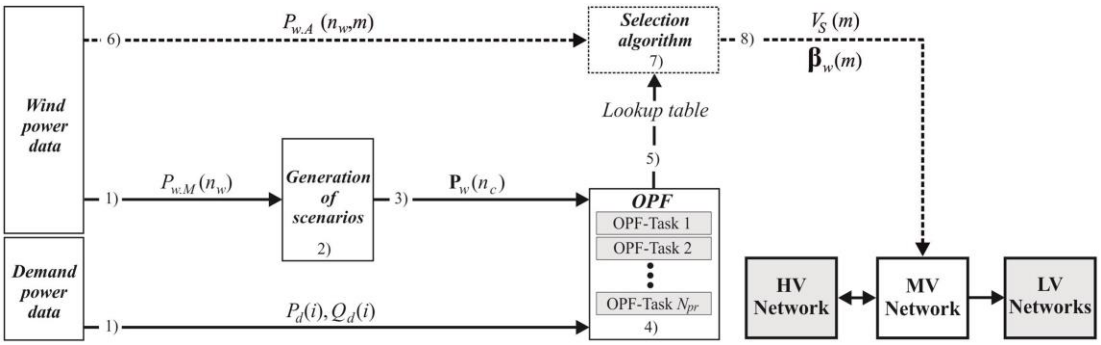

Figure 2.3. Framework of the proposed RT-OPF for a prediction horizon. Here, HV, MV and LV denote high-voltage, medium-voltage and low-voltage, respectively.

conservativeness, so that feasibility of the selected solution to be realized to the grid can be ensured. This conservativeness will be decreased if more scenarios for each WF are used. But then the number of MINLP problems to be solved will be increased correspondingly.

2.3.3 Implementation of the RT-OPF Framework

The RT-OPF framework of the proposed prediction-realization approach is implemented as shown in Figure 2.3 where the execution steps are shown by the numbers. It consists of following eight steps:

1) For the current prediction horizon, provide the forecasted active $P_d(i)$ and reactive $Q_d(i)$ power demand and wind power $P_{w.M}(n_w)$.
2) Generate N_c wind power scenario combinations based on the Beta distribution as described in Section 2.2.
3) Send the generated scenarios as inputs to formulate N_c MINLP OPF problems.
4) Solve the N_c MINLP OPF problems with parallel computing.
5) Send the solution results as a lookup table to the selection algorithm.
6) Provide the actual wind power of WFs, $P_{w.A}(n_w,m)$, available at the current sampling time m (for $m=1,\cdots,M$), to the selection algorithm.
7) Select one of the solutions from the lookup table based on $P_{w.A}(n_w,m)$ and the selection algorithm (see Section 2.3).
8) Send the values of the controls $V_s(m)$ and $\boldsymbol{\beta}_w(m)$ to the grid.

Steps 1–5, as shown with solid lines in Figure 2.3, correspond to the prediction phase, while steps 6–8, presented with dashed lines, denote the realization phase. Step 8 means that, with an optimal value of the slack bus voltage, an optimal amount of wind power is

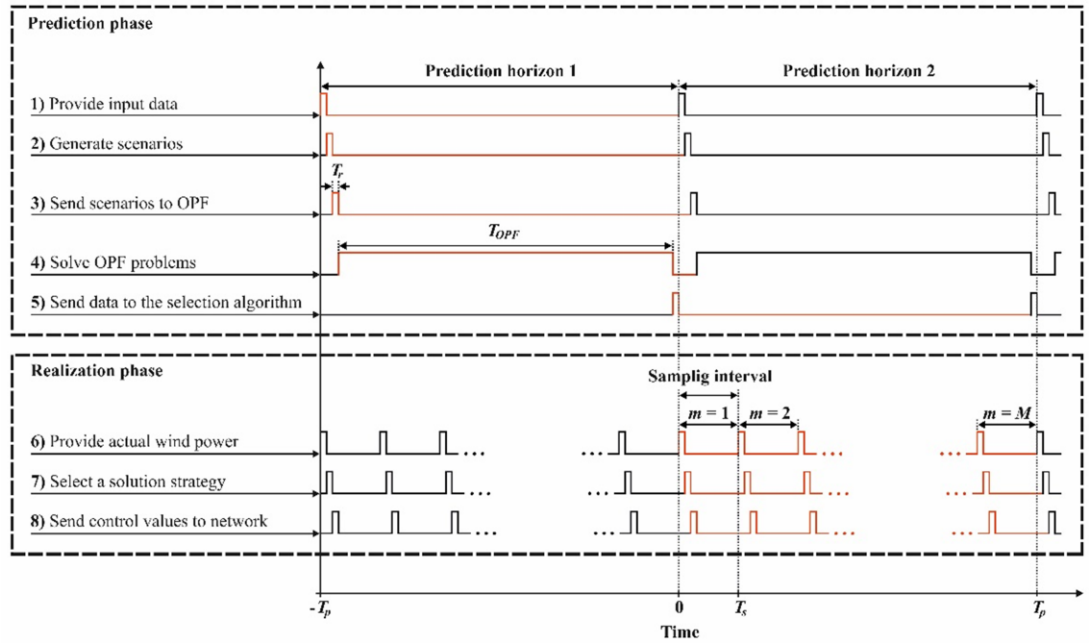

Figure 2.4. Time allocation for the computational tasks of the 8 steps in Figure 2.3.

penetrated to the grid in the current sampling time m. When $m = M$, the computation proceeds to the next prediction horizon.

To online realize the computation framework described above, it is necessary to ensure all 8 steps to be completed inside the time slot of T_P. The implementation is illustrated in Figure 2.4, showing two consecutive prediction horizons. In Figure 2.4, the red lines indicate the execution of the eight tasks along the time. It means when the optimal strategies for the current prediction horizon are realized to the network, the solutions for the upcoming prediction horizon are prepared.

In Figure 2.4, T_r denotes the length of the time reserved for data management (for our case study $T_r = 2\,s$). For steps 1, 3, 5, 6, and 8, T_r means the communication (i.e., sending/receiving data) time. In steps 2, 4, and 7, T_r means the time for processing data after receiving the corresponding inputs. T_{OPF} is the time to solve the N_c OPF problems, which takes the largest part of the time horizon.

T_P is the prediction horizon for which the forecasted data is available and its length should be the summation of the lengths of all the tasks (including OPF computations as shown in Figure 2.4) in the prediction phase:

$$T_P = 4T_r + T_{OPF} \tag{2.25}$$

Here, the greatest time slot is allocated to the computation of the OPF problems corresponding to the generated scenarios (i.e., T_{OPF}). It means that, at the end of the

prediction phase, the OPF results must be ready for the selection algorithm in the realization phase.

The sampling time T_S in which the actual values of wind power are available, could be very short (even less than a second). However, since the realization is also performed at every T_S, the length of T_S should be realistic in order not to damage devices by too frequent control actions in very short time intervals. On the other hand, based on Equation 2.1, T_s theoretically can be equal to T_P (i.e., $M=1$). However, long sampling intervals could not response the intermittency of the wind power.

The wind power spectrum has been investigated for a long time. Using short term and long term records, the Van der Hoven spectrum [209] shows the diurnal and turbulence effects of wind power. It confirms that there are considerable wind power discrepancies in short term (e.g., 1 min) periods. The spectrum has been also studied to evaluate and improve wind power prediction [210, 211]. However, in this study, we assume that the values of wind power prediction are provided by a forecast center. The time period over which the forecasted value is updated, is defined as the prediction horizon. In our case study, the forecasted wind power value is assumed to be available every two minutes. Thus we define the length of the prediction horizon as two minutes. The forecasted wind power profiles for one day are taken from [28] for the case study. Indeed, this is the reason that the blocks 'wind power data' and 'power demand data' are not included in the '8 steps' of the framework in Figure 2.3. This means that the way how the wind and demand power data is obtained is not considered in this study.

Parallel computing is used for solving the individual MINLP problems by multiple processors, each of which solves an equal number of the optimization problems. Therefore, the time needed for the solutions to be available is the maximum time taken by the processors. But we need to allocate T_{OPF} large enough to ensure that none of the processors exceeds this limit. The proposed RT-OPF framework is further described by a flowchart in Figure 2.5. The flowchart shows the prediction and realization phases.

2.4 Case Study

2.4.1 Network and Input Data

The network for the case study is taken from [212, 213]. It is a 41-bus, 27.6 kV typical rural DN, as shown in Figure 2.6. The peak power demand is 16.25 MVA [17] and the substation rating is 20 MVA. Two WFs each with $P_{w.R}=10$ MW and unity power factors are

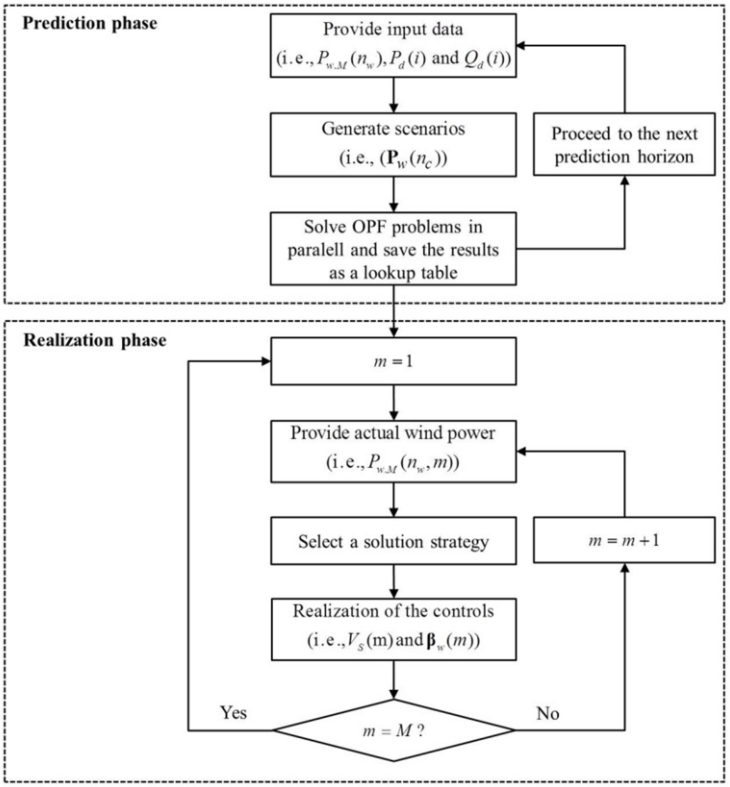

Figure 2.5. The flowchart of the proposed RT-OPF framework.

located at buses 2 and 16, as shown in Figure 2.6. The WFs are subject to different wind profiles which make the problem more complicated. The bus number 1 is considered as the slack bus with zero voltage angle [212, 213]. The active and reactive energy prices are adapted and fixed with 1.67 \$/MW.T_p and 0.4 \$/Mvar.T_p [28, 212], respectively. We assume that the forecasted and measured values of wind power generation are available in every 120 and 20 s, respectively. Therefore, the length of the prediction horizon T_p and the length of the sampling time T_s are taken as 120 and 20 s, respectively. For generating wind scenarios, we take $N_s = 7$ which means we consider seven scenarios for each of the two WFs, leading to

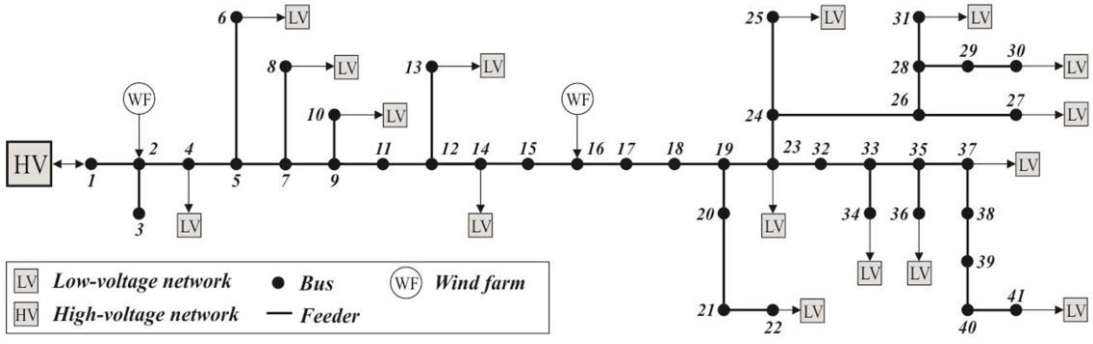

Figure 2.6. DN for the case study.

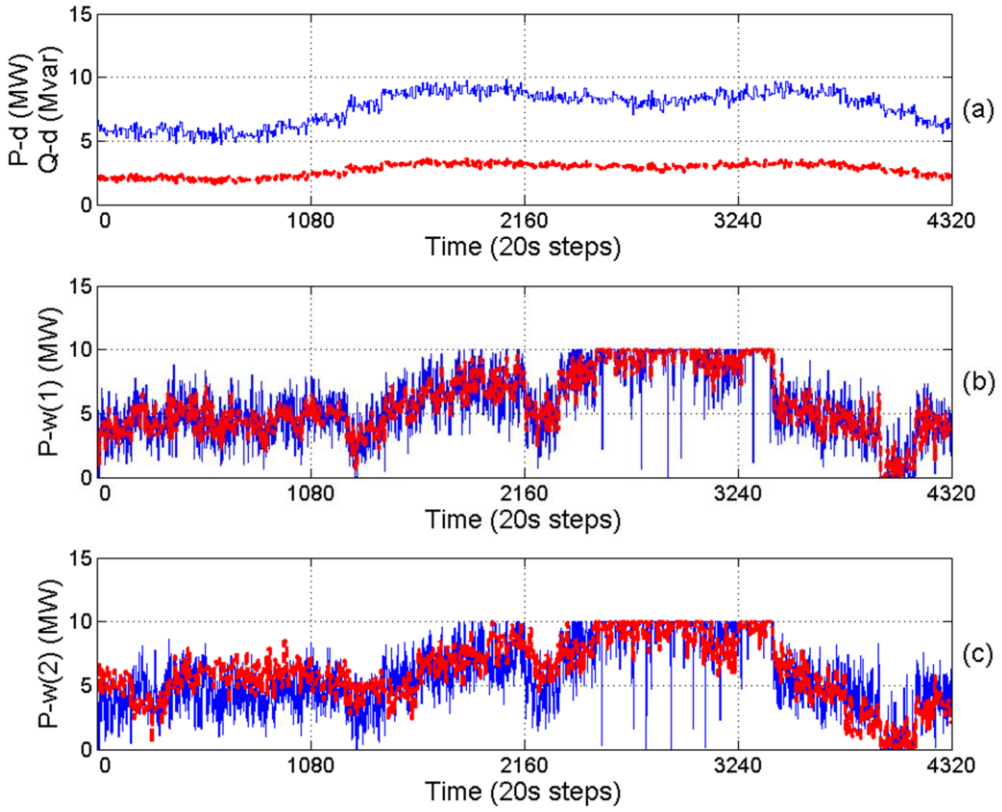

Figure 2.7. Trajectories of one day: (**a**) total active (blue-solid) and reactive (red-dashed) power demand; (**b**) forecasted (red-dashed) and actual (blue-solid) wind power of the first WF; and (**c**) forecasted (red-dashed) and actual (blue-solid) wind power of the second WF.

$N_c = 49$ MINLP OPF problems. To implement parallel computing, we use seven processors to solve the 49 problems (i.e., seven scenario combinations are allocated to each processor).

The computations are carried out on a server with 2 Intel Xeon X5690, CPU 3.47 GHz (six cores, 12 threads) and 64 GB random access memory (RAM). The problem is formulated and coded in the general algebraic modeling system (GAMS) [214] framework and the resulting problem solved by the MINLP solver BONMIN [215], using the usual flat start [17]. Based on the BONMIN manual [215], the algorithms are exact when both the objective function and the constraints are convex, otherwise they are heuristics. It is also noted that there are some possible model status messages in GAMS. In solving our MINLP problems, we always got the message No. 8 (integer solution), meaning that a feasible solution has been found to problems with discrete variables, see details in [214]. However, the solution achieved in this way should be considered as a local solution, since the power flow equations are non-convex.

The active P_d and reactive Q_d power demand are assumed to follow the hourly IEEE-RTS fall season's days [212]. However, inside each hour, the demand profiles are generated for every bus at every 120 s by adding normally distributed random values (with $\mu_d(i) = 0$

and $\sigma_d(i) = 0.01$) to the hourly values [28]. The resulting demand trajectories for one day are shown in Figure 2.7(a).

In the reality, the forecasted and actual wind power profiles can be acquired from environmental data centers and online measurements, respectively. The forecasted wind power profiles for one day are taken from [28] and shown as the red-dashed curves in Figure 2.7(b,c). The actual wind power $P_{w.A}(n_w, m)$ for the two WFs are generated at each 20 s using the Beta distribution with the shape parameters $\alpha_b(n_w)$ and $\beta_b(n_w)$ corresponding to the forecasted wind power, where $\sigma_w(n_w) = 0.1\,\text{pu} = 1\,\text{MW}$ based on Equations 2.7 and 2.8. The resulting curves for the two WFs are shown in Figure 2.7(b,c).

2.4.2 Test Cases

In the case study, possible reverse power flow is considered for the proposed RT-OPF framework. We define the forward and reverse active as well as reactive energy at the slack bus as follows:

- Forward energy flow: The forward active and reactive energy from the HV network to the MV network is to be minimized based on an energy price model.
- Reverse energy flow: The reverse power flow could have impacts on voltage profiles [216] of the upper-level network and may result in specific operational limits being exceeded at the congested primary substations [217]. However, reverse flows have been considered in many studies [208, 218-222] and in reality, they are likely to happen. Therefore, in this study we consider the cases with and without reverse power flows.

Furthermore, in the optimization problem formulation, the slack bus voltage can be either a parameter with a fixed value or a discrete free variable. Based on these considerations, we carry out RT-OPF for four different cases defined as follows:

Case 1): Both reverse active and reactive power to the upstream HV network is not allowed (i.e., $\gamma_{Ps} = \gamma_{Qs} = 0$), and with a fixed value of the slack bus voltage ($V_s(m) = V_s(n_c) = 1\,\text{pu}$).

Case 2): Both reverse active and reactive power to upstream HV network is not allowed (i.e., $\gamma_{Ps} = \gamma_{Qs} = 0$), and with the slack bus voltage as a discrete free variable.

Case 3): Both reverse active and reactive power to upstream HV network is allowed (i.e., $\gamma_{Ps} = \gamma_{Qs} = 1$), and with a fixed value of the slack bus voltage (i.e., $V_s(m) = V_s(n_c) = 1\,\text{pu}$).

Case 4): Both reverse active and reactive power to upstream HV network is allowed (i.e., $\gamma_{Ps} = \gamma_{Qs} = 1$), and with the slack bus voltage as a discrete free variable.

2.4.3 Results and Discussions

We run the RT-OPF for one day for the aforementioned four cases using the same network in Figure 2.6 and the input data in Figure 2.7. To illustrate the prediction phase and the realization phase, we firstly take the first prediction horizon (i.e., $t \in [0, 120\ \text{s}]$) as an example. The forecasted values of wind power for the two WFs in the first prediction horizon are $P_{w.M}(1) = 3.8$ MW and $P_{w.M}(2) = 7.05$ MW. The wind power scenario combinations and the corresponding results for the four cases in the first prediction horizon are shown in Tables 2.2–2.5. In addition, the results of one day for four cases are compared in Table 2.6.

The lookup tables consist of two sections: "scenario combinations" and "optimal results". The scenario combinations are obtained as described in Section 2.2 and optimal results are achieved by solving the corresponding OPF problems (i.e., Equations 2.10–2.24). Based on Equation 2.9, there are 49 scenarios in each lookup table from which one action will be selected in each sampling interval T_S. It is noted that the lookup tables are updated in each prediction horizon T_P based on the new values of forecasted wind and power demand.

In the first sampling time interval (i.e., $t \in [0, 20\ \text{s}]$), the real wind power are $P_{w.A}(1,1) = 3.74$ MW and $P_{w.A}(2,1) = 4.17$ MW, respectively. Therefore, the selection algorithm (shown as Step 7 in Figure 2.3) selects the scenario combination 27 which corresponds to the level higher than the real value of wind power for both WFs. Then the control strategy corresponding to this scenario combination will be realized to the grid.

It can be seen in Tables 2.2 and 2.3 that, for this prediction horizon, the active power at the slack bus is zero when the wind power of WFs is high. This is because of the low total active power demand (6.65 MW) and high active wind power generation. In addition, the high wind power generation leads to high curtailment (i.e., low values of the curtailment factors) to ensure feasibility. In contrast, if reverse power flow is allowed, as in Cases (3) and (4), the surplus active wind power will not be curtailed, i.e., $\boldsymbol{\beta}_w(n_c) = 1$, and it is exported to the upstream HV network, showing negative active power at the slack bus. The reactive power at the slack bus is always positive for all scenarios of the four cases in this time horizon, i.e., it will be imported from the upstream network. This is because of using unity power factors of the WFs and the reactive power compensation of feeder capacitive susceptance [212] (the total reactive power demand is 2.46 Mvar in this time horizon). From another perspective, for this prediction horizon, in Cases (2) and (4) where the optimization

problems are formulated as MINLP, the values of slack bus voltage tend to be more than 1 pu. This is due the fact that a higher slack bus voltage results in less power losses and consequently higher values of the objective function.

Based on the input profiles as shown in Figure 2.7, the optimal strategies are computed online for the network for 24 hours. The resulting trajectories for the four cases are shown in Figures 2.8–2.11. In these figures, subplots (a)–(c) show the curtailment factors of WFs and the slack bus voltages, respectively. From the economic point of view, the optimal strategy has some degree of conservativeness due to the (limited) number of scenarios. This can be seen from the resulting active power imported from the upstream network, shown in subplot (d) in Figures 2.8 and 2.9, which means in most time the really imported value is higher than the expectedly imported value.

However, when the total wind power is much higher than the forecasted value but lower than the total demand plus the losses, the really imported active power will be lower than the expected value, leading to higher total revenue for such sampling intervals as shown in subplots (f) in Figures 2.8 and 2.9. In Cases (3) and (4) where $\gamma_{Ps,rev} = \gamma_{Qs,rev} = 1$, i.e., the reverse power flow to upstream HV network is allowed, there will be no wind power curtailment, i.e., $\boldsymbol{\beta}_w(n_c) = \boldsymbol{\beta}_w(m) = 1$. Thus, high amount of energy is exported through the slack bus leading to negative values of active power as shown in subplots (d) in Figures 2.10 and 2.11. As clearly shown in subplots (e), there is no significant difference between the forecasted and actual values of reactive power at the slack bus. This is due to unity power factors of WFs which means the reactive power imported from the upstream HV network is not sensitive to wind power fluctuations and it mostly follows the same trend as the total reactive power demand in the network. However, comparing subplots (e) in Figures 2.8 and 2.9 with the ones in Figures 2.10 and 2.11, it is clearly seen that the reactive power at the slack bus is increased when the reverse power is allowed. The reason is that increasing the power flow in the network increases both the active and reactive power losses in the grid. Therefore, most of the reactive power losses must be supplied by the upstream network.

As shown in subplots (c) of Figures 2.9 and 2.11, when the slack bus voltage is taken into account as a discrete free variable, it tends to take the values higher than 1 pu which leads to decrease in power losses. At the same time, the slack bus voltage must lead to satisfying the constraints of voltage at PQ buses (i.e., $V_{\min}(i) = 0.94\,\text{pu}$ and $V_{\max}(i) = 1.06\,\text{pu}$). When the reverse power flow is not allowed, the slack bus voltage varies between 1.06 and 1.07 as shown in Figure 2.9(c). Allowing reverse power flow results in increasing the range to be between 1.03 and 1.07 as shown in Figure 2.11(c). This is because power flows from buses with a higher voltage to a lower one, which means that in the case of reverse power flow, the slack bus voltage must be lower than the voltage at bus 2.

Table 2.2. Lookup table for the first prediction horizon (with $P_{w.M}(1)$ = 3.8 MW, $P_{w.M}(2)$ = 7.05 MW) for Case 1.

Scenario Combination			Optimal Results				
n_c	$P_w(n_w,n_s)$ (MW) n_w = 1	$P_w(n_w,n_s)$ (MW) n_w = 2	$\beta_w(1)$ -	$\beta_w(2)$ -	Vs (pu)	P_S (MW)	Q_S (Mvar)
1	$P_w(1,7)$ = 10	$P_w(2,7)$ = 10	0.379	0.288	1	0	2.375
2	$P_w(1,7)$ = 10	$P_w(2,6)$ = 8.04	0.379	0.358	1	0	2.375
3	$P_w(1,7)$ = 10	$P_w(2,5)$ = 7.55	0.379	0.382	1	0	2.375
4	$P_w(1,7)$ = 10	$P_w(2,4)$ = 7.13	0.379	0.404	1	0	2.375
5	$P_w(1,7)$ = 10	$P_w(2,3)$ = 6.67	0.379	0.432	1	0	2.375
6	$P_w(1,7)$ = 10	$P_w(2,2)$ = 6.07	0.379	0.475	1	0	2.375
7	$P_w(1,7)$ = 10	$P_w(2,1)$ = 0	0.669	1	1	0	2.406
8	$P_w(1,6)$ = 4.79	$P_w(2,7)$ = 10	0.792	0.288	1	0	2.375
9	$P_w(1,6)$ = 4.79	$P_w(2,6)$ = 8.04	0.792	0.358	1	0	2.375
10	$P_w(1,6)$ = 4.79	$P_w(2,5)$ = 7.55	0.792	0.382	1	0	2.375
11	$P_w(1,6)$ = 4.79	$P_w(2,4)$ = 7.13	0.792	0.404	1	0	2.375
12	$P_w(1,6)$ = 4.79	$P_w(2,3)$ = 6.67	0.792	0.432	1	0	2.375
13	$P_w(1,6)$ = 4.79	$P_w(2,2)$ = 6.07	0.792	0.475	1	0	2.375
14	$P_w(1,6)$ = 4.79	$P_w(2,1)$ = 0	1	1	1	1.9	2.419
15	$P_w(1,5)$ = 4.22	$P_w(2,7)$ = 10	0.899	0.288	1	0	2.375
16	$P_w(1,5)$ = 4.22	$P_w(2,6)$ = 8.04	0.899	0.358	1	0	2.375
17	$P_w(1,5)$ = 4.22	$P_w(2,5)$ = 7.55	0.899	0.382	1	0	2.375
18	$P_w(1,5)$ = 4.22	$P_w(2,4)$ = 7.13	0.899	0.404	1	0	2.375
19	$P_w(1,5)$ = 4.22	$P_w(2,3)$ = 6.67	0.899	0.432	1	0	2.375
20	$P_w(1,7)$ = 4.22	$P_w(2,2)$ = 6.07	0.899	0.475	1	0	2.375
21	$P_w(1,5)$ = 4.22	$P_w(2,1)$ = 0	1	1	1	2.476	2.427
22	$P_w(1,4)$ = 3.77	$P_w(2,7)$ = 10	1	0.29	1	0	2.375
23	$P_w(1,4)$ = 3.77	$P_w(2,6)$ = 8.04	1	0.361	1	0	2.375
24	$P_w(1,4)$ = 3.77	$P_w(2,5)$ = 7.55	1	0.385	1	0	2.375
25	$P_w(1,4)$ = 3.77	$P_w(2,4)$ = 7.13	1	0.407	1	0	2.375
26	$P_w(1,4)$ = 3.77	$P_w(2,3)$ = 6.67	1	0.435	1	0	2.375
27	$P_w(1,4)$ = 3.77	$P_w(2,2)$ = 6.07	1	0.478	1	0	2.375
28	$P_w(1,4)$ = 3.77	$P_w(2,1)$ = 0	1	1	1	2.927	2.435
29	$P_w(1,3)$ = 3.33	$P_w(2,7)$ = 10	1	0.334	1	0	2.376
30	$P_w(1,3)$ = 3.33	$P_w(2,6)$ = 8.04	1	0.416	1	0	2.376
31	$P_w(1,3)$ = 3.33	$P_w(2,5)$ = 7.55	1	0.443	1	0	2.376
32	$P_w(1,3)$ = 3.33	$P_w(2,4)$ = 7.13	1	0.469	1	0	2.376
33	$P_w(1,3)$ = 3.33	$P_w(2,3)$ = 6.67	1	0.501	1	0	2.376
34	$P_w(1,3)$ = 3.33	$P_w(2,2)$ = 6.07	1	0.551	1	0	2.376
35	$P_w(1,3)$ = 3.33	$P_w(2,1)$ = 0	1	1	1	3.370	2.444
36	$P_w(1,2)$ = 2.81	$P_w(2,7)$ = 10	1	0.387	1	0	2.379
37	$P_w(1,2)$ = 2.81	$P_w(2,6)$ = 8.04	1	0.481	1	0	2.379
38	$P_w(1,2)$ = 2.81	$P_w(2,5)$ = 7.55	1	0.512	1	0	2.379
39	$P_w(1,2)$ = 2.81	$P_w(2,4)$ = 7.13	1	0.542	1	0	2.379
40	$P_w(1,2)$ = 2.81	$P_w(2,3)$ = 6.67	1	0.58	1	0	2.379
41	$P_w(1,2)$ = 2.81	$P_w(2,2)$ = 6.07	1	0.637	1	0	2.379
42	$P_w(1,2)$ = 2.81	$P_w(2,1)$ = 0	1	1	1	3.895	2.457
43	$P_w(1,1)$ = 0	$P_w(2,7)$ = 10	1	0.67	1	0	2.429
44	$P_w(1,1)$ = 0	$P_w(2,6)$ = 8.04	1	0.833	1	0	2.429
45	$P_w(1,1)$ = 0	$P_w(2,5)$ = 7.55	1	0.887	1	0	2.429
46	$P_w(1,1)$ = 0	$P_w(2,4)$ = 7.13	1	0.939	1	0	2.429
47	$P_w(1,1)$ = 0	$P_w(2,3)$ = 6.67	1	1	1	0.025	2.428
48	$P_w(1,1)$ = 0	$P_w(2,2)$ = 6.07	1	1	1	0.619	2.414
49	$P_w(1,1)$ = 0	$P_w(2,1)$ = 0	1	1	1	6.744	2.554

Table 2.3. Lookup table for the first prediction horizon (with $P_{w.M}(1) = 3.8$ MW, $P_{w.M}(2) = 7.05$ MW) for Case 2.

Scenario Combination			Optimal Results				
n_c	$P_w(n_w,n_s)$ (MW) $n_w = 1$	$P_w(n_w,n_s)$ (MW) $n_w = 2$	$\beta_w(1)$ -	$\beta_w(2)$ -	Vs (pu)	P_S (MW)	Q_S (Mvar)
1	$P_w(1,7) = 10$	$P_w(2,7) = 10$	0.379	0.288	1.06	0	2.352
2	$P_w(1,7) = 10$	$P_w(2,6) = 8.04$	0.379	0.359	1.06	0	2.352
3	$P_w(1,7) = 10$	$P_w(2,5) = 7.55$	0.379	0.382	1.06	0	2.352
4	$P_w(1,7) = 10$	$P_w(2,4) = 7.13$	0.379	0.405	1.06	0	2.352
5	$P_w(1,7) = 10$	$P_w(2,3) = 6.67$	0.379	0.432	1.06	0	2.352
6	$P_w(1,7) = 10$	$P_w(2,2) = 6.07$	0.379	0.475	1.06	0	2.352
7	$P_w(1,7) = 10$	$P_w(2,1) = 0$	0.668	1	1.06	0	2.38
8	$P_w(1,6) = 4.79$	$P_w(2,7) = 10$	0.791	0.288	1.06	0	2.352
9	$P_w(1,6) = 4.79$	$P_w(2,6) = 8.04$	0.791	0.359	1.06	0	2.352
10	$P_w(1,6) = 4.79$	$P_w(2,5) = 7.55$	0.791	0.382	1.06	0	2.352
11	$P_w(1,6) = 4.79$	$P_w(2,4) = 7.13$	0.791	0.405	1.06	0	2.352
12	$P_w(1,6) = 4.79$	$P_w(2,3) = 6.67$	0.791	0.433	1.06	0	2.352
13	$P_w(1,6) = 4.79$	$P_w(2,2) = 6.07$	0.791	0.475	1.06	0	2.352
14	$P_w(1,6) = 4.79$	$P_w(2,1) = 0$	1.000	1	1.06	1.896	2.391
15	$P_w(1,5) = 4.22$	$P_w(2,7) = 10$	0.898	0.288	1.06	0	2.352
16	$P_w(1,5) = 4.22$	$P_w(2,6) = 8.04$	0.898	0.359	1.06	0	2.352
17	$P_w(1,5) = 4.22$	$P_w(2,5) = 7.55$	0.898	0.382	1.06	0	2.352
18	$P_w(1,5) = 4.22$	$P_w(2,4) = 7.13$	0.898	0.405	1.06	0	2.352
19	$P_w(1,5) = 4.22$	$P_w(2,3) = 6.67$	0.898	0.433	1.06	0	2.352
20	$P_w(1,7) = 4.22$	$P_w(2,2) = 6.07$	0.898	0.475	1.06	0	2.352
21	$P_w(1,5) = 4.22$	$P_w(2,1) = 0$	1	1	1.06	2.471	2.398
22	$P_w(1,4) = 3.77$	$P_w(2,7) = 10$	1	0.29	1.06	0	2.352
23	$P_w(1,4) = 3.77$	$P_w(2,6) = 8.04$	1	0.361	1.06	0	2.352
24	$P_w(1,4) = 3.77$	$P_w(2,5) = 7.55$	1	0.384	1.06	0	2.352
25	$P_w(1,4) = 3.77$	$P_w(2,4) = 7.13$	1	0.407	1.06	0	2.352
26	$P_w(1,4) = 3.77$	$P_w(2,3) = 6.67$	1	0.435	1.06	0	2.352
27	$P_w(1,4) = 3.77$	$P_w(2,2) = 6.07$	1	0.478	1.06	0	2.352
28	$P_w(1,4) = 3.77$	$P_w(2,1) = 0$	1	1	1.07	2.921	2.401
29	$P_w(1,3) = 3.33$	$P_w(2,7) = 10$	1	0.334	1.06	0	2.353
30	$P_w(1,3) = 3.33$	$P_w(2,6) = 8.04$	1	0.416	1.06	0	2.353
31	$P_w(1,3) = 3.33$	$P_w(2,5) = 7.55$	1	0.443	1.06	0	2.353
32	$P_w(1,3) = 3.33$	$P_w(2,4) = 7.13$	1	0.469	1.06	0	2.353
33	$P_w(1,3) = 3.33$	$P_w(2,3) = 6.67$	1	0.501	1.06	0	2.353
34	$P_w(1,3) = 3.33$	$P_w(2,2) = 6.07$	1	0.551	1.06	0	2.353
35	$P_w(1,3) = 3.33$	$P_w(2,1) = 0$	1	1	1.07	3.364	2.409
36	$P_w(1,2) = 2.81$	$P_w(2,7) = 10$	1	0.386	1.06	0	2.355
37	$P_w(1,2) = 2.81$	$P_w(2,6) = 8.04$	1	0.480	1.06	0	2.355
38	$P_w(1,2) = 2.81$	$P_w(2,5) = 7.55$	1	0.512	1.06	0	2.355
39	$P_w(1,2) = 2.81$	$P_w(2,4) = 7.13$	1	0.542	1.06	0	2.355
40	$P_w(1,2) = 2.81$	$P_w(2,3) = 6.67$	1	0.579	1.06	0	2.355
41	$P_w(1,2) = 2.81$	$P_w(2,2) = 6.07$	1	0.636	1.06	0	2.355
42	$P_w(1,2) = 2.81$	$P_w(2,1) = 0$	1	1	1.07	3.888	2.419
43	$P_w(1,1) = 0$	$P_w(2,7) = 10$	1	0.669	1.06	0	2.4
44	$P_w(1,1) = 0$	$P_w(2,6) = 8.04$	1	0.832	1.06	0	2.4
45	$P_w(1,1) = 0$	$P_w(2,5) = 7.55$	1	0.886	1.06	0	2.4
46	$P_w(1,1) = 0$	$P_w(2,4) = 7.13$	1	0.938	1.06	0	2.4
47	$P_w(1,1) = 0$	$P_w(2,3) = 6.67$	1	1	1.06	0.02	2.399
48	$P_w(1,1) = 0$	$P_w(2,2) = 6.07$	1	1	1.06	0.615	2.387
49	$P_w(1,1) = 0$	$P_w(2,1) = 0$	1	1	1.07	6.731	2.504

Table 2.4. Lookup table for the first prediction horizon (with $P_{w.M}(1) = 3.8$ MW, $P_{w.M}(2) = 7.05$ MW) for Case 3.

Scenario Combination			**Optimal Results**				
n_c	$P_w(n_w,n_s)$ (MW) $n_w = 1$	$P_w(n_w,n_s)$ (MW) $n_w = 2$	$\beta_w(1)$ -	$\beta_w(2)$ -	Vs (pu)	P_S (MW)	Q_S (Mvar)
1	$P_w(1,7) = 10$	$P_w(2,7) = 10$	1	1	1	−13.034	3.091
2	$P_w(1,7) = 10$	$P_w(2,6) = 8.04$	1	1	1	−11.167	2.863
3	$P_w(1,7) = 10$	$P_w(2,5) = 7.55$	1	1	1	−10.697	2.813
4	$P_w(1,7) = 10$	$P_w(2,4) = 7.13$	1	1	1	−10.293	2.773
5	$P_w(1,7) = 10$	$P_w(2,3) = 6.67$	1	1	1	−9.85	2.731
6	$P_w(1,7) = 10$	$P_w(2,2) = 6.07$	1	1	1	−9.27	2.681
7	$P_w(1,7) = 10$	$P_w(2,1) = 0$	1	1	1	−3.301	2.439
8	$P_w(1,6) = 4.79$	$P_w(2,7) = 10$	1	1	1	−7.96	2.755
9	$P_w(1,6) = 4.79$	$P_w(2,6) = 8.04$	1	1	1	−6.069	2.586
10	$P_w(1,6) = 4.79$	$P_w(2,5) = 7.55$	1	1	1	−5.593	2.551
11	$P_w(1,6) = 4.79$	$P_w(2,4) = 7.13$	1	1	1	−5.184	2.524
12	$P_w(1,6) = 4.79$	$P_w(2,3) = 6.67$	1	1	1	−4.736	2.497
13	$P_w(1,6) = 4.79$	$P_w(2,2) = 6.07$	1	1	1	−4.148	2.465
14	$P_w(1,6) = 4.79$	$P_w(2,1) = 0$	1	1	1	1.9	2.419
15	$P_w(1,5) = 4.22$	$P_w(2,7) = 10$	1	1	1	−7.399	2.728
16	$P_w(1,5) = 4.22$	$P_w(2,6) = 8.04$	1	1	1	−5.505	2.566
17	$P_w(1,5) = 4.22$	$P_w(2,5) = 7.55$	1	1	1	−5.029	2.533
18	$P_w(1,5) = 4.22$	$P_w(2,4) = 7.13$	1	1	1	−4.619	2.507
19	$P_w(1,5) = 4.22$	$P_w(2,3) = 6.67$	1	1	1	−4.17	2.481
20	$P_w(1,7) = 4.22$	$P_w(2,2) = 6.07$	1	1	1	−3.582	2.452
21	$P_w(1,5) = 4.22$	$P_w(2,1) = 0$	1	1	1	2.476	2.427
22	$P_w(1,4) = 3.77$	$P_w(2,7) = 10$	1	1	1	−6.959	2.708
23	$P_w(1,4) = 3.77$	$P_w(2,6) = 8.04$	1	1	1	−5.063	2.551
24	$P_w(1,4) = 3.77$	$P_w(2,5) = 7.55$	1	1	1	−4.586	2.519
25	$P_w(1,4) = 3.77$	$P_w(2,4) = 7.13$	1	1	1	−4.176	2.495
26	$P_w(1,4) = 3.77$	$P_w(2,3) = 6.67$	1	1	1	−3.726	2.47
27	$P_w(1,4) = 3.77$	$P_w(2,2) = 6.07$	1	1	1	−3.138	2.442
28	$P_w(1,4) = 3.77$	$P_w(2,1) = 0$	1	1	1	2.927	2.435
29	$P_w(1,3) = 3.33$	$P_w(2,7) = 10$	1	1	1	−6.527	2.69
30	$P_w(1,3) = 3.33$	$P_w(2,6) = 8.04$	1	1	1	−4.629	2.538
31	$P_w(1,3) = 3.33$	$P_w(2,5) = 7.55$	1	1	1	−4.151	2.508
32	$P_w(1,3) = 3.33$	$P_w(2,4) = 7.13$	1	1	1	−3.741	2.484
33	$P_w(1,3) = 3.33$	$P_w(2,3) = 6.67$	1	1	1	−3.29	2.461
34	$P_w(1,3) = 3.33$	$P_w(2,2) = 6.07$	1	1	1	−2.701	2.434
35	$P_w(1,3) = 3.33$	$P_w(2,1) = 0$	1	1	1	3.37	2.444
36	$P_w(1,2) = 2.81$	$P_w(2,7) = 10$	1	1	1	−6.015	2.670
37	$P_w(1,2) = 2.81$	$P_w(2,6) = 8.04$	1	1	1	−4.115	2.524
38	$P_w(1,2) = 2.81$	$P_w(2,5) = 7.55$	1	1	1	−3.636	2.495
39	$P_w(1,2) = 2.81$	$P_w(2,4) = 7.13$	1	1	1	−3.225	2.473
40	$P_w(1,2) = 2.81$	$P_w(2,3) = 6.67$	1	1	1	−2.774	2.451
41	$P_w(1,2) = 2.81$	$P_w(2,2) = 6.07$	1	1	1	−2.184	2.427
42	$P_w(1,2) = 2.81$	$P_w(2,1) = 0$	1	1	1	3.895	2.457
43	$P_w(1,1) = 0$	$P_w(2,7) = 10$	1	1	1	−3.239	2.591
44	$P_w(1,1) = 0$	$P_w(2,6) = 8.04$	1	1	1	−1.325	2.478
45	$P_w(1,1) = 0$	$P_w(2,5) = 7.55$	1	1	1	−0.843	2.457
46	$P_w(1,1) = 0$	$P_w(2,4) = 7.13$	1	1	1	−0.429	2.442
47	$P_w(1,1) = 0$	$P_w(2,3) = 6.67$	1	1	1	0.025	2.428
48	$P_w(1,1) = 0$	$P_w(2,2) = 6.07$	1	1	1	0.619	2.414
49	$P_w(1,1) = 0$	$P_w(2,1) = 0$	1	1	1	6.744	2.554

Table 2.5. Lookup table for the first prediction horizon (with $P_{w.M}(1) = 3.8$ MW, $P_{w.M}(2) = 7.05$ MW) for Case 4.

Scenario Combination			**Optimal Results**				
n_c	$P_w(n_w,n_s)$ (MW) $n_w = 1$	$P_w(n_w,n_s)$ (MW) $n_w = 2$	$\beta_w(1)$ -	$\beta_w(2)$ -	Vs (pu)	P_S (MW)	Q_S (Mvar)
1	$P_w(1,7) = 10$	$P_w(2,7) = 10$	1	1	1.04	−13.057	3.022
2	$P_w(1,7) = 10$	$P_w(2,6) = 8.04$	1	1	1.05	−11.187	2.798
3	$P_w(1,7) = 10$	$P_w(2,5) = 7.55$	1	1	1.05	−10.715	2.753
4	$P_w(1,7) = 10$	$P_w(2,4) = 7.13$	1	1	1.05	−10.31	2.717
5	$P_w(1,7) = 10$	$P_w(2,3) = 6.67$	1	1	1.05	−9.866	2.679
6	$P_w(1,7) = 10$	$P_w(2,2) = 6.07$	1	1	1.05	−9.284	2.634
7	$P_w(1,7) = 10$	$P_w(2,1) = 0$	1	1	1.06	−3.306	2.409
8	$P_w(1,6) = 4.79$	$P_w(2,7) = 10$	1	1	1.05	−7.977	2.701
9	$P_w(1,6) = 4.79$	$P_w(2,6) = 8.04$	1	1	1.05	−6.079	2.547
10	$P_w(1,6) = 4.79$	$P_w(2,5) = 7.55$	1	1	1.05	−5.602	2.516
11	$P_w(1,6) = 4.79$	$P_w(2,4) = 7.13$	1	1	1.05	−5.192	2.491
12	$P_w(1,6) = 4.79$	$P_w(2,3) = 6.67$	1	1	1.05	−4.742	2.466
13	$P_w(1,6) = 4.79$	$P_w(2,2) = 6.07$	1	1	1.06	−4.155	2.432
14	$P_w(1,6) = 4.79$	$P_w(2,1) = 0$	1	1	1.06	1.896	2.391
15	$P_w(1,5) = 4.22$	$P_w(2,7) = 10$	1	1	1.05	−7.414	2.676
16	$P_w(1,5) = 4.22$	$P_w(2,6) = 8.04$	1	1	1.05	−5.515	2.529
17	$P_w(1,5) = 4.22$	$P_w(2,5) = 7.55$	1	1	1.05	−5.037	2.499
18	$P_w(1,5) = 4.22$	$P_w(2,4) = 7.13$	1	1	1.05	−4.626	2.475
19	$P_w(1,5) = 4.22$	$P_w(2,3) = 6.67$	1	1	1.05	−4.176	2.452
20	$P_w(1,7) = 4.22$	$P_w(2,2) = 6.07$	1	1	1.06	−3.588	2.42
21	$P_w(1,5) = 4.22$	$P_w(2,1) = 0$	1	1	1.06	2.471	2.398
22	$P_w(1,4) = 3.77$	$P_w(2,7) = 10$	1	1	1.05	−6.974	2.658
23	$P_w(1,4) = 3.77$	$P_w(2,6) = 8.04$	1	1	1.05	−5.072	2.515
24	$P_w(1,4) = 3.77$	$P_w(2,5) = 7.55$	1	1	1.05	−4.594	2.487
25	$P_w(1,4) = 3.77$	$P_w(2,4) = 7.13$	1	1	1.05	−4.183	2.464
26	$P_w(1,4) = 3.77$	$P_w(2,3) = 6.67$	1	1	1.06	−3.733	2.437
27	$P_w(1,4) = 3.77$	$P_w(2,2) = 6.07$	1	1	1.06	−3.143	2.412
28	$P_w(1,4) = 3.77$	$P_w(2,1) = 0$	1	1	1.07	2.921	2.401
29	$P_w(1,3) = 3.33$	$P_w(2,7) = 10$	1	1	1.05	−6.541	2.642
30	$P_w(1,3) = 3.33$	$P_w(2,6) = 8.04$	1	1	1.05	−4.637	2.504
31	$P_w(1,3) = 3.33$	$P_w(2,5) = 7.55$	1	1	1.05	−4.158	2.476
32	$P_w(1,3) = 3.33$	$P_w(2,4) = 7.13$	1	1	1.05	−3.747	2.455
33	$P_w(1,3) = 3.33$	$P_w(2,3) = 6.67$	1	1	1.06	−3.297	2.428
34	$P_w(1,3) = 3.33$	$P_w(2,2) = 6.07$	1	1	1.06	−2.706	2.405
35	$P_w(1,3) = 3.33$	$P_w(2,1) = 0$	1	1	1.07	3.364	2.409
36	$P_w(1,2) = 2.81$	$P_w(2,7) = 10$	1	1	1.05	−6.028	2.624
37	$P_w(1,2) = 2.81$	$P_w(2,6) = 8.04$	1	1	1.05	−4.122	2.491
38	$P_w(1,2) = 2.81$	$P_w(2,5) = 7.55$	1	1	1.05	−3.643	2.465
39	$P_w(1,2) = 2.81$	$P_w(2,4) = 7.13$	1	1	1.06	−3.232	2.439
40	$P_w(1,2) = 2.81$	$P_w(2,3) = 6.67$	1	1	1.06	−2.78	2.42
41	$P_w(1,2) = 2.81$	$P_w(2,2) = 6.07$	1	1	1.06	−2.189	2.398
42	$P_w(1,2) = 2.81$	$P_w(2,1) = 0$	1	1	1.07	3.888	2.419
43	$P_w(1,1) = 0$	$P_w(2,7) = 10$	1	1	1.05	−3.249	2.551
44	$P_w(1,1) = 0$	$P_w(2,6) = 8.04$	1	1	1.06	−1.332	2.443
45	$P_w(1,1) = 0$	$P_w(2,5) = 7.55$	1	1	1.06	−0.849	2.425
46	$P_w(1,1) = 0$	$P_w(2,4) = 7.13$	1	1	1.06	−0.435	2.411
47	$P_w(1,1) = 0$	$P_w(2,3) = 6.67$	1	1	1.06	0.02	2.399
48	$P_w(1,1) = 0$	$P_w(2,2) = 6.07$	1	1	1.06	0.615	2.387
49	$P_w(1,1) = 0$	$P_w(2,1) = 0$	1	1	1.07	6.731	2.504

Table 2.6. Comparison of results of one day for four cases.

Case	P_{loss} Average (kW)	$\sum_1^{4320} f_1$ ($/day)	$\sum_1^{4320} f_2$ ($/day)	$\sum_1^{4320} f_3$ ($/day)	$\sum_1^{4320} f_4$ ($/day)	$\sum_1^{4320} f$ ($/day)
1	29.61	7654.76	35.54	1540.61	773.73	5304.88
2	26	7651.96	31.2	1539.07	766.30	5315.39
3	97.94	14007.64	117.52	−4730.28	821.61	17798.78
4	88.95	14007.63	106.74	−4741.06	811.02	17830.94

As mentioned earlier, the optimization results from the proposed approach ensure feasible operations. To illustrate this, we compare our results with those by the operation strategies based on the forecasted wind power. In the latter approach, the forecasted wind power is used for the optimization and the results are directly applied to the grid. Since no correction of the solutions is made based on the realized wind power, we call it the forecasted approach. The results of the feasibility obtained by the new approach and by the forecasted approach are compared in subplots (g) of Figures 2.8–2.11. In Case (1), as shown in Figure 2.8(g), using the results of the forecasted approach leads to 2066 infeasible sampling intervals. This takes place because the actual wind power is higher than the forecasted value at these sampling intervals, and thus, the forecasted curtailment factors cannot satisfy the active power balance (Equation 2.15).

In Figure 2.9(g), there are 2110 infeasible sampling intervals for Case (2), most of which are violating the active power balance (Equation 2.15) and the others are violating the other inequality constraints, in particular the voltage bounds at bus 2. This happens when the realized wind power is higher than the forecasted value, and meanwhile, the forecasted active power at the slack bus is greater than zero. Thus, in the reality, the active power from the slack bus is decreased and the voltage drop in the cables between the slack bus and bus 2 is reduced. Since the voltage at the slack bus is fixed, the voltage at bus 2 has to be increased which leads to violating its upper bound. This situation also occurs in Case (4) in the sampling intervals during which the forecasted active power at the slack bus is greater than zero.

Moreover, in Case (4), during the time in which the forecasted active power at the slack bus is negative, if the total actual wind power is higher than the forecasted value, the exported power to the HV network will be increased (i.e., $P_S(m)$ is increased in the reverse direction). Again, the voltage drop in the feeders between the slack bus and bus 2 is increased which leads to violating the upper bound of the voltage at this bus. In Case (4), totally 625 infeasible sampling intervals are observed, among which none of them is due to the power balance since the surplus power can be exported to the HV network. In Case (3), as shown in Figure 2.10(g), the control strategies by the forecasted approach are also feasible, since the slack bus

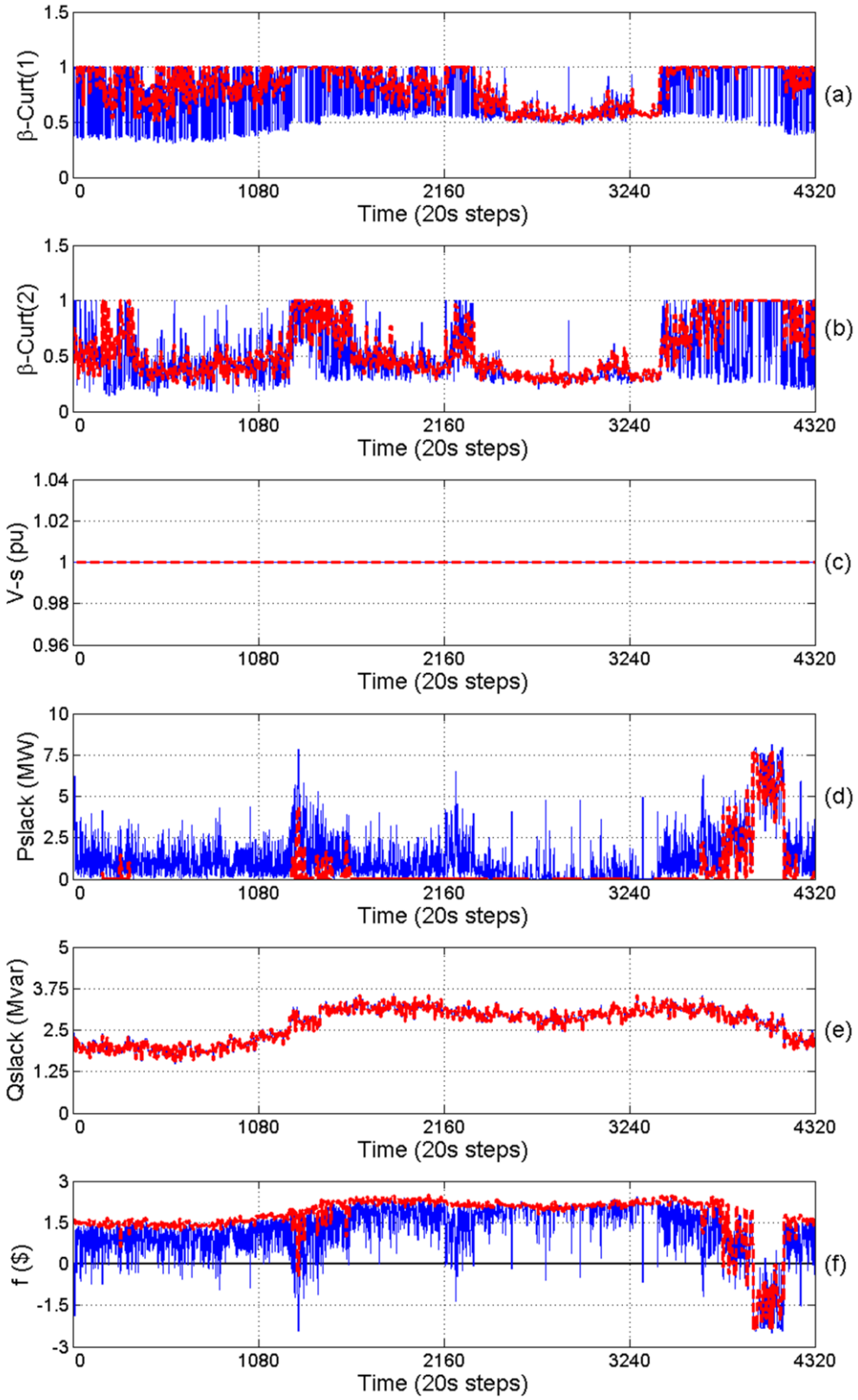

Figure 2.8. Trajectories of one day for Case 1 (red-dashed denotes forecasted and blue-solid denotes actual values). (a)(b) Curtailment factors for the first and second WF, respectively; (c) Slack bus voltage; (d) Slack bus active power; (e) Slack bus reactive power; (f) Total objective function value.

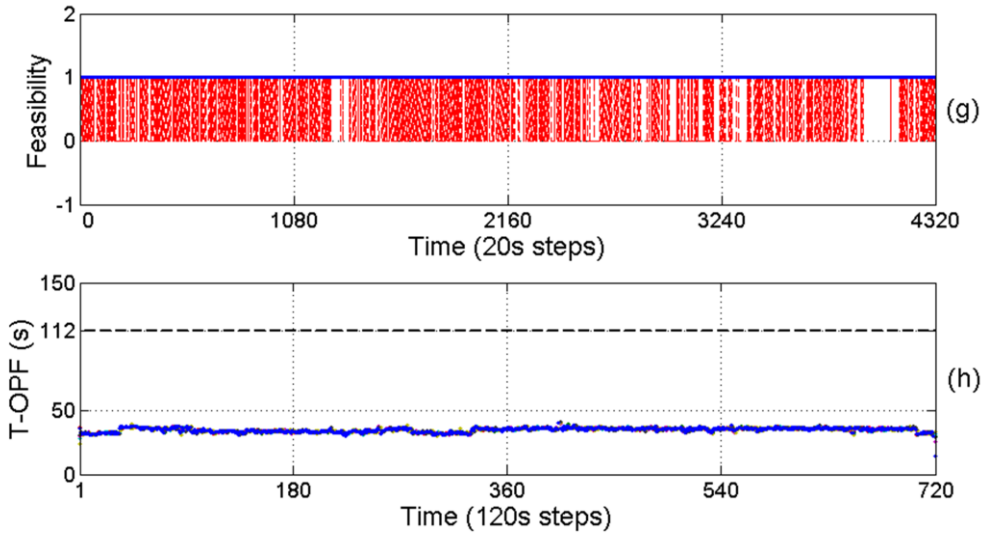

Figure 2.8 (Continued). Trajectories of one day for Case 1. (g) Feasibility status of the deterministic (red-dashed) and prediction-realization (blue-solid) approaches. Here, 1 denotes feasible and 0 denotes infeasible solution; and (h) computational time of the seven processors.

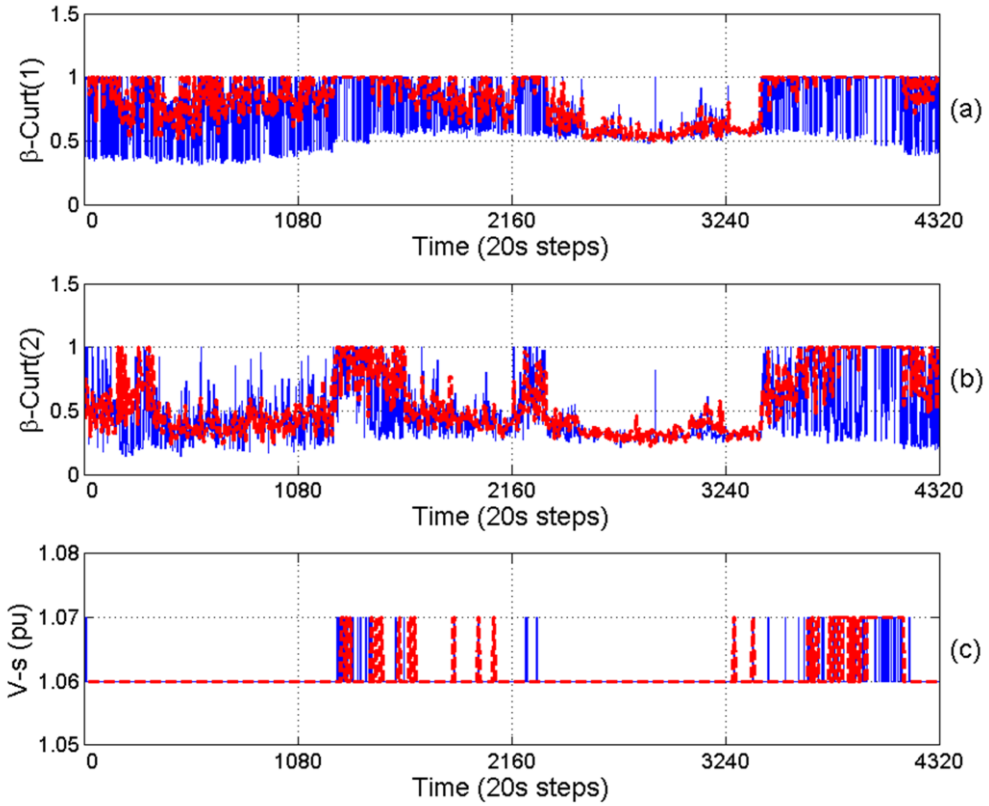

Figure 2.9. Trajectories of one day for Case 2. (a) Forecasted (red-dashed) and actual (blue-solid) curtailment factors for first WF; (b) Forecasted (red-dashed) and actual (blue-solid) curtailment factors for second WF; (c) Forecasted (red-dashed) and actual (blue-solid) values of voltage at the slack bus.

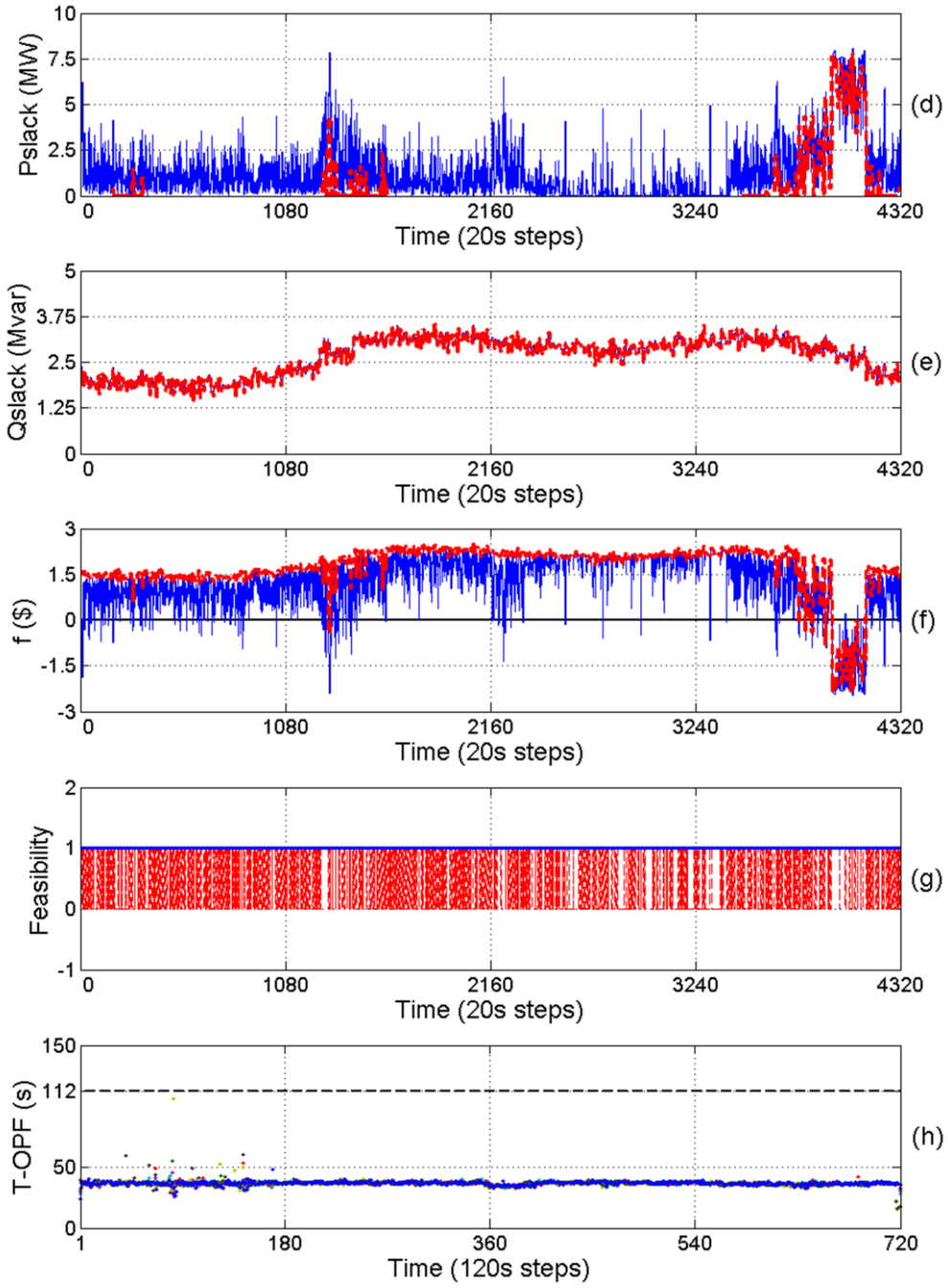

Figure 2.9 (Continued). Trajectories of one day for Case 2. (**d**) Forecasted (red-dashed) and actual (blue-solid) slack bus active power; (**e**) Forecasted (red-dashed) and actual (blue-solid) slack bus reactive power; (**f**) Forecasted (red-dashed) and actual (blue-solid) total objective function value; (**g**) Feasibility status of the deterministic (red-dashed) and prediction-realization (blue-solid) approaches when applying actual wind power. Here, 1 denotes feasible and 0 denotes infeasible solution; (**h**) computational time of the seven processors.

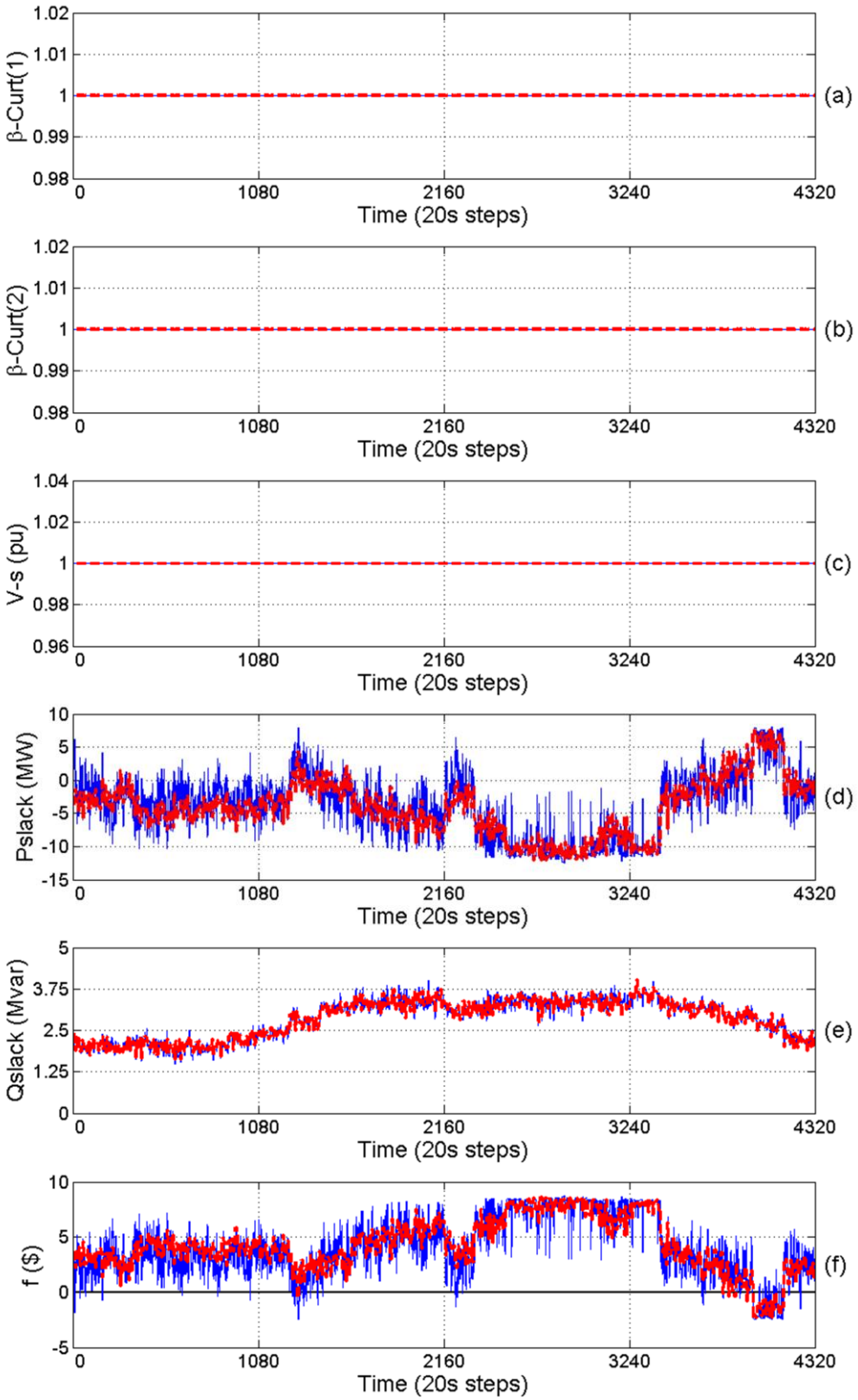

Figure 2.10. Trajectories of one day for Case 3 (red-dashed denotes forecasted and blue-solid denotes actual values). (a)(b) Curtailment factors for the first and second WFs, respectively; (c) Slack bus voltage; (d) Slack bus active power; (e) Slack bus reactive power; (f) Total objective function value.

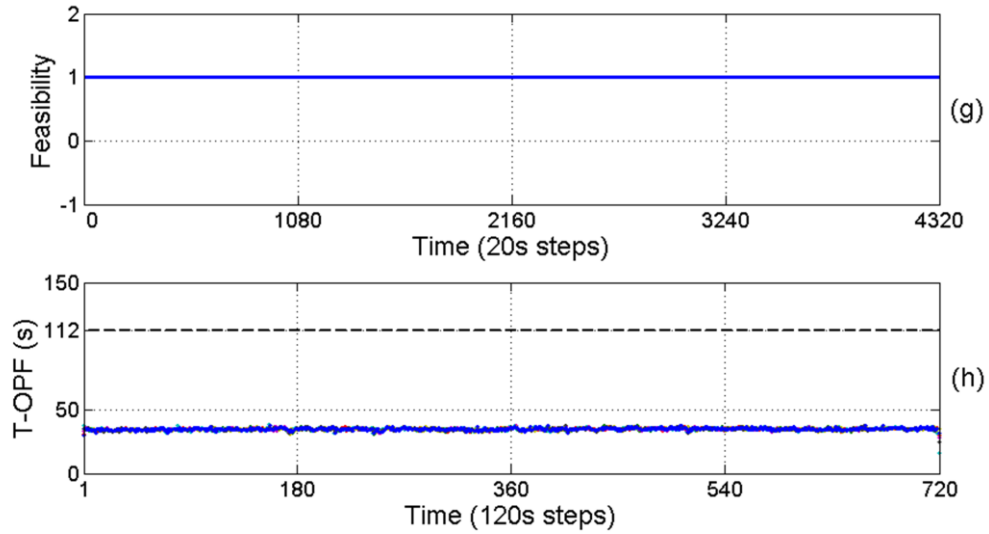

Figure 2.10 (Continued). Trajectories of one day for Case 3. (**g**) Feasibility status of the deterministic (red-dashed) and prediction-realization (blue-solid) approaches when applying actual wind power. Here, 1 denotes feasible and 0 denotes infeasible solution; (**h**) computational time of the seven processors.

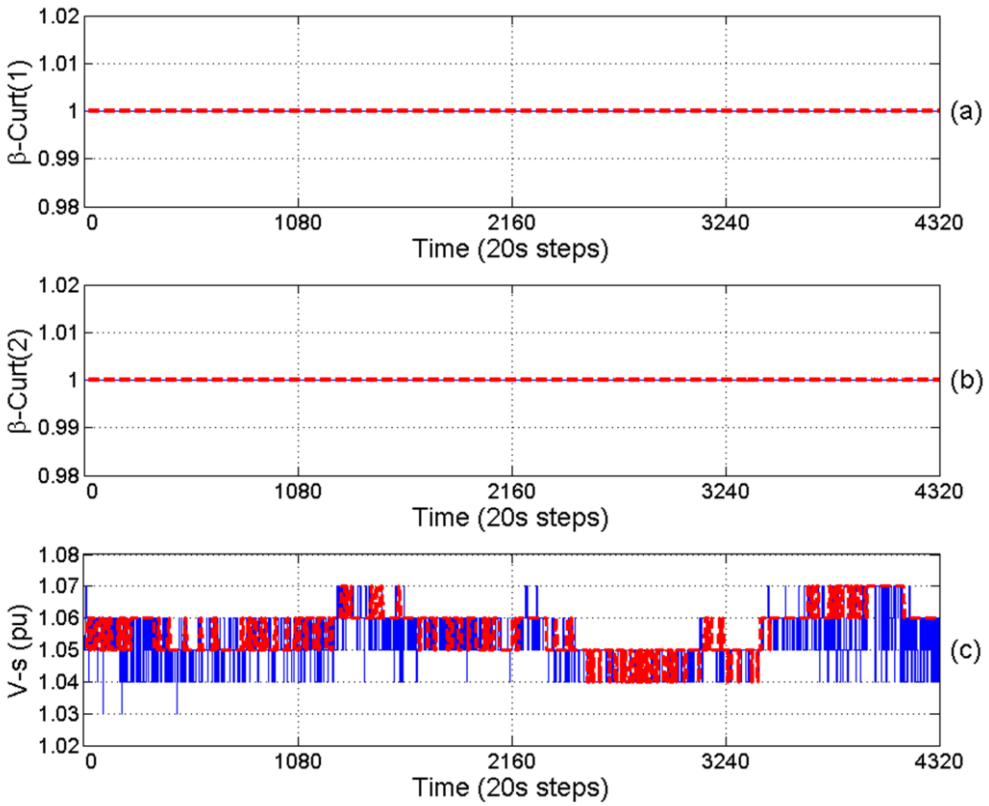

Figure 2.11. Trajectories of one day for Case 4. (**a**) Forecasted (red-dashed) and actual (blue-solid) curtailment factors for first WF; (**b**) Forecasted (red-dashed) and actual (blue-solid) curtailment factors for second WF; (**c**) Forecasted (red-dashed) and actual (blue-solid) values of voltage at the slack bus.

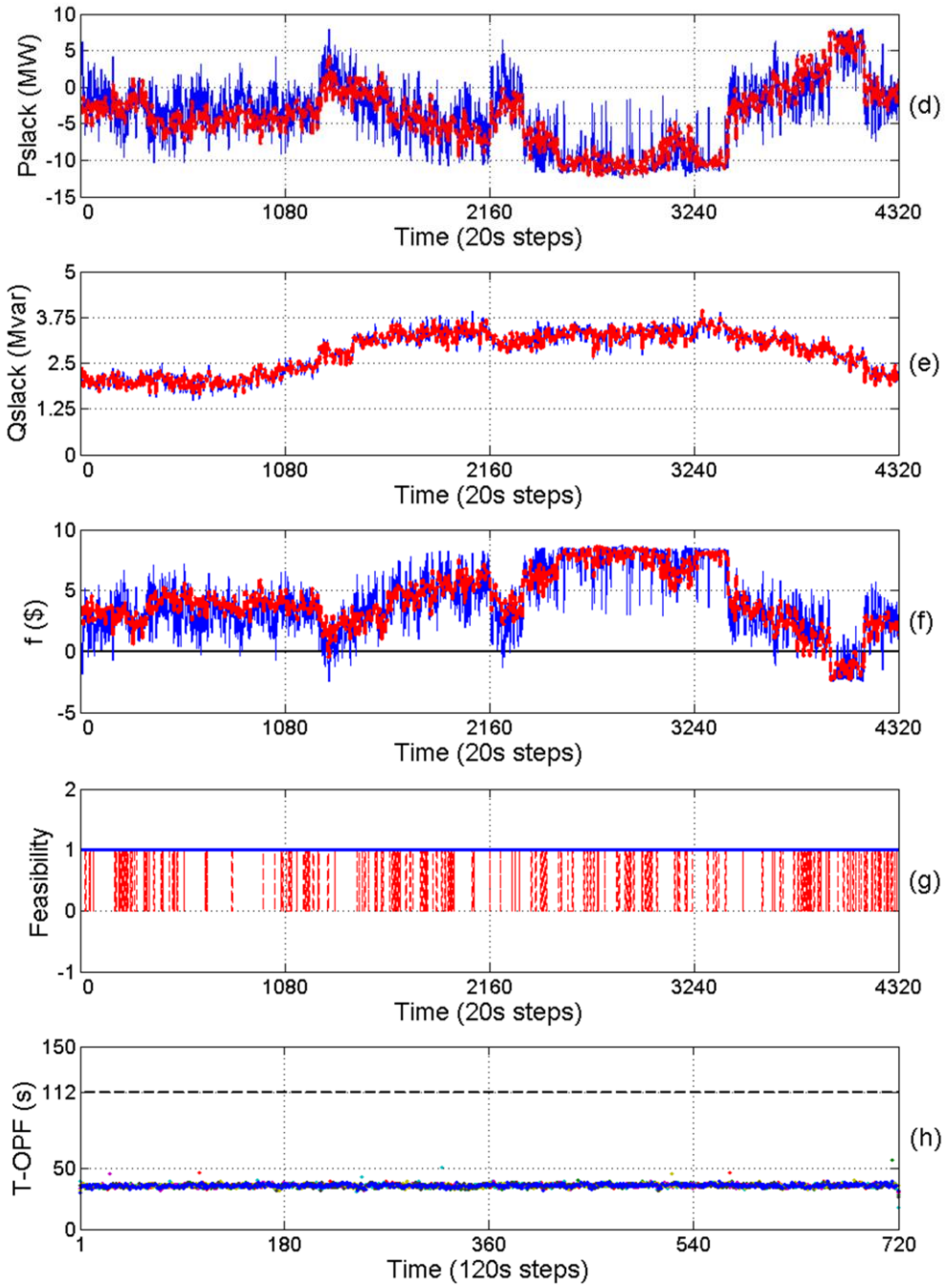

Figure 2.11 (Continued). Trajectories of one day for Case 4 (red-dashed denotes forecasted and blue-solid denotes actual values). (**d**) Slack bus active power; (**e**) Slack bus reactive power; (**f**) Total objective function value; (**g**) Feasibility status of the deterministic (red-dashed) and prediction-realization (blue-solid) approaches. Here, 1 denotes feasible and 0 denotes infeasible solution; (**h**) computational time of the seven processors.

voltage is fixed in the middle position (i.e., 1 pu) and the surplus wind power can be exported to the HV network.

The feasibility of the control strategies by the proposed prediction-realization approach for all the four cases are shown with the blue line in subplots (g) of Figures 2.8–2.11. It can

be seen that there is no infeasible operations at all, i.e., the proposed approach can ensure the operation feasibility in any case of the wind power generation.

Subplots (h) of Figures 2.8–2.11 give the computation time taken by the seven processors to solve the MINLP OPF problems for 49 scenario combinations in real-time. It can be seen that the computation time of each processor is less than the reserved time ($T_{OPF} = 112$ s) which ensures the applicability of the RT-OPF.

Table 2.6 compares the results in the scope of profitability of one-day operation in the four cases. It is shown that, in Cases (2) and (4), the total yield (i.e., the objective function value) will be increased in comparison to Cases (1) and (3), if the slack bus voltage is considered as a variable and optimized, since, in this way, the active power losses are decreased. In contrary, when the reverse power flow is allowed (i.e., Cases (3) and (4)), the active power losses increase dramatically owing to higher power flow in the network. However, the effect of allowable reverse power flow is much more significant as the total yield is increased by more than three times, due to the export of the surplus wind power to the upstream HV network.

2.5 Conclusions

RT-OPF is indispensable for network operations under intermittent wind power, but its numerical implementation poses a significant challenge. In this chapter, a prediction-realization approach RT-OPF is introduced for energy systems to deal with fast changing wind power. In addition, our OPF simultaneously considers curtailment factors as continuous free variables, the reference voltage at the slack bus as discrete free variables, and possible reverse power flow to an upstream network. This leads to a large-scale MINLP OPF problem with uncertain wind power generation. To address this problem, we employ the available information of wind power, i.e., forecasted value in a long time cycle (as the prediction horizon) and measured value in a short time cycle (as the sampling time interval), and developed a two-phase solution approach. In the prediction phase, most probable wind power scenarios are generated based on the Beta distribution for the prediction horizons. The corresponding MINLP OPF problems are then solved in parallel. The results are saved as a lookup table which provides a base for selecting a decision when the actual wind power value is available from one sampling interval to the next. As a result, the proposed RT-OPF framework ensures feasible solutions for the cases with and without reverse power flow to an upstream network. The solutions can be realized in a very short sampling time. The results from a case study demonstrate the applicability of the proposed RT-OPF framework.

One important point we discussed in the chapter is the insurance of the operation feasibility. A series of wind power scenarios are generated according to the stochastic distribution of wind power and the corresponding optimization problems are solved in a predictive way. In the realization phase, when the measured wind power is different from the predefined scenarios, we choose the solution of the optimization problem with the scenario exactly higher than the measured value. The selection leads to a higher curtailment of the generated wind power, i.e., it guarantees the feasibility with a certain degree of conservativeness (with a lower yield). In fact, a reservation of some conservativeness to ensure feasibility is also commonly used in industrial practice.

3 Real-Time OPF with Reactive Power of Wind Farms

It is extremely difficult to realize real-time active-reactive optimal power flow (RT-AR-OPF) in DNs with WFs due to the conflict between the fast changes in wind power and the slow response from the optimization computation. To address this problem, a new lookup-table-based RT-AR-OPF framework is developed in this chapter. According to the forecasted wind power for a prediction horizon, scenarios are generated based on its stochastic distribution. The corresponding MINLP problems are solved online which simultaneously optimize the *active* and *reactive* power dispatch of WFs, active-reactive reverse power flow, and discrete slack bus voltage, resulting in a lookup table. Based on the actual wind power available in a sampling time, one of the solutions will be selected and realized to the DN. A new reconciliation algorithm is proposed to ensure both the feasibility and optimality of the realized operation strategy. The applicability of the proposed framework is shown using a medium-voltage DN.

3.1 RT-AR-OPF Framework

The aim of our RT-AR-OPF framework is to find optimal and feasible operation strategies which are autonomously updated according to the rapid changes of wind power penetration. For this purpose, a lookup-table-based framework is developed in this chapter, as shown in Figure 3.1, where the execution steps are shown by numbers. The parts with dashed lines in Figure 3.1 mean that the data is updated in each *prediction horizon* T_P (e.g., 120s), while the parts in solid lines denote updating in each *sampling interval* T_S (e.g., 20s). This means that the prediction horizon T_P is divided into several sampling intervals T_S.

The proposed RT-AR-OPF framework consists of the following 12 steps:

1) Provide input data (i.e., forecasted wind power, demand and price values) in advance of each prediction horizon.
2) Generate N_s wind power scenarios for each WF to describe uncertain wind power. The scenarios for each WF are generated based on a continuous bounded stochastic distribution in a way that an identical probability between two neighboring

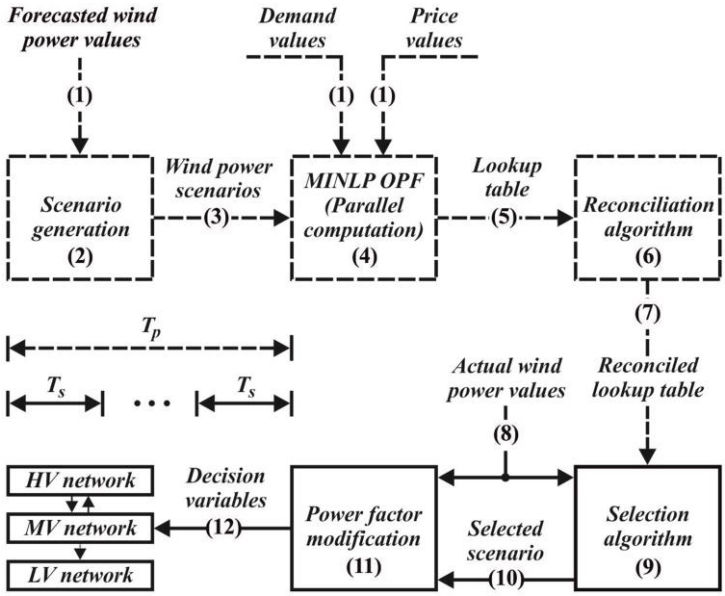

Figure 3.1. The proposed framework for RT-AR-OPF.

scenarios is ensured. For this we define $N_s - 1$ intervals for the wind power $P_w(n_w, n_s)$, $n_s = 1,...,N_s$ such that [35]:

$$\Pr\{P_w(n_w, n_s) - P_w(n_w, n_s - 1)\} = \frac{1}{N_s - 1}, \quad \text{for } n_s \geq 2 \tag{3.1}$$

where Pr is the probability operator and the scenarios are the boundaries of the intervals. To this end, N_s wind power scenarios will be generated for each individual WF. Thus, N_c wind power scenario combinations are formed for each prediction horizon [35]. For a network with N_w WFs, the total number of scenario combinations will be

$$N_c = (N_s)^{N_w} \tag{3.2}$$

3) Send the generated N_c wind power scenario combinations to the MINLP OPF.
4) Solve the N_c MINLP OPF problems corresponding to each wind power scenario combination $\mathbf{P}_w(n_c)$ (i.e., the vector of active power of WFs for scenario combination n_c) in parallel. The objective of the OPF is to minimize the costs of the imported active and reactive energies from the HV transmission network [17]. The MINLP OPF problem formulation is described in detail in Section 3.2.
5) Send the N_c solution results as a lookup table to the reconciliation algorithm.
6) Reconcile the OPF results. The reconciliation algorithm ensures the feasibility and optimality of the solutions (see Section 3.3) and updates the lookup table correspondingly.
7) Send the reconciled lookup table to the selection algorithm.

8) Send the values of actual wind power to the selection and the power factor modification algorithms.

9) Select one of the reconciled solution strategies in the lookup table for each sampling time T_S. The selection is made by comparing the actual wind power $P_{w.A}(n_w, m)$ measured in each sampling time with the generated wind power scenarios of each WF based on the following algorithm:

Algorithm 3.1. Selection algorithm

for each WF $n_w = 1,..., N_w$ and $n_s \geq 2$
If $P_w(n_w, (n_s - 1)) < P_{w.A}(n_w, m) \leq P_w(n_w, n_s)$
Then consider $P_{w.A}(n_w, m)$ as $P_w(n_w, n_s)$
end
Achieve $\mathbf{P}_w(n_c)$
Based on n_c, set $\boldsymbol{\beta}_w(m) = \boldsymbol{\beta}_w(n_c)$ and $V_S(m) = V_S(n_c)$

The algorithm selects a solution which ensures both the safety of the operation and the minimum of the objective function. This means, for each WF n_w, if $P_{w.A}(n_w, m)$ is not equal to $P_w(n_w, (n_s - 1))$, the algorithm considers it to be *the nearest higher* scenario. This is because a higher wind power associates with a lower curtailment factor, leading to a feasible operation strategy [35].

10) Send the selected scenario to the power factor modification algorithm.

11) Modify the power factors of WFs before realizing the selected solution strategies. This is necessary since the random behavior of wind power generation will result in possible discrepancy between the selected and the actual active wind power. Consequently, realizing the reactive power dispatch of the selected scenario $\mathbf{P}_w(n_c, m)$ may lead to violations of the power factor limits of WFs. For this reason, we introduce a power factor modification algorithm to adjust the reactive power dispatch before realizing to the network. The resulting operation strategy ensures satisfaction of the operation constraints (including bus voltages and apparent powers in feeders) of the DN. The power factor modification algorithm is described in more detail in Section 3.4.

12) Send the selected and modified control values to the network.

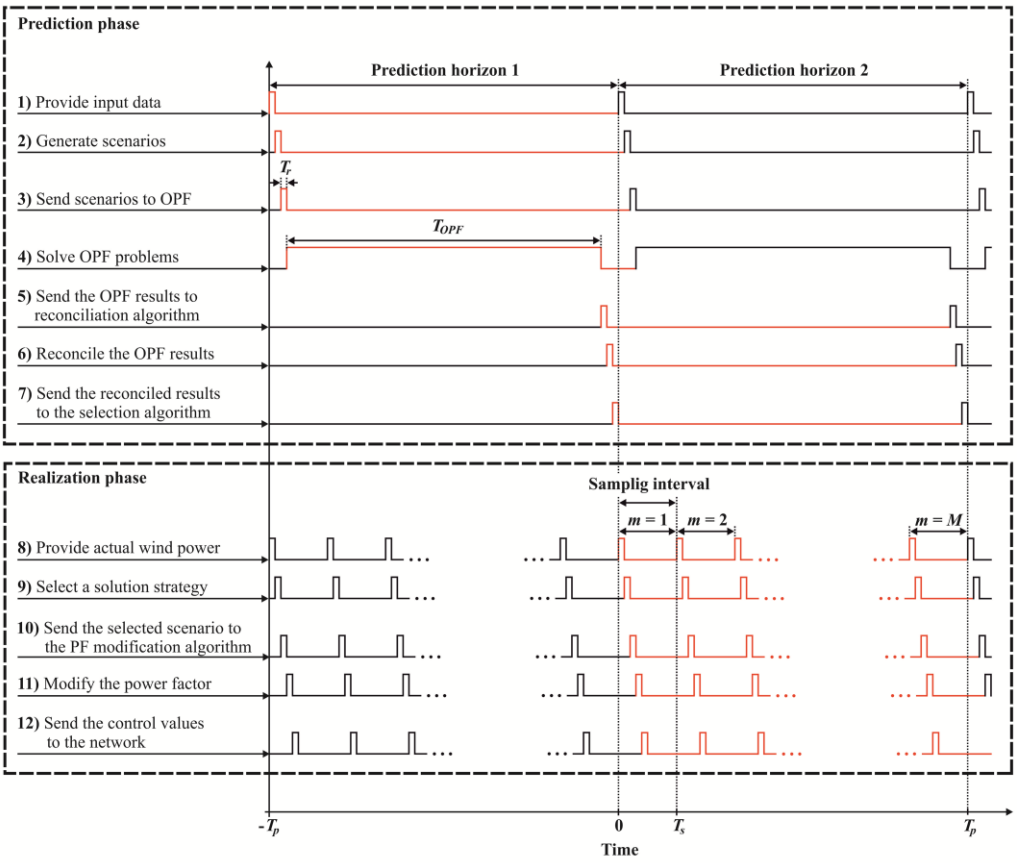

Figure 3.2. Time allocation for the tasks of the 12 steps in Figure 3.1.

For the applicability of the real-time framework, it is necessary to ensure that all 12 steps are completed inside their pre-specified time slots. The time slots and the implementation are illustrated in Figure 3.2 in which two consecutive prediction horizons are shown.

In Figure 3.2, the red lines indicate the execution of the 12 tasks along the time. T_r denotes the length of the time reserved for data management (for our case study $T_r = 2\ s$ [35]), i.e., sending the data (in steps 1, 3, 5, 7, 8, 10, and 12) and processing the data (in steps 2, 6, 9, and 11). Here, T_{OPF} denotes the reserved time to solve the N_c MINLP OPF problems. It is noted that the summation of the lengths of tasks in the prediction phase must be equal to the length of the prediction horizon:

$$T_p = 6T_r + T_{OPF}. \tag{3.3}$$

It is shown in Figure 3.2 that when the optimal strategies for the current prediction horizon are realized to the network, the solutions for the upcoming prediction horizon are prepared. The proposed framework is further described by a flowchart in Figure 3.3. The flowchart demonstrates the prediction and realization phases of the RT-AR-OPF framework.

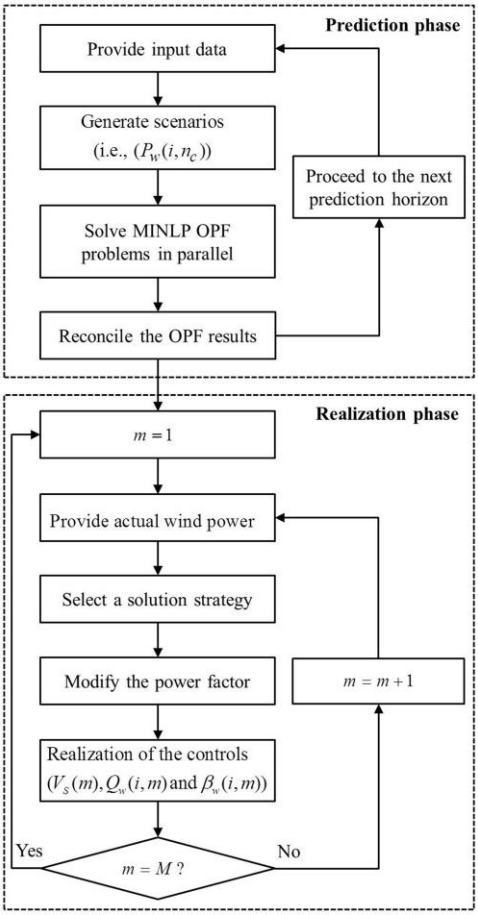

Figure 3.3. The flowchart of the proposed RT-AR-OPF framework.

3.2 AR-OPF Formulation

For each prediction horizon T_P, our real-time framework solves N_c number of uncoupled MINLP AR-OPF problems. The active and reactive power demand as well as energy prices are assumed to be fixed in each T_P and updated according to their current values. The optimization problem for each T_P is defined as follows:

$$\min_{\beta_w(i,n_c),Q_w(i,n_c),V_s(n_c)} f(n_c) = C_{PP} P_s(n_c) + C_{PQ} Q_s(n_c) \tag{3.4}$$

subject to

$$f_P(n_c) - \left(P_w(i,n_c)\beta_w(i,n_c)\right) + P_d(i) - P_s(n_c) = 0, \qquad i \in S_b \tag{3.5}$$

$$f_Q(n_c) - Q_w(i,n_c) + Q_d(i) - Q_s(n_c) = 0, \qquad i \in S_b \tag{3.6}$$

$$\sqrt{\left(P_s(n_c)\right)^2 + \left(Q_s(n_c)\right)^2} \le S_{s.\max} \tag{3.7}$$

$$\gamma_{Ps} S_{s.\max} \le P_s(n_c) \le S_{s.\max}, \qquad -1 \le \gamma_{Ps} \le 0 \tag{3.8}$$

$$\gamma_{Qs} S_{s.\max} \le Q_s(n_c) \le S_{s.\max}, \qquad -1 \le \gamma_{Qs} \le 0 \tag{3.9}$$

$$S(i, j, n_c) \le S_{l.\max}(i, j), \qquad i, j \in S_b; \quad i \ne j \tag{3.10}$$

$$V_{s.\min} \le V_s(n_c) \le V_{s.\max} \tag{3.11}$$

$$V_s(n_c) = 1 \pm \Delta V_s(n_c), \quad \Delta V_s(n_c) = \{0.01, 0.02, ..., 0.1\} \tag{3.12}$$

$$V_{lo.in}(i) \le V(i, n_c) \le V_{up.in}(i), \qquad i \in S_b; \quad i \ne 1 \tag{3.13}$$

The objective function in Equation 3.4 aims to minimize the total costs of the active and reactive energy at the slack bus for each scenario combination $\mathbf{P}_w(n_c, m)$. In practice, the active-reactive energy prices are set based on agreements between medium voltage (MV) and HV network operators [223, 224]. In this work, the energy prices are assumed to be the same when active-reactive power flows from MV to HV network (i.e., export) and from HV to MV network (i.e., import) [35, 221]. But they can be any price values defined by the user.

Equations 3.5-3.6 represent the active and reactive power balance, in which $f_P(n_c)$ and $f_Q(n_c)$ are the network active and reactive power functions [17], respectively. Here, $\beta_w \in [0,1]$ is the curtailment factor of a WF [35], which is a continuous control variable.

Equations 3.7-3.9 define active and reactive power bounds at the slack bus. The parameters γ_{Ps} and γ_{Qs} denote the permissible amount of active and reactive power export to the upstream network and Equation 3.10 represents the constraint for apparent power in the feeders. Equation 3.11-3.12 denote the constraints on slack bus voltage V_s consisting of discrete variables in the range of [0.9, 1.1] with the step length of 0.01, representing the tap positions of the OLTC. Equation 3.13 indicates the voltage limits of PQ buses. Since the voltages are particularly sensitive to the reactive power dispatch of WFs, a back-off strategy similar to [225, 226] is utilized for the OPF to ensure safe voltage levels. For this reason, a tube with an inner and an outer bound is defined as voltage constraints for PQ buses, as shown in Figure 3.4. The inner bound should be satisfied in the optimization stage, while the outer bound is to be held in the realization phase. This means the outer bounds are the real voltage constraints (i.e., $V_{\min} = V_{lo.out}$ and $V_{\max} = V_{up.out}$). In the AR-OPF problem formulation, $V_{lo.in}$ and $V_{up.in}$ are the lower and upper limits of voltage for the inner tube, respectively. These constraints, however, are allowed to be violated in the realization phase during which $V_{lo.out}$ and $V_{up.out}$ (the lower and upper limits of voltage for the outer tube) must be held.

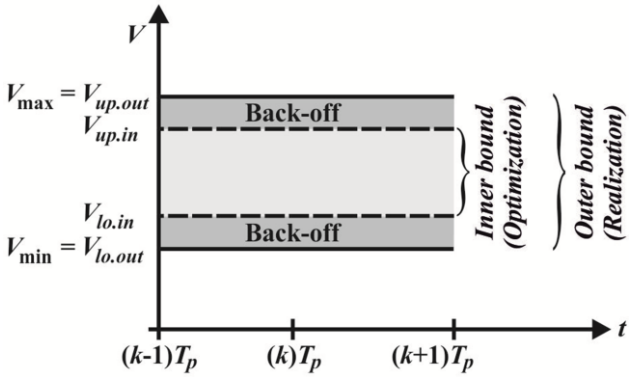

Figure 3.4. Back-off description of voltage constraints for PQ buses.

The formulation of Equations 3.4-3.13 leads to a MINLP OPF problem for each scenario combination n_c. The solutions of these problems provide a lookup table consisting of options for operation strategies for the coming prediction horizon. The operation strategies will be reconciled and then one of the options will be selected, modified, and realized to the DN for each sampling time T_S.

3.3 Reconciliation Algorithm

For the RT-AR-OPF, the online computation should provide solutions of the above formulated problems prior to the coming prediction horizon. However, there can be cases that the MINLP problem fails to converge. Therefore, we propose a reconciliation algorithm to analyze the convergence status and address this problem. The lookup table consists of optimal solutions and convergence status for N_c scenario combinations. We emphasize that the scenarios are listed from the highest to the least wind power values [35] to be utilized in our reconciliation of the un-converged cases.

As shown in Figure 3.5, the reconciliation algorithm begins to check the convergence status of the OPF problem of the first scenario combination (i.e., $n_c = 1$). If it is converged, the control values $\boldsymbol{\beta}_w(n_c)$ (i.e., the vector of curtailment factors of wind power of WFs) and $V_s(n_c)$ will be kept. If it is not converged, $\boldsymbol{\beta}_w(n_c)$ will be set to zero (i.e., the curtailment factors of the worst case scenario) and $V_s(n_c)$ to 1 pu (i.e., the middle value of the slack bus voltage). Then it goes down to the next scenario combination (i.e., $n_c \neq 1$). If the corresponding MINLP OPF is converged, the computed control values (i.e., $\boldsymbol{\beta}_w(n_c)$ and $V_s(n_c)$) will be kept without any modification.

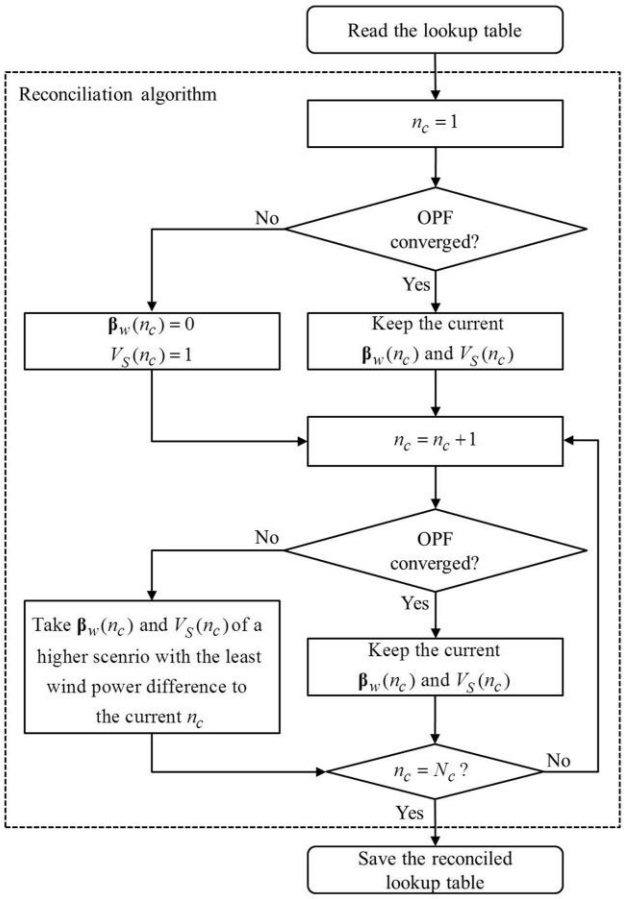

Figure 3.5. Reconciliation algorithm.

If it fails to converge, we take the MINLP solution of another scenario which ensures a feasible operation under the current wind power scenario. This means that a scenario with a higher wind power than the current scenario will be selected and, in this way, the resulting operation will have some degree of conservatism. To minimize the degree of this conservatism, the scenario with a higher value of wind power and meanwhile the least difference to the value of the current scenario should be chosen. For a DN with N_w WFs, there are N_w scenarios which have one level higher than that of the current scenario. Thus, what we need to do is to find, among these scenarios, the scenario which has the least difference to the current scenario.

To illustrate this algorithm, we assume that there are three WFs in the DN. Let us assume that the MINLP problem for the current scenario (in Table 3.1) fails to converge. Then, the three scenario options listed in the table have exactly one level higher than the current scenario. It can be seen that the minimum difference is between the current scenario and the scenario option 1. Therefore, the MINLP solution corresponding to this scenario combination (option 1) will be chosen for the current solution.

Table 3.1. Illustrative example to the reconciliation algorithm. Here, the values are in per unit.

Current scenario	$P_w(n_w, n_s)$ $P_w(1,2) = 0.09$	$P_w(n_w, n_s)$ $P_w(2,2) = 0.44$	$P_w(n_w, n_s)$ $P_w(3,2) = 0.81$
Option 1	$P_w(1,3) = 0.13$	$P_w(2,2) = 0.44$	$P_w(3,2) = 0.81$
Option 2	$P_w(1,2) = 0.09$	$P_w(2,3) = 0.51$	$P_w(3,2) = 0.81$
Option 3	$P_w(1,2) = 0.09$	$P_w(2,2) = 0.44$	$P_w(3,3) = 0.86$

3.4 Realization Phase

In the prediction phase, a lookup table consisting of the optional operation strategies is generated and reconciled for each prediction horizon T_P (e.g., 120 s). The generation of the scenarios is based on the forecasted values of wind power and a stochastic distribution as described in Chapter 2. In the realization phase, one of the operation strategies in the reconciled lookup table is selected in real-time by the selection algorithm [35] for each sampling interval T_S (e.g., 20 s). The selection algorithm compares the scenarios in the lookup table with the actual wind power measured in each sampling time interval T_S. Accordingly, the algorithm selects a scenario combination with the solution which ensures both the safety of the operation and the minimum of the objective function. This means, in the realization phase, no OPF problem is solved and only selection and modification are carried out. This is accomplished in short time intervals (as shown in Figure 3.2) making the framework applicable for real-time operation.

Due to the possible discrepancy between the selected and the actual *active* wind power, realizing the *reactive* power dispatch of the corresponding scenario may lead to violations of the power factor limits of WFs. Therefore, the operation strategies should be modified prior to the realization. For this purpose, we introduce a power factor modification algorithm which is suitable for WFs with different operation modes as illustrated in Figure 3.6. A WF can operate in three different modes: unity power factor (Mode (a)), fixed non-unity power factor (Mode (b)), and flexible power factor(Mode (c)). In Mode (a), the WF does not supply and/or absorb any reactive power, i.e., $\cos(\varphi_{\min}) = \cos(\varphi_{\max}) = 1$. In Mode (b), the WF supplies reactive power with a fixed non-unity power factor, i.e., $\cos(\varphi_{\min}) = \cos(\varphi_{\max}) \neq 1$. In Mode (c), the WF can supply reactive power to the network by a power factor in a given range, i.e., $\cos(\varphi_{\min}) \neq \cos(\varphi_{\max})$.

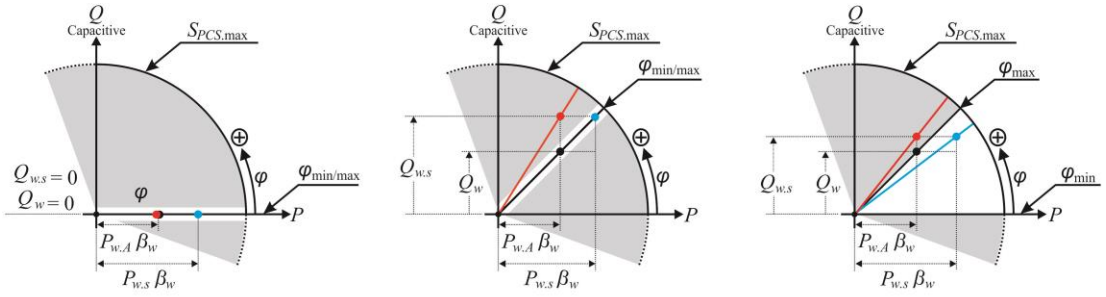

Figure 3.6. Active and reactive power capability diagram of WFs for three different operation modes: (a) unity, (b) fixed non-unity, and (c) flexible power factor. Here, white and gray colors denote feasible and infeasible operation regions, respectively.

For instance in Mode (c) in Figure 3.6, the blue point denotes the operating point of a selected scenario. This point corresponds to the selected active power to be injected to the DN (i.e., $P_{w.s}\beta_w$) and the selected reactive power dispatch (i.e., $Q_{w.s}$). If the actual active wind power $P_{w.A}$ is different from the selected wind power scenario $P_{w.s}$, realizing $Q_{w.s}$ can lead to violation of the power factor limit. The operating point in this case is shown by the red point. Therefore, $Q_{w.s}$ should be modified to Q_w in order to satisfy the power factor limit. This modification is carried out by Algorithm 3.2.

Algorithm 3.2. Power factor modification algorithm

For each wind farm n_w

If $\arctan\left(\frac{Q_{w.s}}{P_{w.A}\beta_w}\right) \le \varphi_{\max}$

then consider Q_w as $Q_{w.s}$

End

and if $\arctan\left(\frac{Q_{w.s}}{P_{w.A}\beta_w}\right) > \varphi_{\max}$

then consider Q_w as $\left(P_{w.A}\beta_w \tan(\varphi_{\max})\right)$

End

After realization of Q_w and $P_w\beta_w$, the new operating point will be the black point which satisfies the power factor limits. Since $Q_w \le Q_{w.s}$, applying Q_w to the DN can lead to decrease in the voltage amplitude at the nodes connecting WFs and/or nearby buses. Therefore, a tube with inner and outer bounds is defined as voltage constraints for PQ buses in the RT-AR-OPF. The inner bounds are the ones used in the optimization problem formulation (see Section 3.2) which have some degree of conservatism while the outer bounds are the real voltage constraints (i.e., $V_{\min} = V_{lo.out}$ and $V_{\max} = V_{up.out}$).

It is noted that the reference values of the slack bus voltage are not incorporated in the power factor modification algorithm. To this end, the control variables (i.e., the discrete slack bus voltage, curtailment factor of active wind power, and reactive power dispatch) have been computed. The realization of the control variables is carried out at each sampling interval. Consequently, our RT-AR-OPF framework provides online operation strategies which ensure both feasibility and optimality.

3.5 Case Study

Here, a 41-bus medium-voltage DN [17, 97, 213, 227] is taken as a case study to demonstrate the effectiveness of the proposed RT-AR-OPF framework. The DN is shown in Figure 3.7. There are two WFs each with rated power of 10 MVA. Based on Equations 3.1-3.2, N_s wind power scenarios for each WF are formed for each prediction horizon leading to N_c wind power scenario combinations. This results in N_c MINLP AR-OPF problems to be solved in each prediction horizon. The length of the prediction horizon T_P and sampling interval T_S are considered to be 120 and 20 s, respectively [35]. Parallel computing is utilized in our work to speed up the computation to be accomplished within the reserved time for computing the OPF problems (i.e., T_{OPF} in Figure 3.2). Therefore, the number of wind power scenarios for each WF should be related to the computer speed, number of processors, number of WFs , and the reserved time for the computation (i.e., T_{OPF}). Here, we use seven processors on a server with two Intel Xeon X5690, CPU 3.47 GHz (6 cores, 12 threads) and 64 GB RAM. Therefore, seven scenarios for each WF [28, 35, 207] are generated based on the Beta probability distribution function [35, 149-151] which leads to 49 scenario combinations. Each processor takes seven scenarios ensuring the equal number of scenarios for each processor. It is noted that based on Equation 3.1, the only limitation for the number of scenarios is that it should be greater than or equal to 2. This is because the scenarios must cover the whole range of [0,1] pu (i.e., from zero to the rated power). In this way, the RT-AR-OPF can deal with any actual values of wind power generation. Theoretically, a higher number of scenarios will lead to a more accurate description to reflect the random property of uncertain wind power. But the computation burden will also be higher. Therefore, a compromise between the description accuracy and the computation demand needs to be made.

Population-based stochastic optimization algorithms (e.g., GA [79, 80] and particle swarm optimization (PSO) [228]) have been widely used to solve MINLP problems in power systems [10, 51, 130, 229, 230]. Such methods can provide satisfactory solutions in a

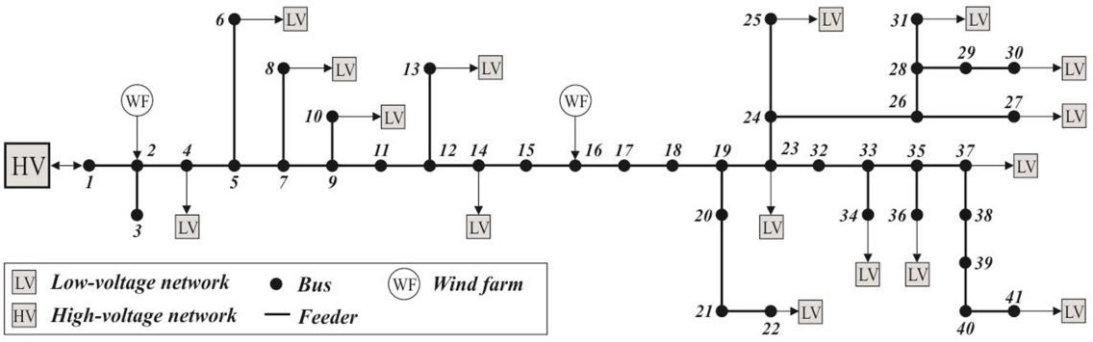

Figure 3.7. DN for the case study.

reasonable time when the algorithm-specific parameters are tuned properly [231]. For each prediction horizon, several number of MINLP AR-OPF problems should be solved within a reserved time T_{OPF}. Since GA is not so fast [232], it could not be suitable for our 'real-time' AR-OPF optimization as it may exceed this time limit. In comparison, PSO is faster but not so successful in finding close to optimal solutions [233, 234]. In our RT-AR-OPF framework, the problem is coded in GAMS [214] and solved by the MINLP solver BONMIN [215]. The algorithms in BONMIN are exact and ensures global optimal when both the objective function and constraints are convex, otherwise they are heuristics [215, 235] which is the case in the OPF problem. Since BONMIN uses branch-and-bound based algorithms which utilize NLPs for bounding, it often finds good solutions (but not necessarily global) also for non-convex problems [235]. This is in contrast with pure outer approximation based algorithms which may easily run into infeasible LP or mixed-integer programming (MIP) relaxations due to wrong cutting-planes [235].

The length of the prediction horizon T_P and sampling interval T_S are considered to be 120 and 20 s, respectively. The active and reactive energy prices are assumed to be 1.67 $\$/\text{MW}.T_P$ and 0.4 $\$/\text{Mvar}.T_P$ [35]. The inner and outer bounds of the voltage tube for PQ buses are considered to be $1\text{ pu} \pm 0.06$ [17, 184] and $1\text{ pu} \pm 0.1$ [236, 237], respectively.

We perform RT-OPF for six different cases: 1) WFs with unity power factors and without reverse active-reactive power flow to the HV network; 2) WFs with unity power factors and with reverse active-reactive power flow to the HV network; 3) WFs with fixed non-unity power factors and without reverse active-reactive power flow to the HV network; 4) WFs with fixed non-unity power factors s and with reverse active-reactive power flow to the HV network; 5) WFs with flexible power factors and without active-reactive reverse power flow to the HV network; and 6) WFs with flexible power factors and with reverse active-reactive power flow to the HV network. The input data for the DN are taken from [35] and shown in Figure 3.8. We run the RT-AR-OPF for one day for the six cases using the same input data. In Case 1 (Figure 3.9), where the WFs operate with unity power factor and the

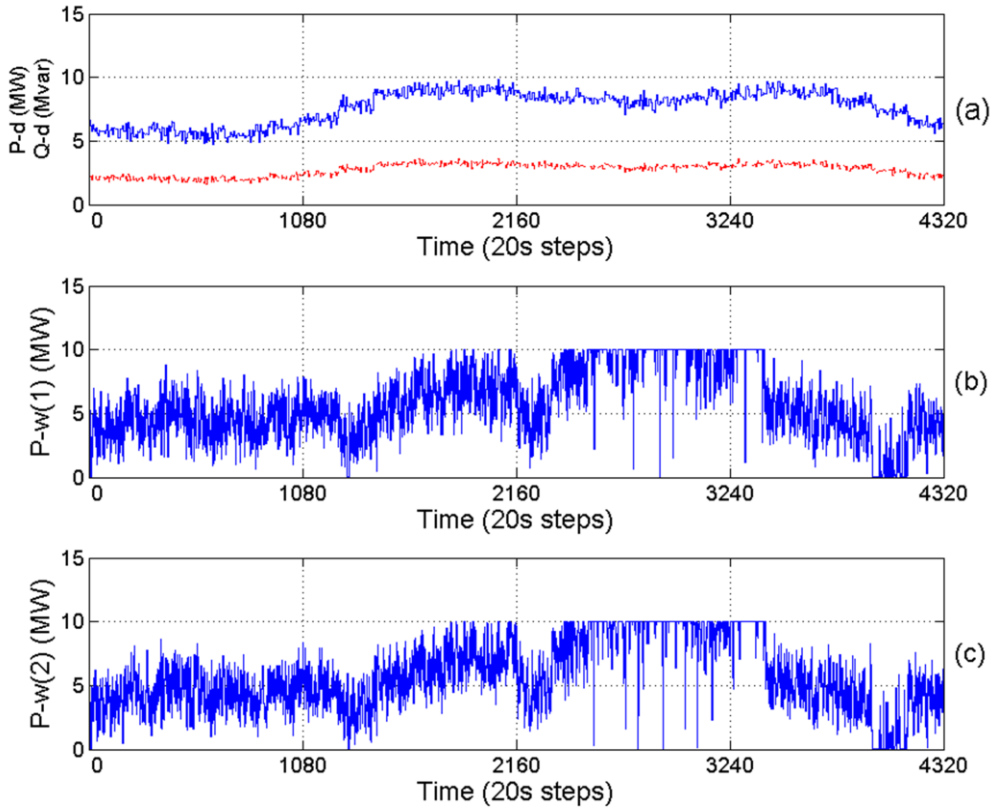

Figure 3.8. Trajectories for one day: (a) total active (black-solid) and reactive (red-dashed) power demand; (b) actual wind power for the first WF; (c) actual wind power for the second WF.

reverse active-reactive power flow is not allowed, some amount of wind power will be curtailed (as shown in subplots (a) and (b)) to satisfy the active power balance equation. The WFs in Cases 1 and 2 do not supply any reactive power to the DN as shown in subplots (c) and (d) in Figures 3.9 and 3.10. In Case 2, since the reverse power flow is allowed, the available wind power is totally injected to the DN (as shown in subplots (a) and (b)).

In Cases 3 and 4, the power factors of WFs are fixed at 0.85 lagging (i.e., supplying reactive power [17]). Therefore, WFs can provide reactive power as shown in subplots (c) and (d) in Figures 3.11 and 3.12. However, in Case 3, where the reverse active-reactive power flow is not allowed, a huge amount of wind power is curtailed (as shown in subplots (a) and (b)) to satisfy the power factor. In contrast, in Case 4 where the reverse active-reactive power flow is allowed, the surplus reactive power in the network will be exported which leads to high reactive power dispatch of WFs. Satisfying the power factor limits, the active power of WFs can also be high (i.e., the curtailment factors of WFs are high) as shown in subplots (a) and (b) for Case 4.

In Cases 5 and 6, the power factors of WFs are free and between 0.85 lagging and 1. For Case 5, where the reverse active-reactive power flow is not allowed, the optimization prefers to inject less reactive power to the network in order to be able to provide more active power

as shown in subplots (a)-(d) in Figure 3.13. This is due to the higher price of active power. In Case 6, where the reverse active-reactive power is allowed, a high amount of active and reactive power will be injected to the network as shown in subplots (a)-(d) in Figure 3.14. It is worth noting that in Cases (4) and (6), regardless of the allowed reverse active-reactive power flow, there is still a small amount of wind power curtailment. This is because the optimization prefers to supply a certain amount of reactive power for some instances to minimize the objective function while holding all the constraints.

Subplots (e) show the discrete slack bus voltage for different cases. It can be seen that at most time instances the slack bus voltage tends to take high values leading to decrease in active and reactive power losses. The exception is Case 3, where the slack bus voltage is mostly kept to be low to 'increase' the reactive power losses in the network or in other words to decrease the reactive power generation by the network feeders. In this case, since surplus reactive power generation in the network cannot be exported, the total reactive power generation in the network must be limited.

Subplots (f) and (g) show the active and reactive power at the slack bus, respectively. Case 6 has the highest amount of active power export (negative value), while Case 4 results in the highest amount of reactive power export. Since the price of the active energy is higher than that of the reactive power, it can be seen in subplots (h) that the objective function value in Case 6 is, at most time instances, the least comparing to the other cases. Subplots (i) show that in all the six cases, the nodal voltages can go beyond the inner tubes (i.e., the blue dashed lines) but they are always in the predefined outer tube (i.e., the red lines). Subplots (j) indicate that the apparent powers in the feeders are always within their constraints. Thus the safety of the operations is ensured for all the defined operation modes.

To compare our proposed RT-AR-OPF method with a deterministic approach, we calculate the value-of-stochastic-solution (VSS) [238-241], which is a measure to show the potential benefit from solving a stochastic problem over solving a deterministic problem. Here, we define the VSS as

$$VSS = F_{TD} - F_T \tag{3.14}$$

where, F_{TD} and F_T are the total values of objective functions obtained by the deterministic approach and the proposed approach, respectively. Table 3.2 presents the results for the six cases for one day. It can be clearly seen that using the deterministic method leads to relatively better values of total objective function for all the cases i.e., negative values of VSS. This is due to the possible deviation of actual values of wind power from the generated wind power scenarios [35]. It is, however, noted that the results obtained in a deterministic way could lead to infeasible operations.

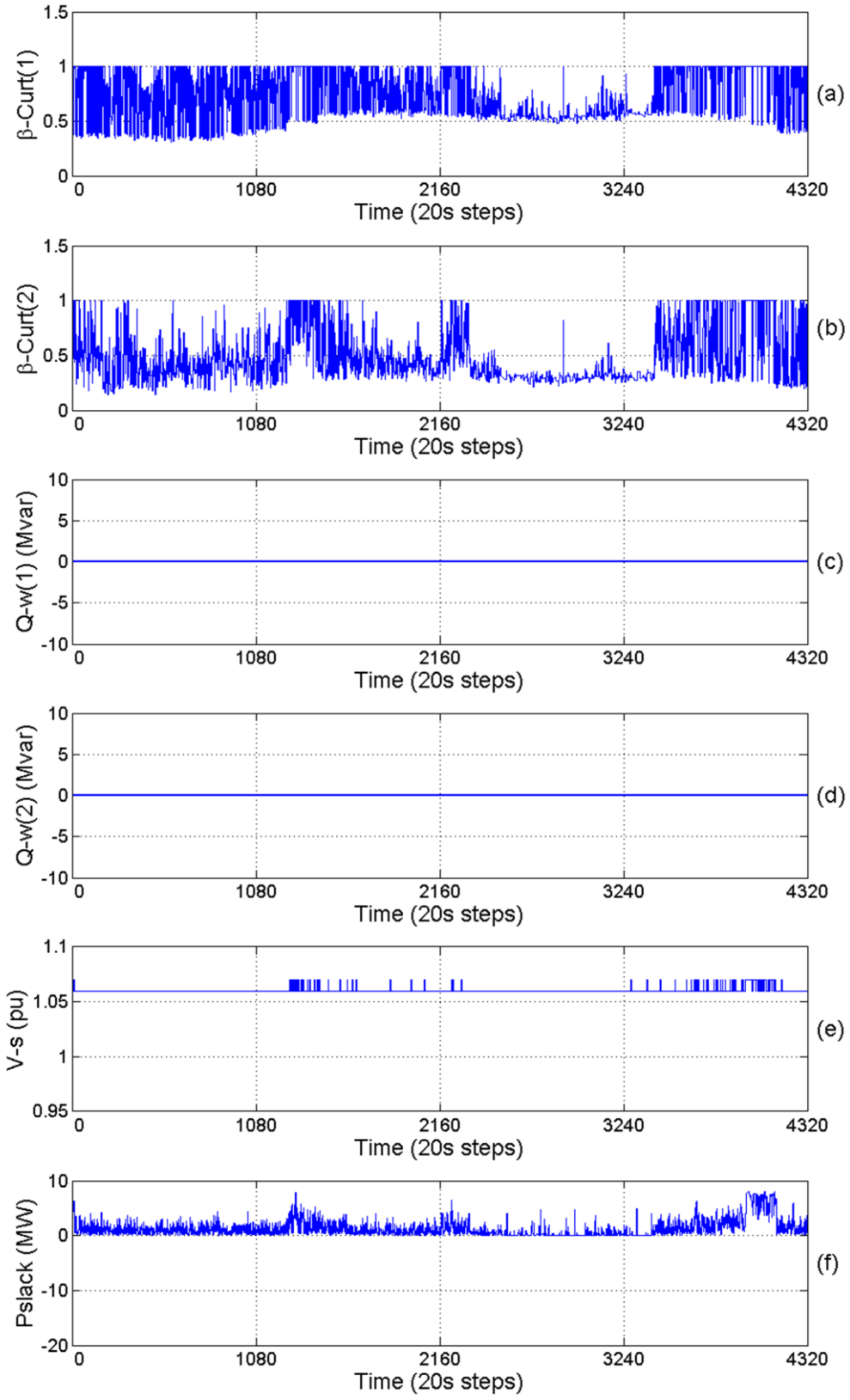

Figure 3.9. Trajectories for Case 1. (a), (b) Curtailment factors for the first and second WF, respectively. (c), (d) Reactive power dispatch of the first and second WF, respectively. (e) Slack bus voltage. (f) Active power at the slack bus.

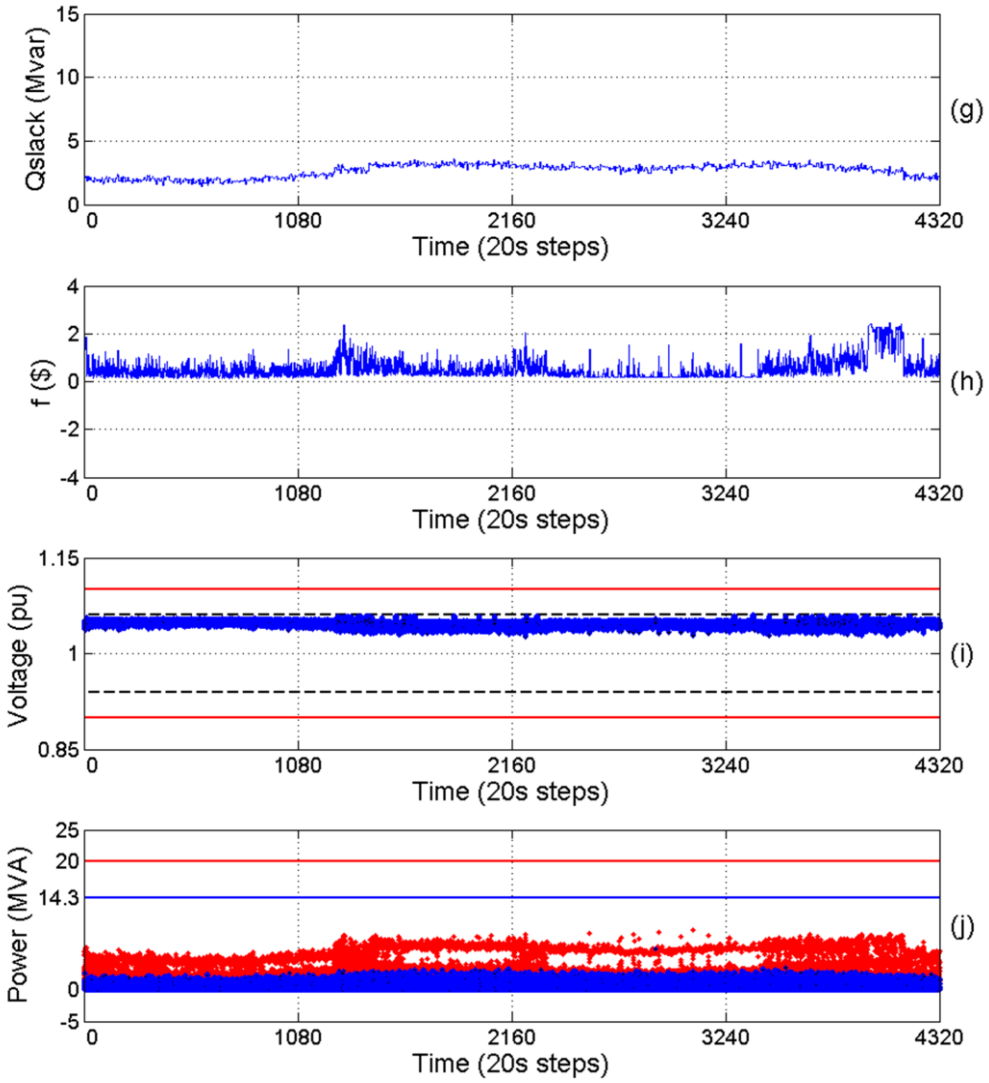

Figure 3.9 (Continued). Trajectories for Case 1. (g) Reactive power at the slack bus. (h) Total objective function value. (i) Bus voltages with inner and outer bounds. (j) Feeders apparent power (2 types of feeders: red and blue).

Figure 3.15 shows the computation time and feasibility status of the proposed RT-AR-OPF (denoted by black color) and the deterministic method [17, 208] (denoted by red color) for the defined modes of operations. It can be clearly seen that the deterministic approach takes much less time as it only solves one MINLP OPF for each prediction horizon. This is in contrast with the proposed RT-AR-OPF framework which solves 49 scenarios in parallel. It is noted that both methods accomplish the computation within the reserved time for OPF computation (here $T_{OPF} = 108\,\text{s}$).

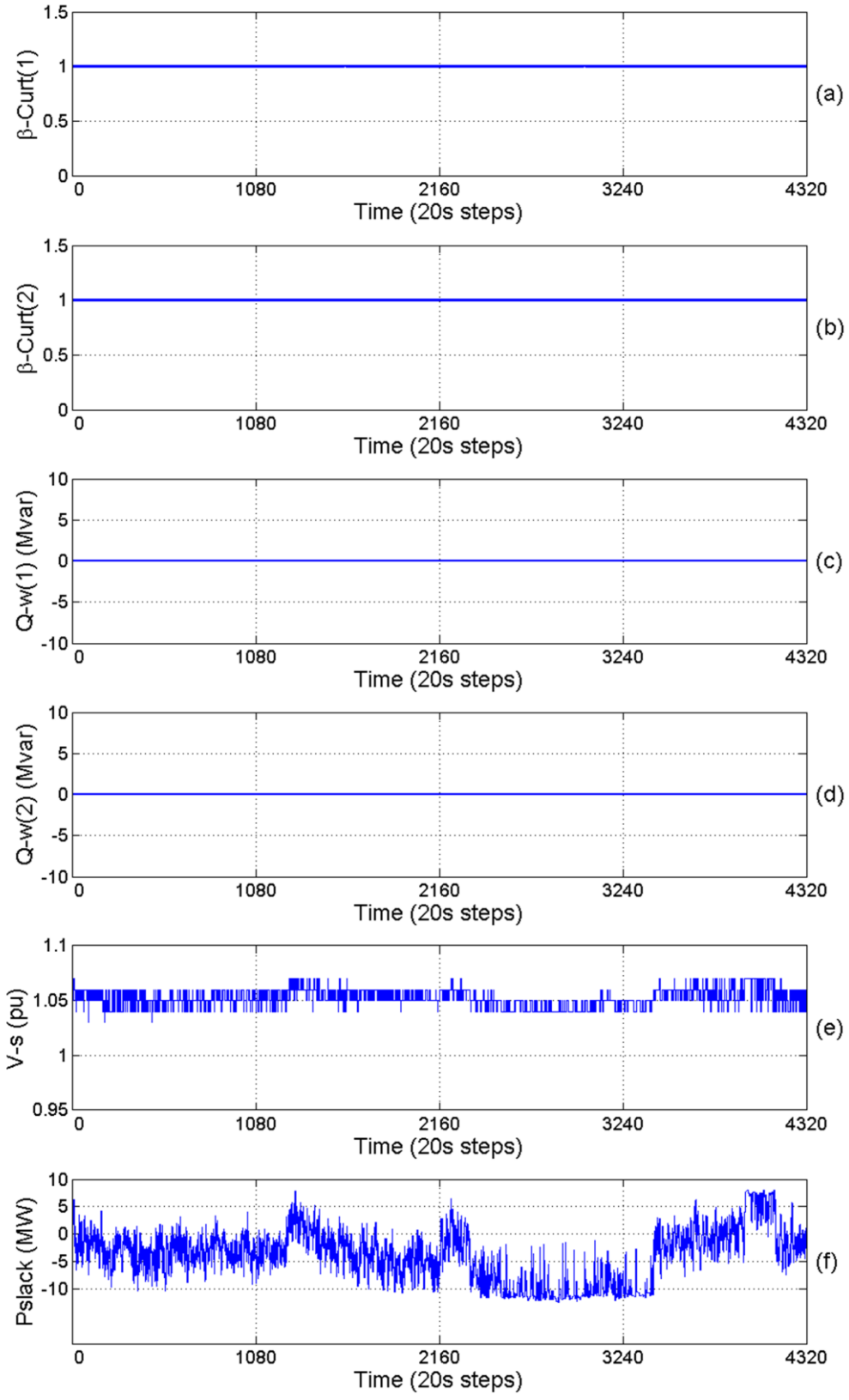

Figure 3.10. Trajectories for Case 2. (a), (b) Curtailment factors for the first and second WF, respectively. (c), (d) Reactive power dispatch of the first and second WF, respectively. (e) Slack bus voltage. (f) Active power at the slack bus.

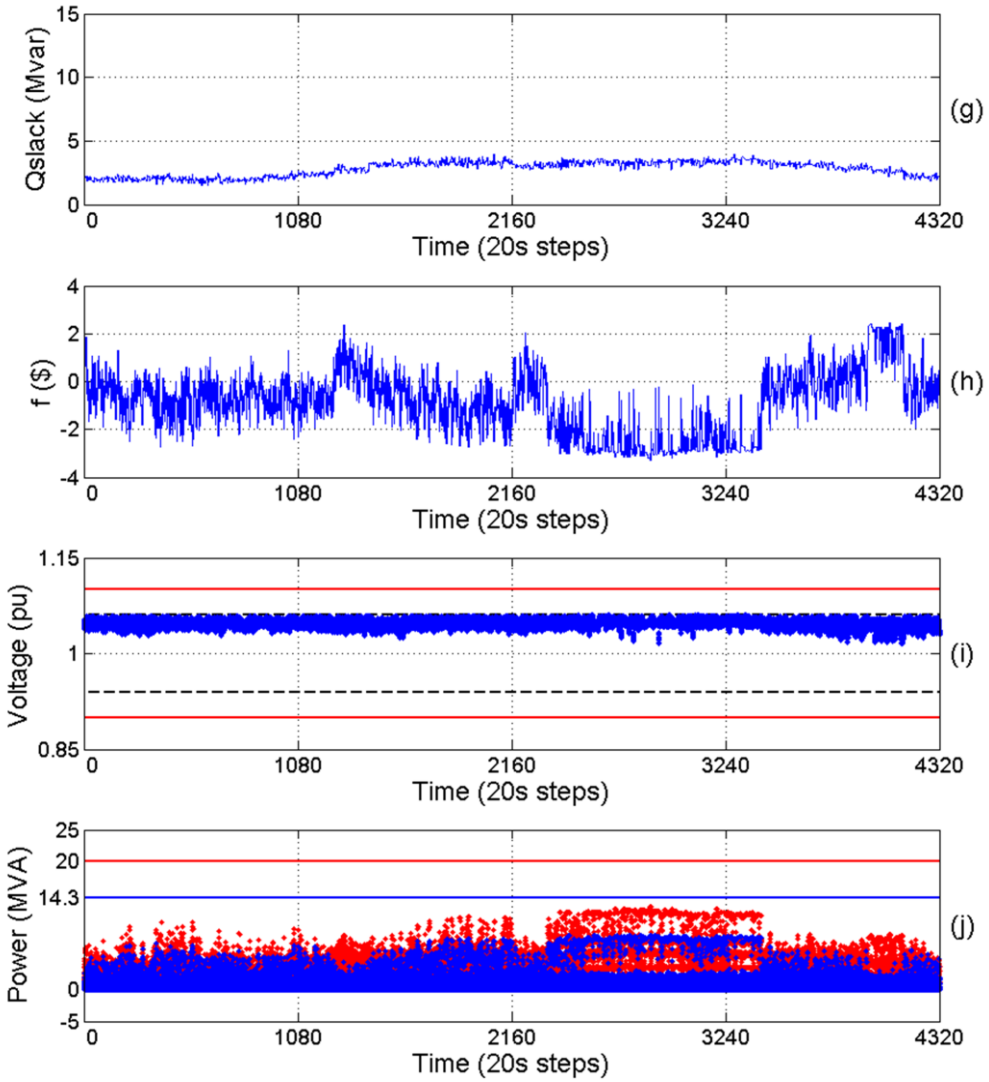

Figure 3.10 (Continued). Trajectories for Case 2. (g) Active and reactive power at the slack bus, respectively. (h) Total objective function value. (i) Bus voltages with inner and outer bounds. (j) Feeders apparent power (2 types of feeders: red and blue).

Figure 3.16 compares the feasibility of the solutions for the deterministic and the proposed method 'after realization' of their operation strategies. This means that after realization of the computed decision, the actual values of wind power could be different from those used in the OPFs. The deterministic method (denoted by red color) leads to infeasible operations for many time instances; For Cases 1 and 2 (i.e., subplots (a)-(b)), the infeasibilities in the deterministic method are mostly due to the violation of equality and/or the voltage constraints (the interested readers are referred to [35] for details).

For Cases 3 and 4 (i.e., subplots (c)-(d)), in addition to the equality and/or the voltage constraints, the violations of power factors of WFs lead to infeasibility for all time instances for the deterministic method. The violations of power factors also affect the feasibility of operations for the deterministic method in Cases 5 and 6 (i.e., subplots (e)-(f)). The details of

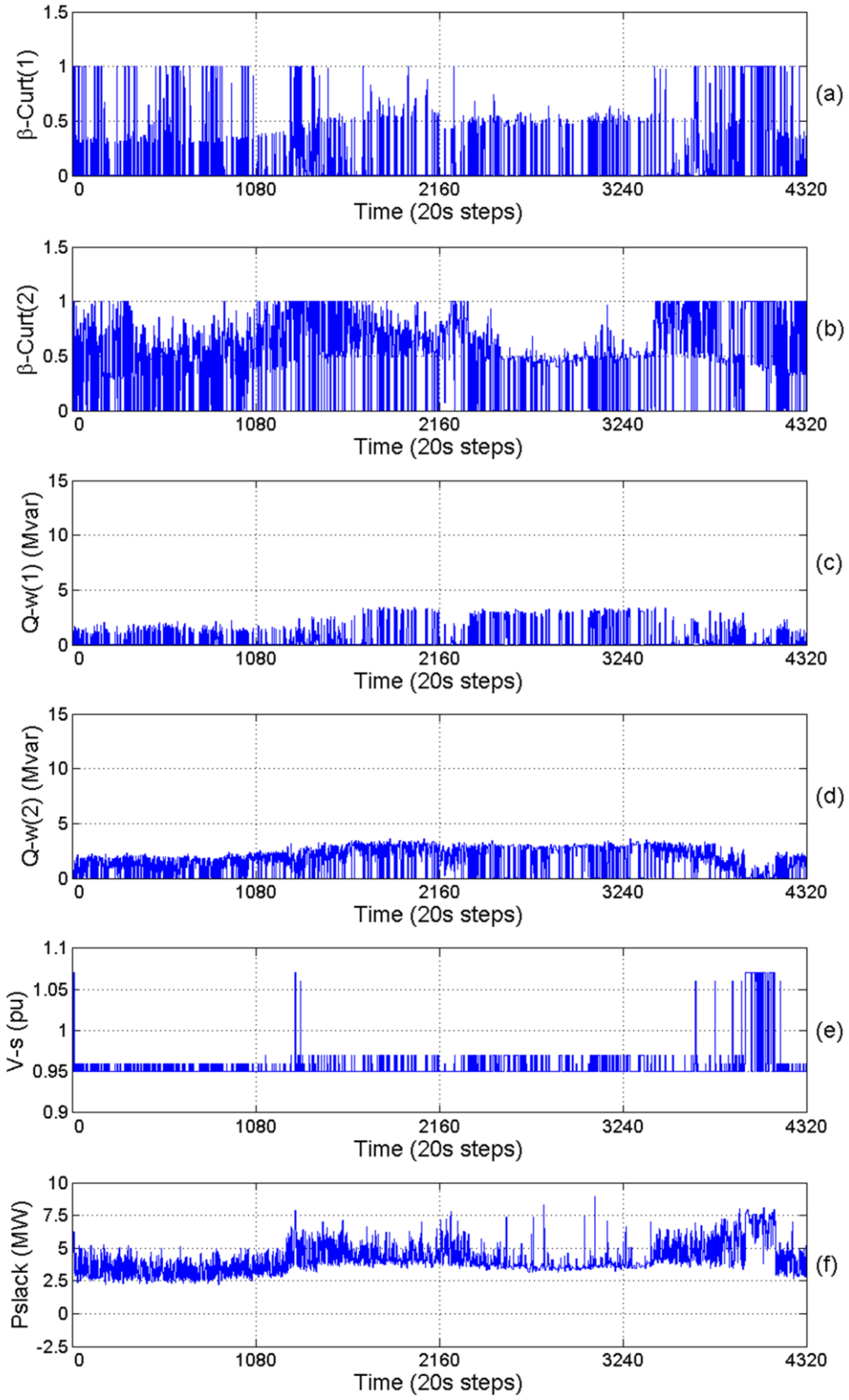

Figure 3.11. Trajectories for Case 3. (a), (b) Curtailment factors for the first and second WF, respectively. (c), (d) Reactive power dispatch of the first and second WF, respectively. (e) Slack bus voltage. (f) Active power at the slack bus.

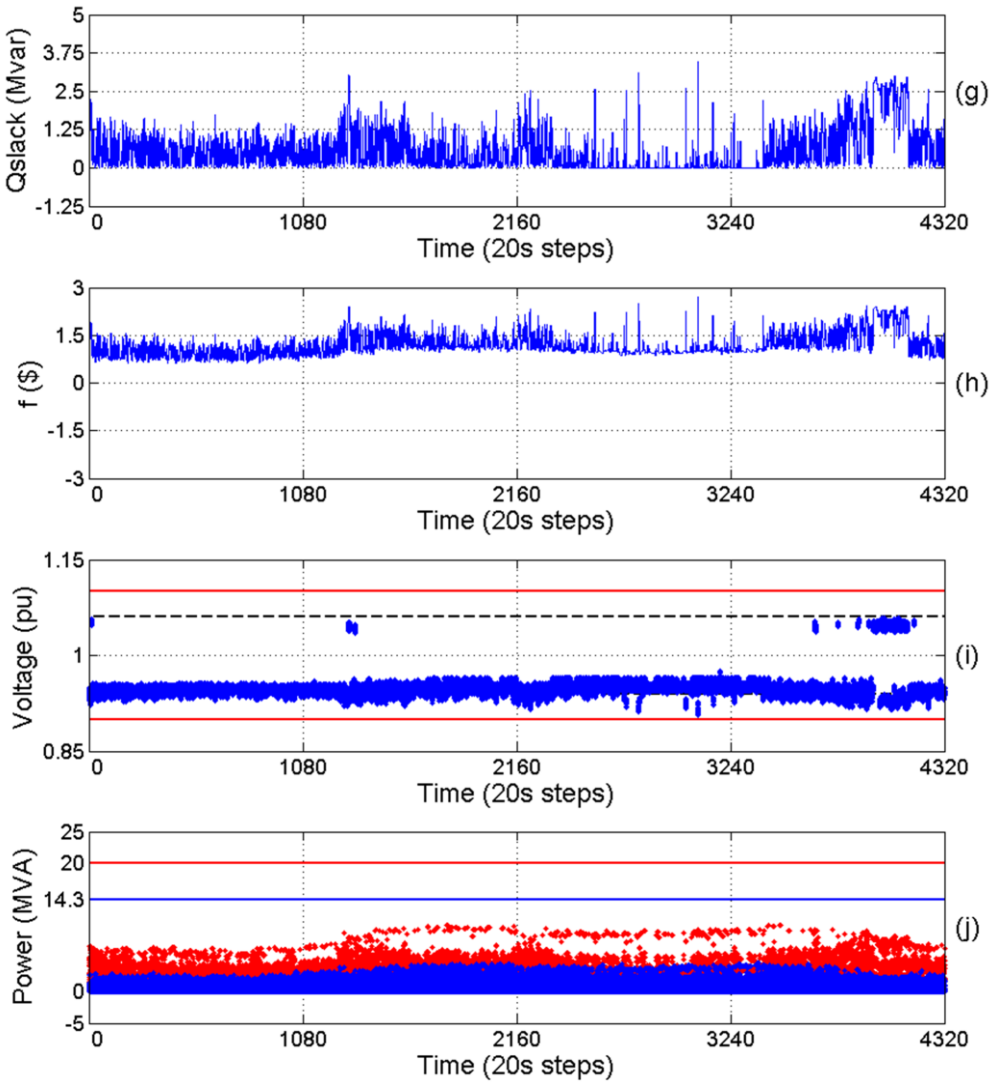

Figure 3.11 (Continued). Trajectories for Case 3. (g) Active and reactive power at the slack bus, respectively. (h) Total objective function value. (i) Bus voltages with inner and outer bounds. (j) Feeders apparent power (2 types of feeders: red and blue).

violation of power factor constraints are shown in Figure 3.6 and discussed in Section 3.4. The superiority of the proposed approach over the deterministic approach [17, 208] can be clearly seen in Figure 3.16, where the feasibility of the RT-AR-OPF is always guaranteed (1 denotes feasible). It means, in the proposed approach, ensuring safety has priority over decreasing costs.

The proposed framework is a general method and thus can be applied to larger networks. The only concern is the capacity of the computation facility. For the numerical implementation in the case study, we use seven processors to solve the MINLP AR-OPF problems in parallel. The proposed RT-AR-OPF framework can be used for different sizes of

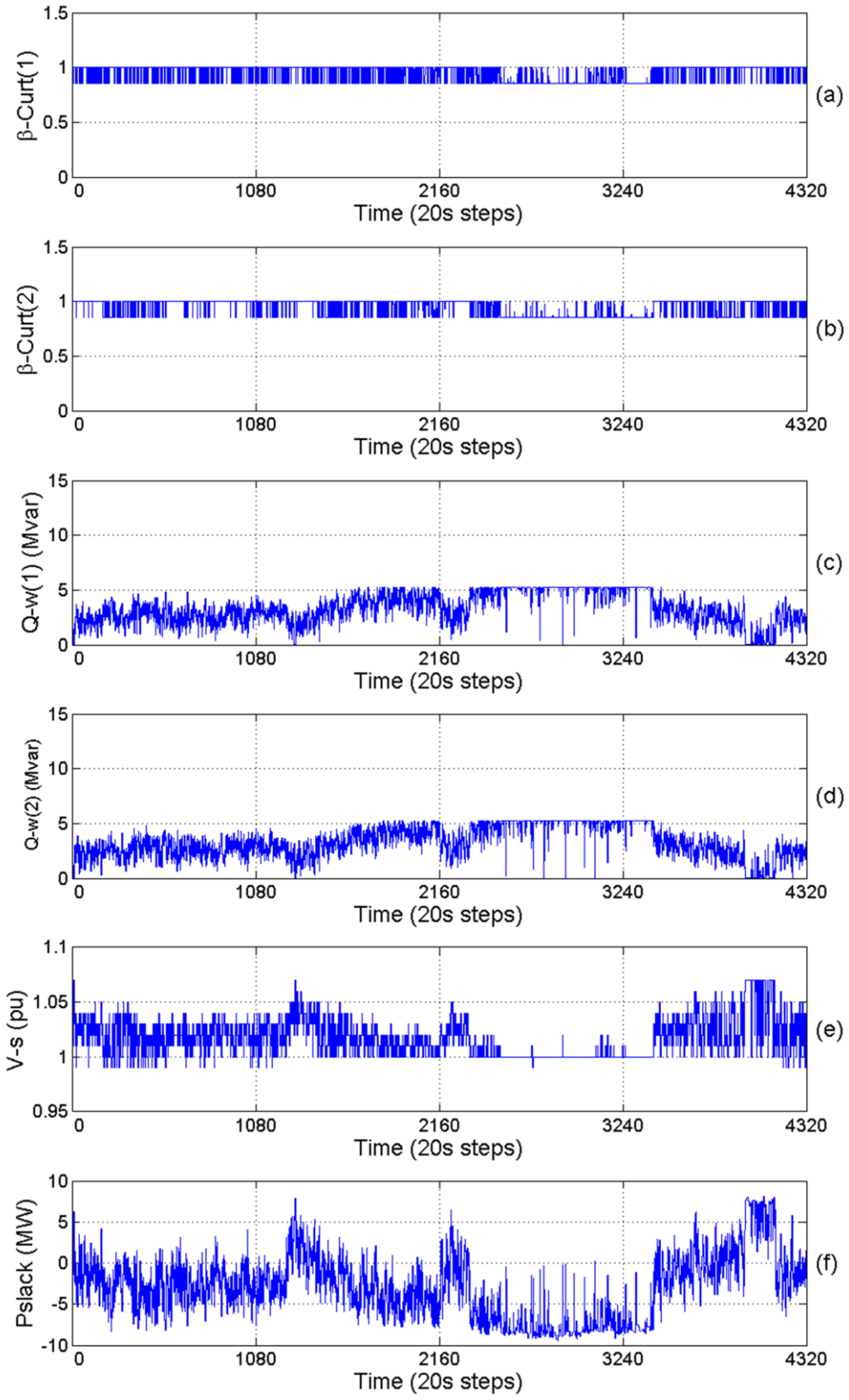

Figure 3.12. Trajectories for Case 4. (a), (b) Curtailment factors for the first and second WF, respectively. (c), (d) Reactive power dispatch of the first and second WF, respectively. (e) Slack bus voltage. (f) Active power at the slack bus.

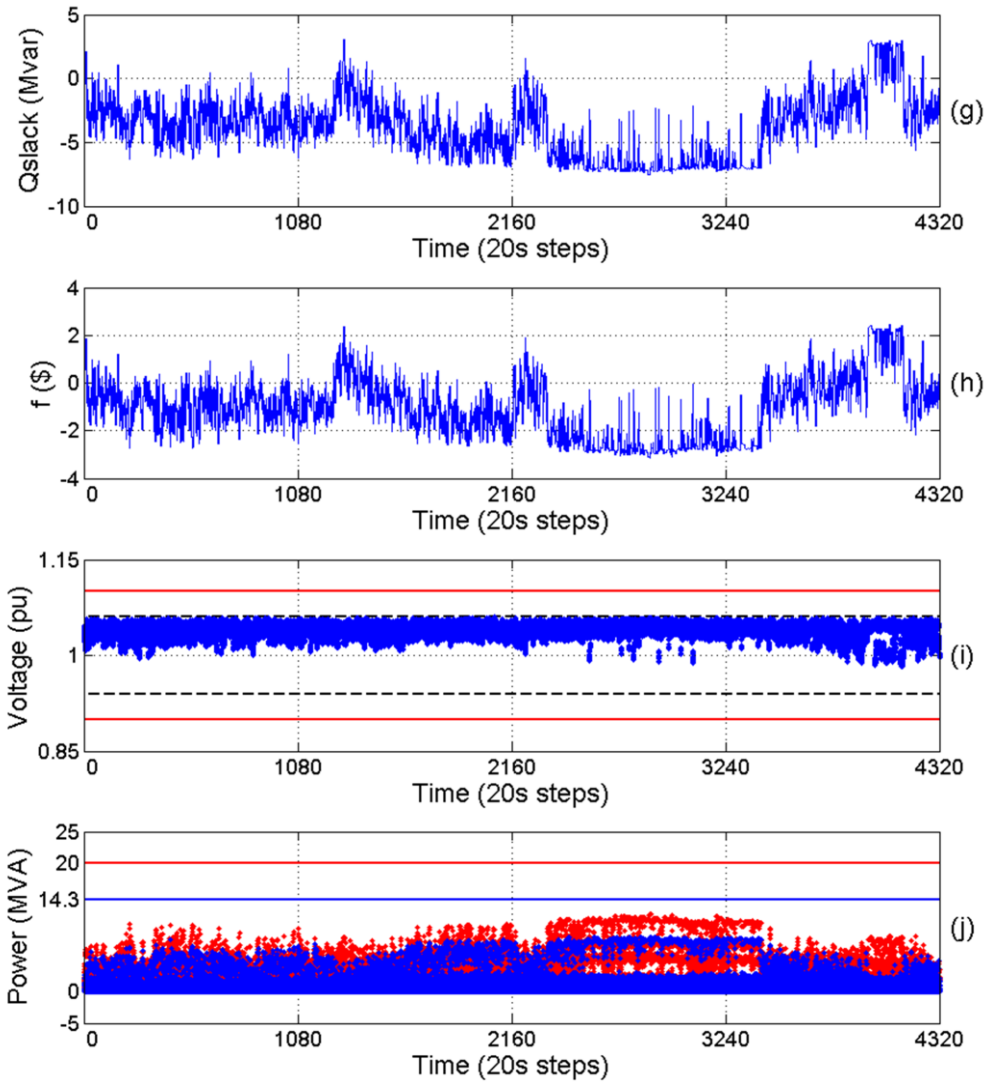

Figure 3.12 (Continued). Trajectories for Case 4. (g) Reactive power at the slack bus. (h) Total objective function value. (i) Bus voltages with inner and outer bounds. (j) Feeders apparent power (2 types of feeders: red and blue).

networks as far as the maximum computation time taken by the processors, $T_{OPF.\max}$ is less than the reserved time for computing OPF problems T_{OPF} (here $T_{OPF} = 108\,\text{s}$). Table 3.3 confirms that $T_{OPF.\max}$, is always less than T_{OPF}, ensuring the applicability of the proposed RT-AR-OPF framework. Increasing the size of the model (i.e., the number of continuous/integer variables, parameters and constraints) could increases the computation time, although the increase ratio cannot be clearly determined [242]. Computing for larger networks requires more efficient computation facilities.

Comparing the results in Table 3.3, it is seen that the reverse active-reactive power flow can lead to increase in active and reactive power losses in the network. However, exporting the surplus amount of power to the upstream HV network results in improving the value of

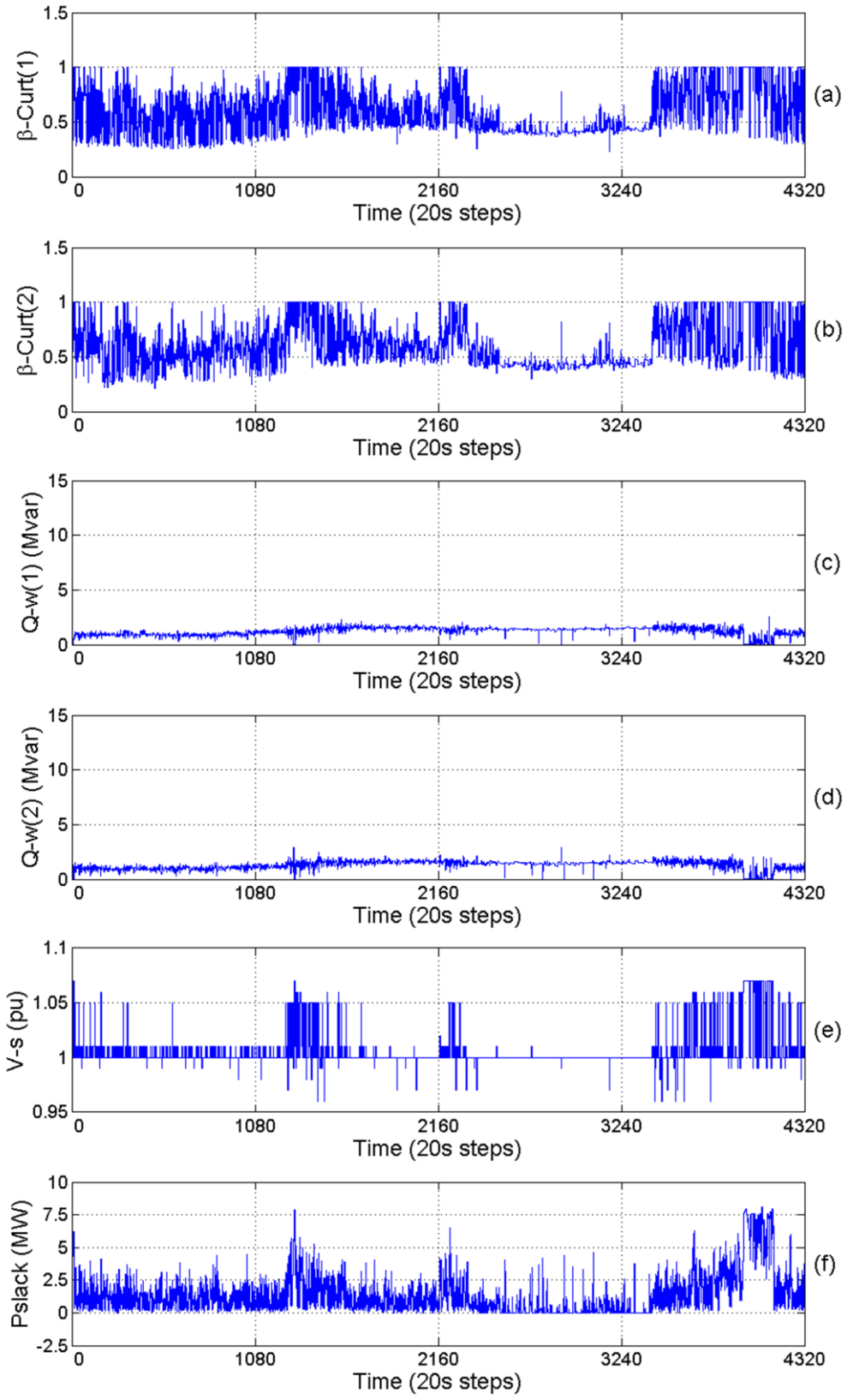

Figure 3.13. Trajectories for Case 5. (a), (b) Curtailment factors for the first and second WF, respectively. (c), (d) Reactive power dispatch of the first and second WF, respectively. (e) Slack bus voltage. (f) Active power at the slack bus.

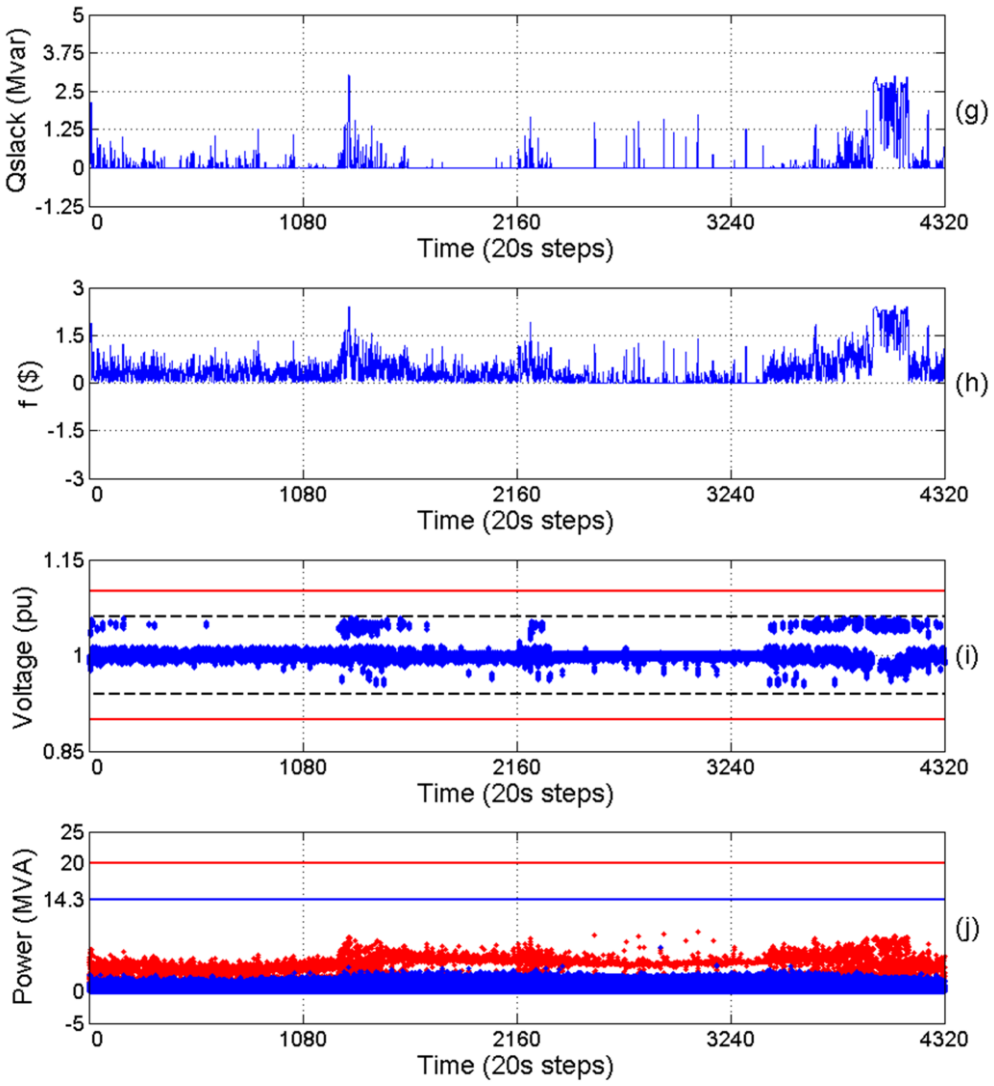

Figure 3.13 (Continued). Trajectories for Case 5. (g) Reactive power at the slack bus. (h) Total objective function value. (i) Bus voltages with inner and outer bounds. (j) Feeders apparent power (2 types of feeders: red and blue).

the total objective function. Looking at Case 3 which is the worst case in terms of objective function value, it can be concluded that, when the reverse active-reactive power flow is not allowed, fixing power factors of WFs to a non-unity value will lead to increasing the costs of the network operation. This is due to the high curtailment of the active wind power to satisfy the power factor limits. It is also clearly seen that making the power factor as a free variable to be optimized leads to decreasing the costs of network operation. In addition, allowing reverse active-reactive power flow at the same time could make this operation mode (i.e., Case 6) to have the best value of the objective function among the others.

To the best of the authors' knowledge, simultaneous optimization of the fluctuating 'reactive' power dispatch of WFs, active wind power curtailment, discrete slack bus voltage, and reverse active-reactive power flow has not been considered in the existing literature of

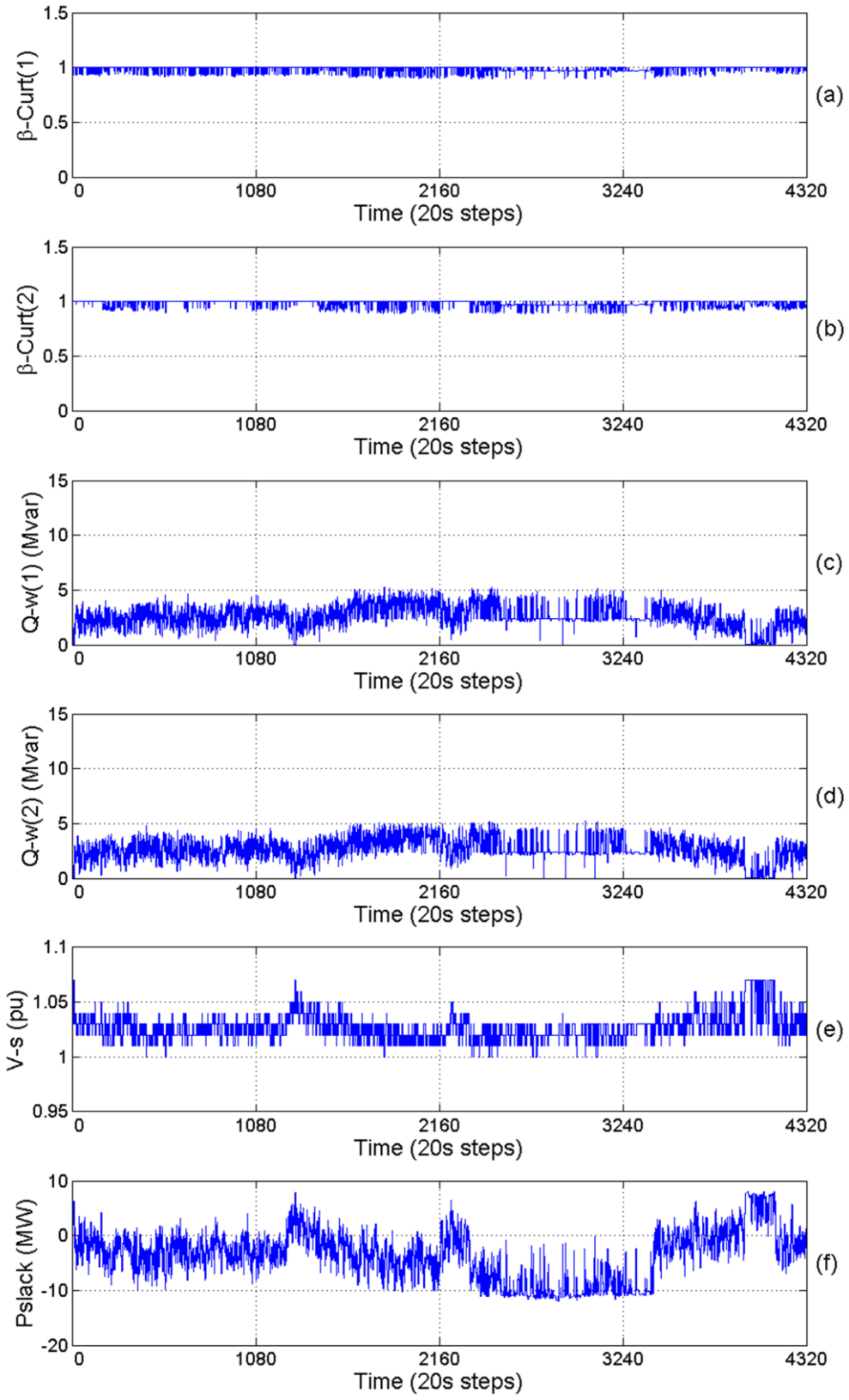

Figure 3.14. Trajectories for Case 6. (a), (b) Curtailment factors for the first and second WF, respectively. (c), (d) Reactive power dispatch of the first and second WF, respectively. (e) Slack bus voltage. (f) Active power at the slack bus.

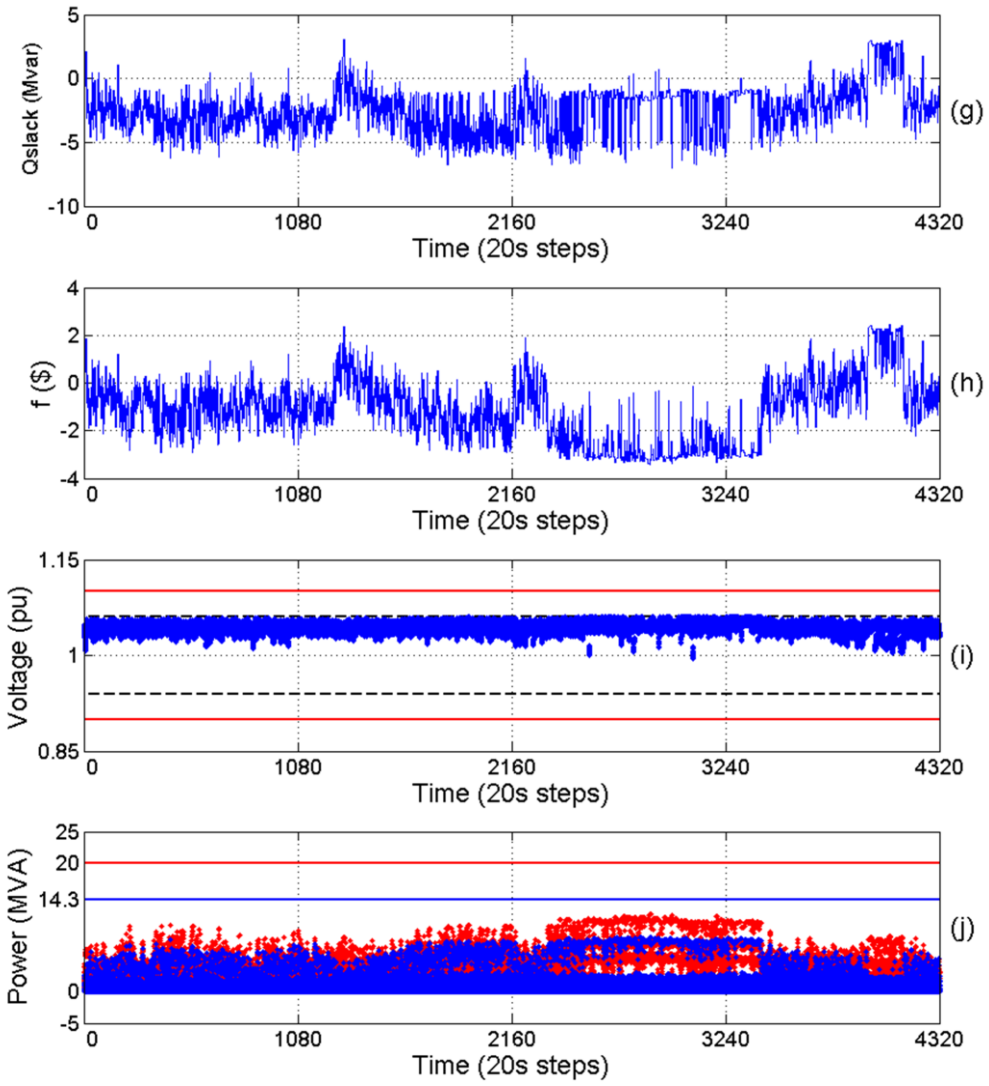

Figure 3.14 (Continued). Trajectories for Case 6. (g) Reactive power at the slack bus, respectively. (h) Total objective function value. (i) Bus voltages with inner and outer bounds. (j) Feeders apparent power (2 types of feeders: red and blue).

'real-time' OPF. As shown in Subplots (g) in Figures 3.11-3.14, the incorporation of the reactive power of WFs can lead to a significance reduction in the amount of reactive power imported from the upstream HV network for Cases 3 and 5, and even exporting reactive power for Cases 4 and 6.

The total effect of the reactive power on the objective function value (Equation 3.4) is shown in Table 3.3. The proposed 'active-reactive' approach with reverse power flow (i.e., Case 6) leads to a significant economic improvement comparing to the one with only active power and reverse power flow (i.e., Case 2). Moreover, Figure 3.16 confirms that the proposed reconciliation algorithm and power factor modification scheme can ensure the feasibility of the optimal operations in real-time.

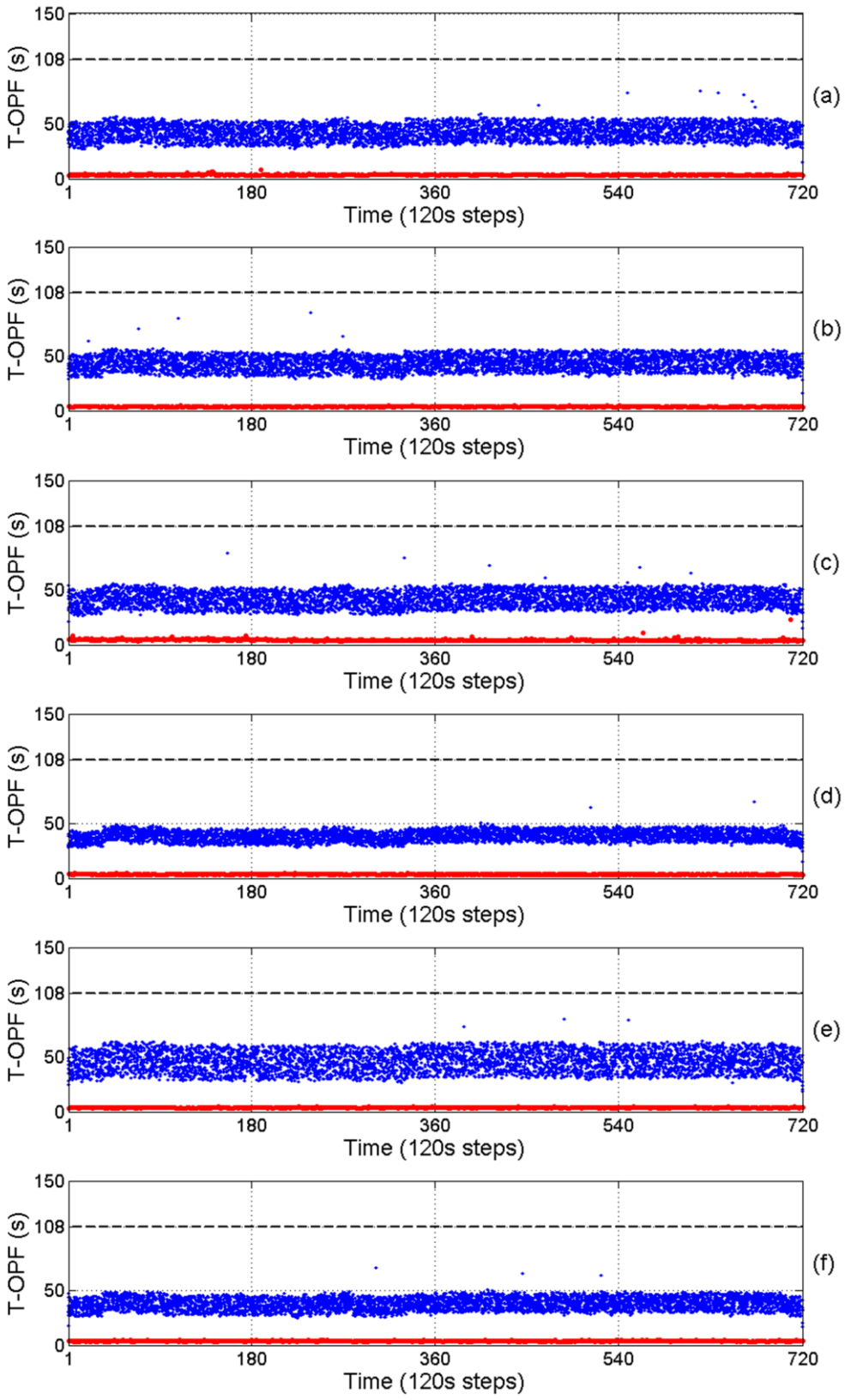

Figure 3.15. Computation time for (a) Case 1, (b) Case 2, (c) Case 3, (d) Case 4, (e) Case 5, (f) Case 6. Here, the trajectories of deterministic approach and the proposed RT-AR-OPF are denoted by red and blue, respectively.

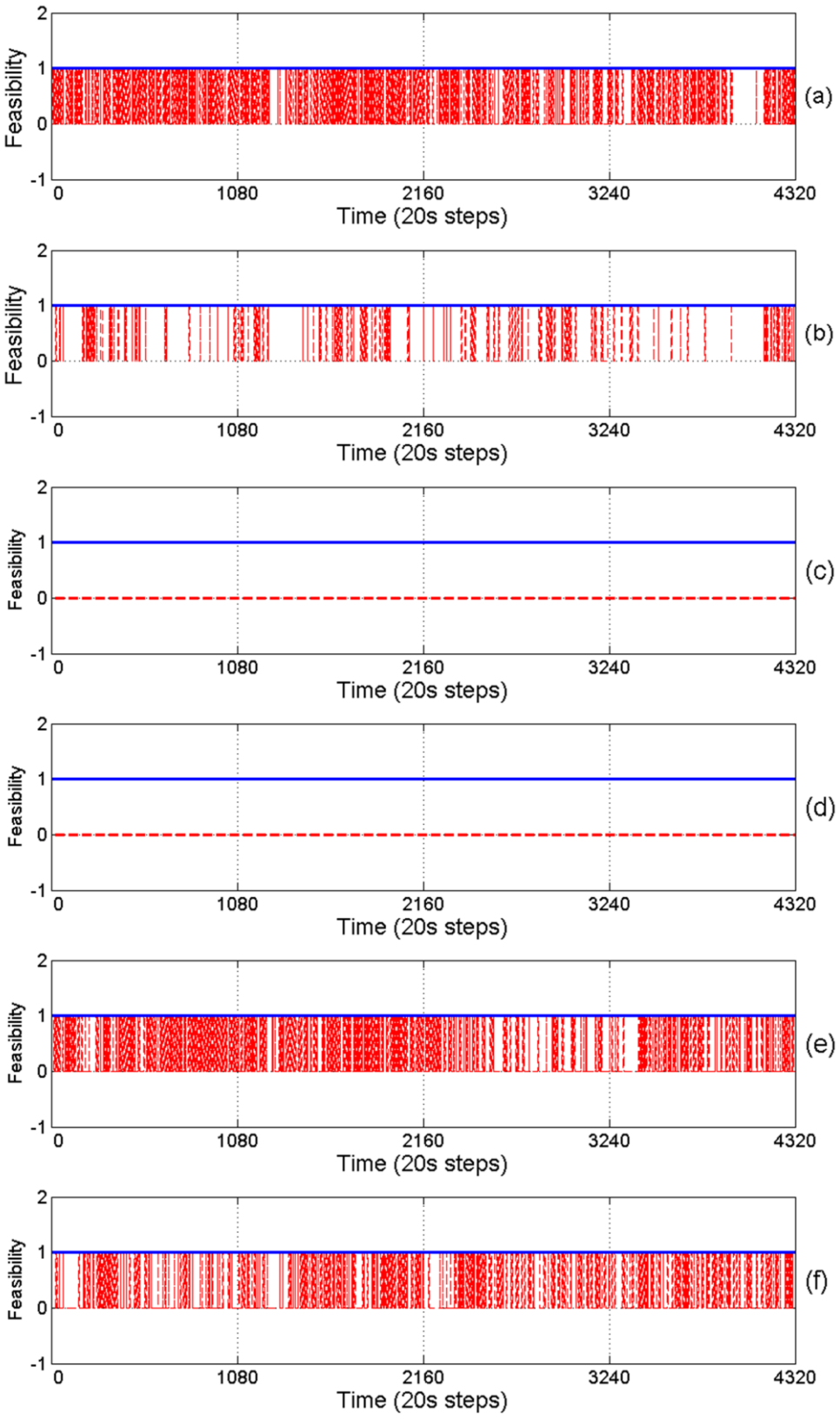

Figure 3.16. Feasibility status for (a) Case 1, (b) Case 2, (c) Case 3, (d) Case 4, (e) Case 5, (f) Case 6. Here, the trajectories of deterministic approach and the proposed RT-AR-OPF are denoted by red and blue, respectively.

Table 3.2. Comparison of the proposed approach and deterministic method for one day (4320×20s).

Case	Power factor (PF)	Reverse power flow	F_{TD} ($/day)	F_T ($/day)	**VSS**
1	PF=1	Not allowed	1241.7	2305.69	**-1063.99**
2	PF=1	Allowed	-4249.98	-3929.9	**-320.08**
3	PF=0.85 lagging	Not allowed	4077.5	5139.69	**-1062.19**
4	PF=0.85 lagging	Allowed	-5759.48	-4752.21	**-1007.27**
5	0.85≤PF≤1 lagging	Not allowed	491.54	1676.92	**-1185.38**
6	0.85≤PF≤1 lagging	Allowed	-5914.64	-5140.1	**-774.54**

3.6 Conclusions

In this chapter, we developed a lookup-table-based RT-AR-OPF framework to deal with intermittent wind power in medium-voltage DNs. Scenario-based MINLP problems are solved in real-time to simultaneously optimize the active wind power curtailment, reactive wind power dispatch, reverse active-reactive power flow, and discrete slack bus voltage. To deal with the cases that the MINLP problems fail to converge, a new reconciliation algorithm is proposed to safeguard both the feasibility and the optimality of the operation strategies to be realized to the network. Furthermore, despite the fluctuating reactive power dispatch of WFs, the framework ensures satisfactions of nodal voltage limits by introducing a power factor modification scheme. Case studies with and without reverse active-reactive power flow and different operation modes in terms of the power factor of WFs were presented to demonstrate the effectiveness of the proposed RT-AR-OPF framework.

Table 3.3. Comparison of results for one day (4320×20s) for six MINLP OPF cases.

Case	Power factor (PF)	Reverse power flow	$T_{OPF.\min}$ (s)	$T_{OPF.\max}$ (s)	$T_{OPF.ave}$ (s)	Average P_{loss} (kW)	Average Q_{loss} (kvar)	$\boldsymbol{F_T}$ **($/day)**
1	PF=1	Not allowed	15.4	79.95	42.3	26	-90.93	**2305.69**
2	PF=1	Allowed	15.6	90.1	43.68	88.95	64.35	**-3929.9**
3	PF=0.85 lagging	Not allowed	15.18	84.04	41.79	47.91	-10.92	**5139.69**
4	PF=0.85 lagging	Allowed	14.77	69.39	38.64	94.62	80.87	**-4752.21**
5	0.85≤PF≤1 lagging	Not allowed	18.39	84.53	45.97	19.96	-93.85	**1676.92**
6	0.85≤PF≤1 lagging	Allowed	16.79	70.42	37.86	90.96	70.48	**-5140.1**

4 Real-Time AR-OPF with Battery Storage Systems

In this chapter, a multi-phase multi-time-scale RT-DAR-OPF framework is developed to optimally deal with spontaneous changes in wind power in DNs with BSSs. The most challenging issue hereby is that a large-scale dynamic MINLP problem has to be solved in real-time[243]. In addition, considering both active and reactive power capabilities of BSSs with flexible operation strategies, as well as minimizing the expended life costs of BSSs further increases the complexity of the problem. To solve this problem, in the first phase, we implement simultaneous optimization of a huge number of mixed-integer decision variables to compute optimal operation strategies of BSSs on a day-to-day base. In the second phase, based on the forecasted wind power values for short prediction horizons, wind power scenarios are generated to describe uncertain wind power with non-Gaussian distribution. Then MINLP AR-OPF problems corresponding to the scenarios are solved and reconciled in advance of each prediction horizon. In the third phase, based on the measured actual values of wind power, one of the solutions is selected, modified and finally realized to the network for very short intervals. The applicability of the proposed RT-DAR-OPF is demonstrated using a medium-voltage DN.

4.1 Problem Formulation

The aim of the RT-DAR-OPF is to compute optimal operation strategies to be realized to DNs with BSSs under uncertain penetration of wind power [243]. A general formulation of the optimization problem can be expressed as:

$$
\begin{aligned}
\min_{\mathbf{u}(t),\mathbf{l}(t),\mathbf{y}(t)} \quad & f\left(\mathbf{x}(t),\mathbf{u}(t),\mathbf{l}(t),\mathbf{y}(t),\boldsymbol{\xi}(t)\right) \\
s.t. \quad & \dot{\mathbf{x}}(t) = \mathbf{g}\left(\mathbf{x}(t),\mathbf{u}(t),\mathbf{l}(t),\mathbf{y}(t),\boldsymbol{\xi}(t)\right), \quad \mathbf{x}(t_0) = \mathbf{x}_0 \\
& \mathbf{x}_{\min}(t) \le \mathbf{x}(t) \le \mathbf{x}_{\max}(t) \\
& \mathbf{u}_{\min}(t) \le \mathbf{u}(t) \le \mathbf{u}_{\max}(t) \\
& \mathbf{l}(t) \in \{0,1,2,...,L\} \\
& \mathbf{y}(t) \in \{0,1\} \\
& \boldsymbol{\xi}(t) \in \Omega \\
& t_0 \le t \le t_f
\end{aligned}
\tag{4.1}
$$

where $f(.)$ is the objective function to be minimized, $\mathbf{x}$ is the vector of state variables, $\mathbf{u}$ is the vector of continuous decision variables, $\mathbf{l}$ is the vector of discrete decision variables, $\mathbf{y}$ is the vector of binary decision variables, ξ is the vector of random variables, and t is time. The objective function is subject to equality and inequality constraints. Here, $\mathbf{g}(.)$ denotes dynamic nonlinear model equations, $\mathbf{x}_0$ denotes the initial states at t_0, $\mathbf{x}_{\mathbf{min/max}}$ are the lower/upper limits on state variables, $\mathbf{u}_{\mathbf{min/max}}$ are the lower/upper limits on continuous decision variables, and t_f is the final time. Equation 4.1 is a large-scale complex stochastic dynamic MINLP optimization problem which is difficult to solve.

4.2 RT-DAR-OPF Framework

To solve the optimization problem in Equation 4.1, we propose a multi-phase multi-time-scale RT-DAR-OPF framework as illustrated in Figure 4.1. The framework consists of three phases (Phases 2 and 3 are adapted from [35, 109]) with three different time scales (e.g., $T_{P1} = 24$ h, $T_{P2} = 2$ min and $T_S = 20$ s) and 15 steps as follows:

1) Provide hourly forecasted wind power, demand, and price profiles in advance of each prediction horizon T_{P1}.
2) Solve the corresponding dynamic MINLP AR-OPF problem. In this step, optimal flexible operation strategies for BSSs are computed for the upcoming T_{P1} (e.g., 24 hours, with hourly discretization). The detailed problem formulation is described in Section 4.3.
3) The variables of BSSs computed in Phase 1 will be used as fixed input parameters for the second phase. Note that other decision variables will be recomputed in Phase 2.
4) Provide forecasted values of wind power, demand, and price ahead of each prediction horizon T_{P2} (e.g., 2 min). Note that the length of the prediction horizon T_{P2} should depend on the availability of the forecasted data as well as the computation time in Step (7).
5) To describe uncertain wind power, generate N_s wind power scenarios for each WF using a continuous bounded stochastic distribution with an identical probability between two adjacent scenarios. For this purpose, $N_s - 1$ intervals are defined for the wind power $P_w(n_w, n_s)$, $n_s = 1,...,N_s$, such that

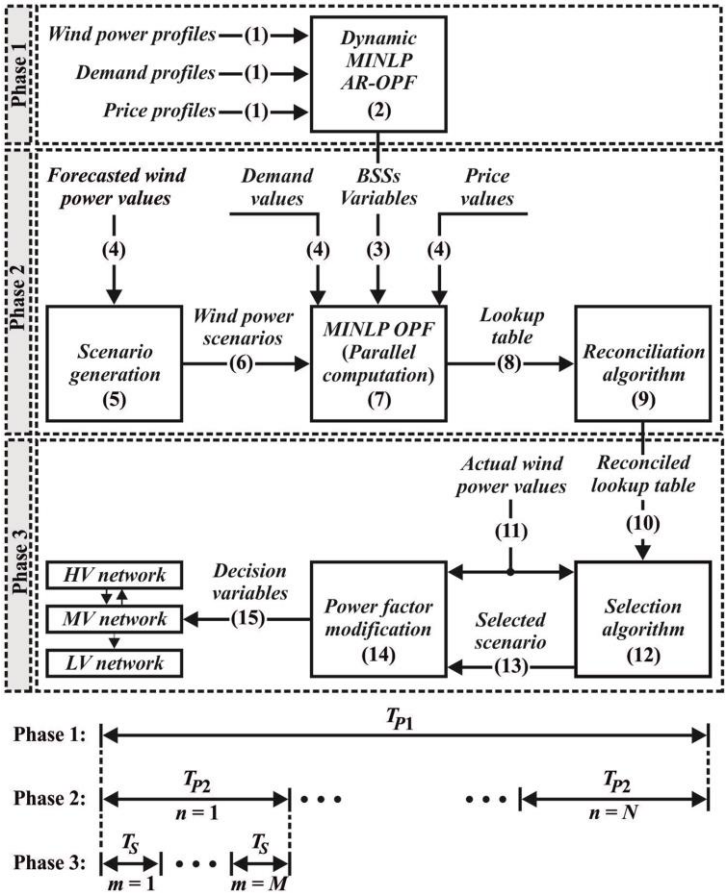

Figure 4.1. The proposed framework for RT-DAR-OPF.

$$\Pr\{P_w(n_w, n_s) - P_w(n_w, n_s - 1)\} = \frac{1}{N_s - 1}, \quad \text{for } n_s \geq 2 \tag{4.2}$$

where n_w and n_s are the indices for WFs and wind power scenarios, respectively. Pr is the probability operator and the scenarios are margins of the defined intervals. To this end, N_s wind power scenarios are generated for each WF. Then, N_c wind power scenario combinations are formed for each prediction horizon T_{P2}. The total number of scenario combinations will be

$$N_c = (N_s)^{N_w} \tag{4.3}$$

where N_w is the total number of WFs.

6) Send the generated N_c wind power scenario combinations (obtained in Step 5) to the MINLP AR-OPF.

7) Solve the MINLP AR-OPF problems corresponding to each scenario combination for the upcoming T_{P2}. Note that the optimization problems at this step are not dynamic as the optimal operation strategies of BSSs are already given as input parameters. Since reactive power flow has influence on nodal voltages [244, 245], reactive power dispatch of the WFs can lead to voltage violations, in particular

when the wind power fluctuates. For this reason, we use a back-off strategy [109] to satisfy voltage constraints in the RT-OPF. Since the optimization problems in this step are independent, they are solved using parallel computation in order to ensure that the solutions for all the scenario combinations are available within the prediction horizon T_{P2}.

8) Send the solutions of the MINLP AR-OPF problems (obtained in Step 7) as a lookup table to a reconciliation algorithm.
9) Using the reconciliation algorithm, reconcile the lookup table by substituting the un-converged problems with solutions by which the safety of the operations are ensured while minimizing the degree of conservatism.
10) Send the reconciled lookup table for the T_{P2} to a selection algorithm.
11) Provide the values of wind power measured at each sampling interval T_S (e.g., 20 s) to the selection and power factor modification algorithms.
12) The selection algorithm selects a solution strategy based on the measured values of wind power for each sampling interval T_S. The selected scenario ensures the safety of the operation with the minimum of the objective function.
13) Send the selected scenario to the power factor modification algorithm.
14) Modify the power factor of WFs before realizing the solution using the power factor modification algorithm. Due to the possible difference between the measured wind power and the selected scenario, realizing the reactive power dispatch can lead to violations of power factor limits. Therefore, the power factor modification algorithm ensures satisfaction of the power factor constraints.
15) Send the decision variables to the network at each sampling interval T_S.

The above 15 steps repeated for the next T_{P1} so that the proposed real-time framework aims at autonomously updating the operation strategies according to spontaneous changes of wind power while optimally manages the operation of BSSs.

4.3 Dynamic MINLP AR-OPF

4.3.1 Operation Modes of BSSs

It was shown in [246] that the lifetime of a battery is strongly influenced by the depth of discharge (DoD) and the number of charge-discharge cycles in the prediction horizon. Therefore, in many studies [17, 18, 112, 113], N_{cyc} was limited in order to increase the

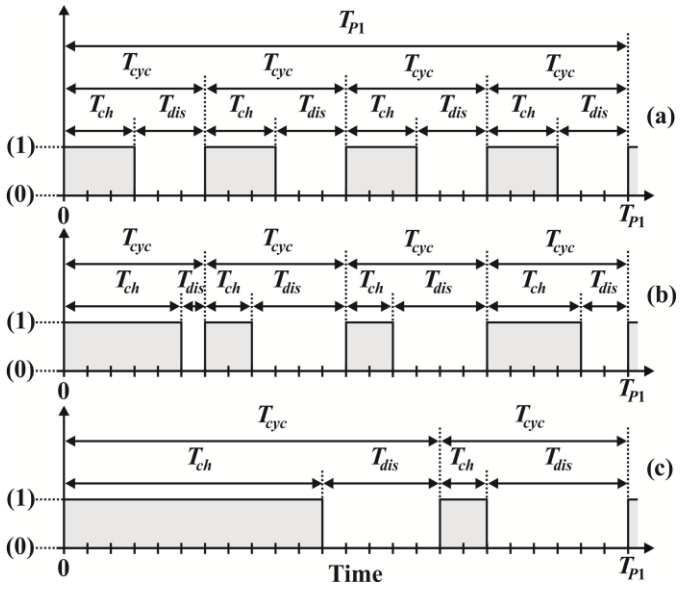

Figure 4.2. Different operation modes for BSSs: a) Mode 1, b) Mode 2, c) Mode 3.

lifetime. Considering this limitation, three types of operation modes can be defined for BSSs in active-reactive OPF as shown in Figure 4.2.

Mode 1: Fixed charge and discharge periods, and a fixed number of charge-discharge cycles in the prediction horizon T_{P1}. In this operation mode, the decision variables of the BSSs are $P_{ch}(i,t)$, $P_{dis}(i,t)$, $Q_b(i,t)$).

Mode 2: Flexible charge and discharge periods, and a fixed number of charge-discharge cycles in the prediction horizon T_{P1}. In this operation mode, the decision variables of the BSSs are $P_{ch}(i,t)$, $P_{dis}(i,t)$, $Q_b(i,t)$, $T_{ch}(i,n_{cyc})$, and $T_{dis}(i,n_{cyc})$).

Mode 3 (proposed): Flexible charge and discharge periods and optimal number of charge-discharge cycles in the prediction horizon T_{P1}. In this operation mode, the decision variables of the BSSs are $P_{ch}(i,t)$, $P_{dis}(i,t)$, $Q_b(i,t)$, $T_{ch}(i,n_{cyc})$, $T_{dis}(i,n_{cyc})$, $T_{cyc}(i,n_{cyc})$ and $N_{cyc}(i)$.

It can be seen that Mode 3 allows higher flexibility comparing to the other modes of operation. However, it leads to higher complexity as the number of decision variables in the optimization problem increases. Therefore, in this chapter the dynamic AR-OPF is formulated and a solution approach is presented for BSSs to operate in Mode 3. For comparison purposes, we also test our new framework with the other operation modes in the case study.

4.3.2 Detailed Problem Formulation

The dynamic optimization problem in Phase 1 of the RT-DAR-OPF framework is formulated as follows

$$\begin{aligned}
&\min_{\mathbf{u}(t),\mathbf{I}(t),\mathbf{y}(t)} \quad (F_1 + F_2 + F_3) \\
&F_1 = \sum_{t=1}^{t_f} C_{pp}(t) P_s(t) \\
&F_2 = \sum_{t=1}^{t_f} C_{pq}(t) Q_s(t) \\
&F_3 = \sum_{i \in S_{BSS}} ELC(i).
\end{aligned} \tag{4.4}$$

The objective function in Equation 4.4 minimizes the total costs of active and reactive energy F_1 and F_2 imported from an upstream network, and meanwhile minimizes the total expended life costs of the BSSs F_3. The significance of our proposed dynamic AR-OPF is that all continuous, discrete and binary decision variables are simultaneously optimized for the prediction horizon T_{P1}. Here, the vector of continuous decision variables $\mathbf{u}(t)$ includes curtailment factors of WFs $\beta_w(i,t)$, reactive power dispatch of WFs $Q_w(i,t)$, active power charge of BSSs $P_{ch}(i,t)$, active power discharge of BSSs $P_{dis}(i,t)$, and reactive power dispatch of BSSs $Q_b(i,t)$. The vector of discrete decision variables $\mathbf{I}(t)$ includes slack bus voltage $V_S(t)$, charge periods of the BSSs $T_{ch}(i,n_{cyc})$, discharge periods of the BSSs $T_{dis}(i,n_{cyc})$, length of charge-discharge cycles of batteries $T_{cyc}(i,n_{cyc})$, and number of charge-discharge cycles of the BSSs in the prediction horizon $N_{cyc}(i)$. The vector of binary decision variables $\mathbf{y}(t)$ includes $\alpha(i,t)$ which represents the status of charge/discharge for each BSS.

Equation 4.4 is subject to the following equality and inequality constraints:

$$f_P + P_d(i,t) + P_{ch}(i,t) - P_{dis}(i,t) - P_w(i,t)\beta_w(i,t) - P_s(t) = 0, \; i \in Sb \tag{4.5}$$

$$f_Q + Q_d(i,t) - Q_b(i,t) - Q_w(i,t) - Q_s(t) = 0, \; i \in S_b \tag{4.6}$$

where Equations 4.5 and 4.6 are the active and reactive power flow equations at the buses, respectively. Here, f_P and f_Q denote the network active and reactive power functions [17]. The active-reactive power constraints at the slack bus are

$$\left(P_s(t)\right)^2 + \left(Q_s(t)\right)^2 \le (S_{s.\max})^2 \tag{4.7}$$

$$\gamma_{Ps} S_{s.\max} \le P_s(t) \le S_{s.\max} \tag{4.8}$$

$$\gamma_{Qs} S_{s.\max} \le Q_s(t) \le S_{s.\max} \tag{4.9}$$

$$-1 \le \gamma_{P_s,rev} \le 0 \tag{4.10}$$

$$-1 \le \gamma_{Q_s,rev} \le 0. \tag{4.11}$$

The nodal voltages are constrained as follows [35, 109]:

$$V_{\min}(i) \le V(i,t) \le V_{\max}(i), \qquad i \in S_b; i \ne 1 \tag{4.12}$$

$$V_{s.\min} \le V_s(t) \le V_{s.\max} \tag{4.13}$$

$$V_s(t) = 1 + \Delta V_s(t) \tag{4.14}$$

$$\Delta V_s(t) = \{-0.1, -0.09, ..., 0.09, 0.1\}. \tag{4.15}$$

The feeder limits are

$$S(i,j,t) \le S_{l.\max}(i,j), \qquad i,j \in S_b; i \ne j \tag{4.16}$$

The constraints of the curtailment factors of WFs are

$$0 \le \beta_w(i,t) \le 1, \qquad i \in S_w \tag{4.17}$$

The constraints of the power factors of WFs are

$$PF_{w.\min} \le PF_w(i,t) \le PF_{w.\max}, \qquad i \in S_w \tag{4.18}$$

4.3.3 Equations of BSSs

In this work, with the aid of power conditioning systems (PCSs), the BSSs can provide and absorb both active and reactive power. The active power charge and discharge are constrained to the capacity of the PCSs:

$$0 \le P_{ch}(i,t) \le S_{PCS.\max}, \qquad i \in S_{BSS} \tag{4.19}$$

$$0 \le P_{dis}(i,t) \le S_{PCS.\max}, \qquad i \in S_{BSS} \tag{4.20}$$

The reactive power dispatch of the BSSs is constrained to

$$-S_{PCS.\max} \le Q_b(i,t) \le S_{PCS.\max}, \qquad i \in S_{BSS} \tag{4.21}$$

The apparent power of the BSSs is constrained to:

$$S_{PCS}(i,t) = \begin{cases} \sqrt{\left(P_{ch}(i,t)\right)^2 + \left(Q_b(i,t)\right)^2} \\ \sqrt{\left(P_{dis}(i,t)\right)^2 + \left(Q_b(i,t)\right)^2} \end{cases} \tag{4.22}$$

$$S_{PCS}(i,t) \le S_{PCS.\max} \tag{4.23}$$

Here, we define a binary decision variable α to avoid charge and discharge at the same time:

$$(1-\alpha(i,t))\,P_{ch}(i,t) = 0, \qquad i \in S_{BSS} \tag{4.24}$$

$$\alpha(i,t)\, P_{dis}(i,t) = 0, \qquad i \in S_{BSS} \tag{4.25}$$

where $\alpha = 1$ indicates the charging of the battery while $\alpha = 0$ denotes the discharging operation. The energy level of a BSS is calculated as follows:

$$E_b(i,t) = E_b(i,t-1) + \eta_{ch} P_{ch}(i,t) t_d - \frac{P_{dis}(i,t) t_d}{\eta_{dis}}, i \in S_{BSS} \tag{4.26}$$

$$E_b(i,t_0) = E_{b.\min}(i) \tag{4.27}$$

$$E_{b.\min}(i) \le E_b(i,t) \le E_{b.\max}(i), \qquad i \in S_{BSS} \tag{4.28}$$

Equation 4.26 shows the dynamic behavior of a battery with initial states in Equation 4.27. The expended life cost of each BSS [246] is a function of number of cycles in the prediction horizon as well as the average value of DoD:

$$ELC(i) = SUC_T \frac{N_{cyc}(i)}{N_{cyc.T}(i)}, i \in S_{BSS} \tag{4.29}$$

where

$$SUC_T = SUC_u S_{PCS.\max} \tag{4.30}$$

$$N_{cyc.T}(i) = \left(a\, DoD_{avg}(i)\right) + b, i \in S_{BSS} \tag{4.31}$$

$$DoD_{avg}(i) = \frac{1}{24} \sum_{t=1}^{24} \left(1 - E_b(i,t)\right), i \in S_{BSS} \tag{4.32}$$

$$N_{cyc} \le N_{cyc.\max}. \tag{4.33}$$

In Equations 4.29 and 4.33 $N_{cyc}(i)$ can be calculated as follows:

$$N_{cyc} = \frac{\left(\sum_{t=1}^{t_f} |\Delta\alpha(t)|\right)}{2}. \tag{4.34}$$

where

$$\Delta\alpha(t) = \alpha(t) - \alpha(t-1) \tag{4.35}$$

$$\alpha(t_0) = 0. \tag{4.36}$$

4.4 Case Study

In this study, a 41-bus medium voltage DN [17, 18, 109, 227] is used as a case study to demonstrate the effectiveness of the proposed approach. Two WFs (each with rated power of

Table 4.1. Data for the case study taken and adapted from [109, 246].

$T_{P1} = 24$ h	$PF_{w.\min} = 0.85$	$S_{PCS.\max} = 6$ MVA
$T_{P2} = 2$ min	$PF_{w.\max} = 1$	$E_{b.\min} = 5.4$ MWh
$T_S = 20$ s	$S_{s.\max} = 20$ MVA	$E_{b.\max} = 18$ MWh
$V_{\min} = 0.94$ pu	$SUC_u = 150$ \$/kVA	$\eta_{ch} = \eta_{dis} = 1$
$V_{\max} = 1.06$ pu	$a = -4775$	$N_{cyc.\max} = 4$
$\gamma_{Ps} = \gamma_{Qs} = -1$	$b = 6542$	$t_d = 1$ h

10 MW) and two BSSs are located at buses 2 and 16, respectively. The input data for the case study is adapted from [109, 246] and given in Table 4.1 as well as Subplots (a)-(c) in Figures 4.3 and 4.4. The dynamic MINLP optimization problem in Phase 1 is solved using the SBB solver and the optimization problems in Phase 2 are solved using the BONMIN solver in GAMS.

Subplots (d)-(l) in Figure 4.3 show the outputs of the dynamic MINLP AR-OPF solved in phase 1. The length of the prediction horizon is 24 h with hourly discretization and the maximum number of cycles in the prediction horizon is 4 [246]. Based on the forecasted profiles, all the mixed-integer variables are simultaneously solved for the upcoming day.

Beside the demand and wind power profiles, energy prices play a significant role in determining the optimal operations of BSSs. It means the batteries tend to be charged when the active energy price is low and discharged when it is high. In addition, the BSSs also dispatch reactive power to cover the reactive power demand in the network as well as exporting the surplus amount to the upstream HV network. It is noted that in Phase 1, only BSSs variables (hourly discretized) are transferred to Phase 2 as input parameters. It means, the other decision variables are recomputed in Phase 2 (with 2min discretization) and modified in Phase 3 (with 20s discretization) before realization. The results of the realization phase are shown in subplots (d)-(k) in Figure 4.4. For comparison purposes, we run the proposed RT-DAR-OPF for three different modes of operation defined in Section 4.3 and show the results in Table 4.2. In Modes 1 and 2, the number of cycles per day is fixed to 4, while in the flexible approach the number of cycles for each BSS is a free variable to be optimized by the solver.

Due to Equations 4.4 and 4.29-4.36, the optimizer tends to decrease the number of cycles and DoD in order to minimize the expended life costs of the BSSs. However, the effect of the number of cycles on expended life cost is more significant in our case study as seen in Table 4.2. Therefore, the total expended life costs of the BSSs are decreased significantly in Mode 3 comparing to the other operation modes. Moreover, the costs of active and reactive energy at

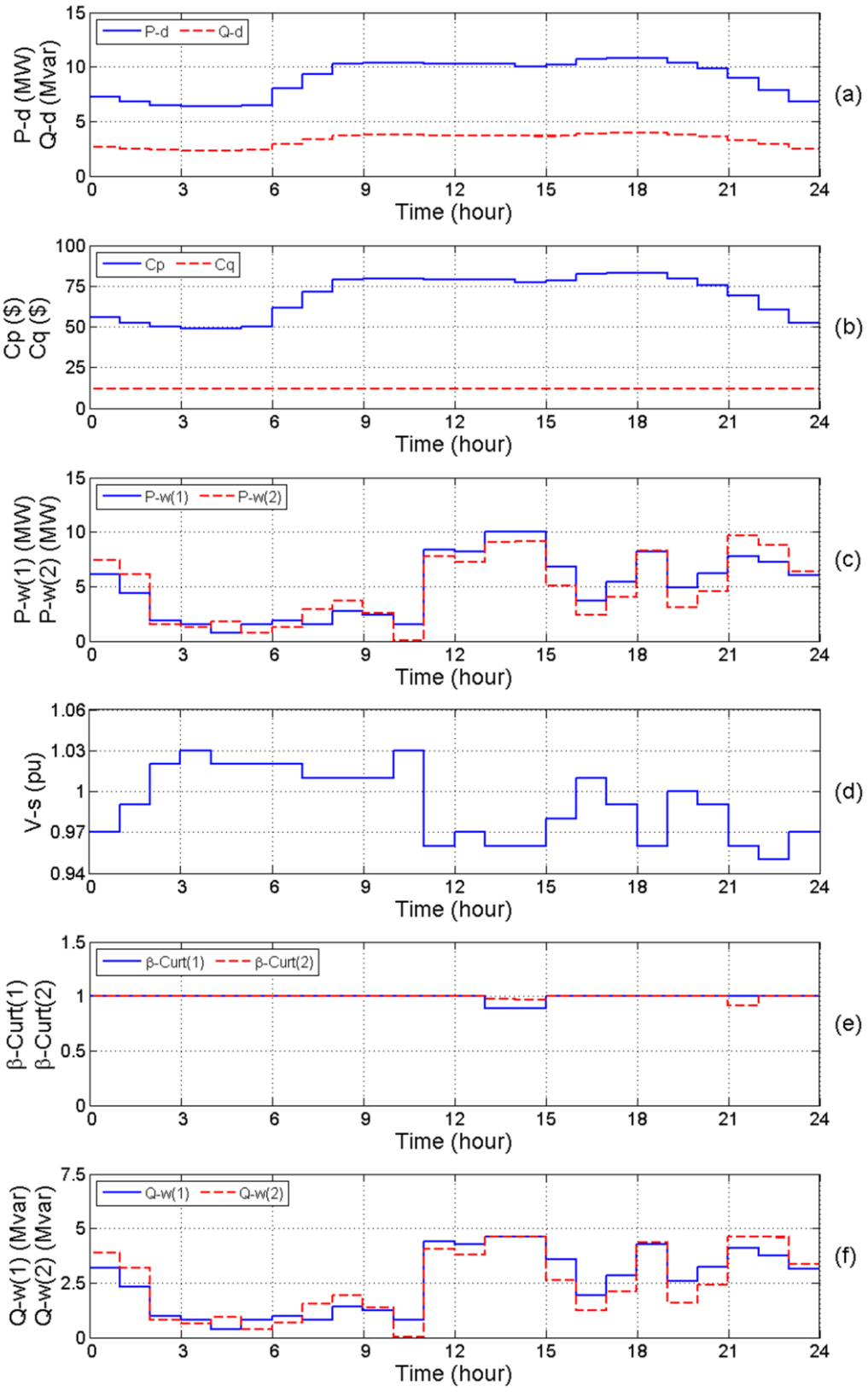

Figure 4.3. (a) Total active and reactive power demand; (b) Energy prices; (c) Wind power; (d) Slack bus voltage; (e) Curtailment factors of WFs; (f) Capacitive reactive power of WFs.

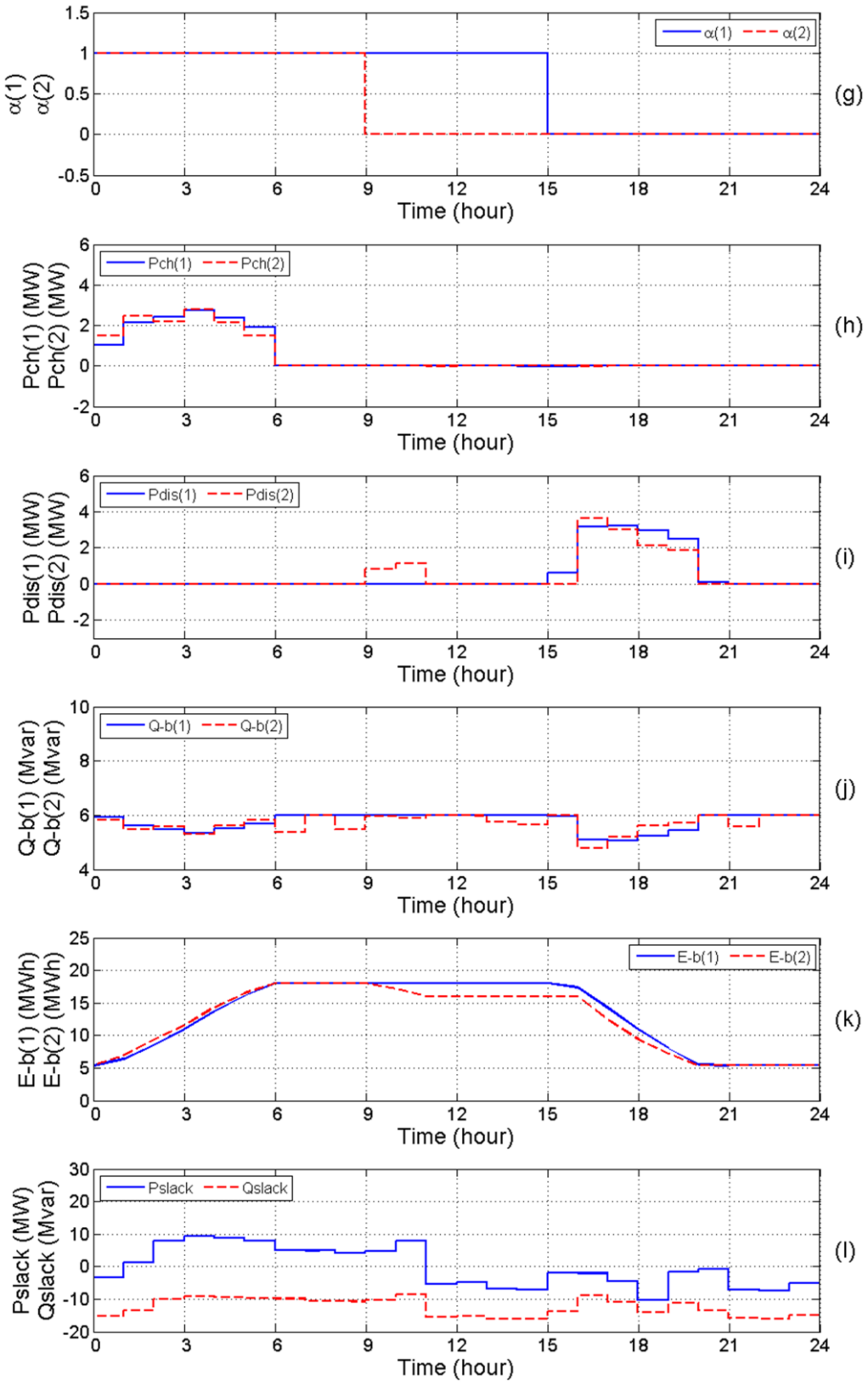

Figure 4.3. (Continued). (g) Binary variables for charge/discharge of BSSs; (h),(i) Active power charge and discharge of BSSs, respectively; (k) Energy levels in BSSs; (l) Active and reactive power at the slack bus.

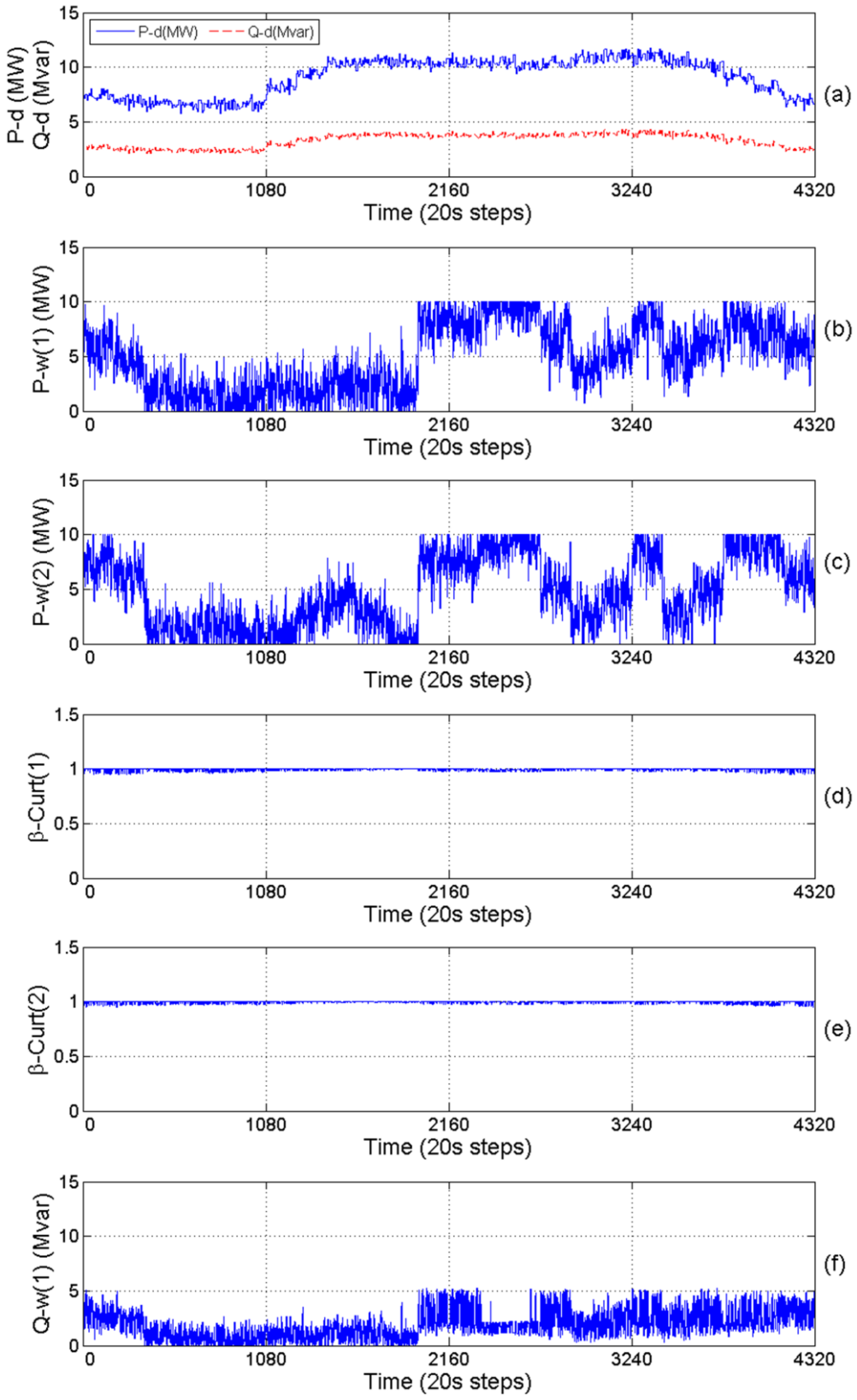

Figure 4.4. (a) Total active and reactive power demand; (b),(c) Actual wind power of the first and second WF; (d),(e) Curtailment factors of the first and second WF, respectively; (f) Capacitive reactive power dispatch of the first WF.

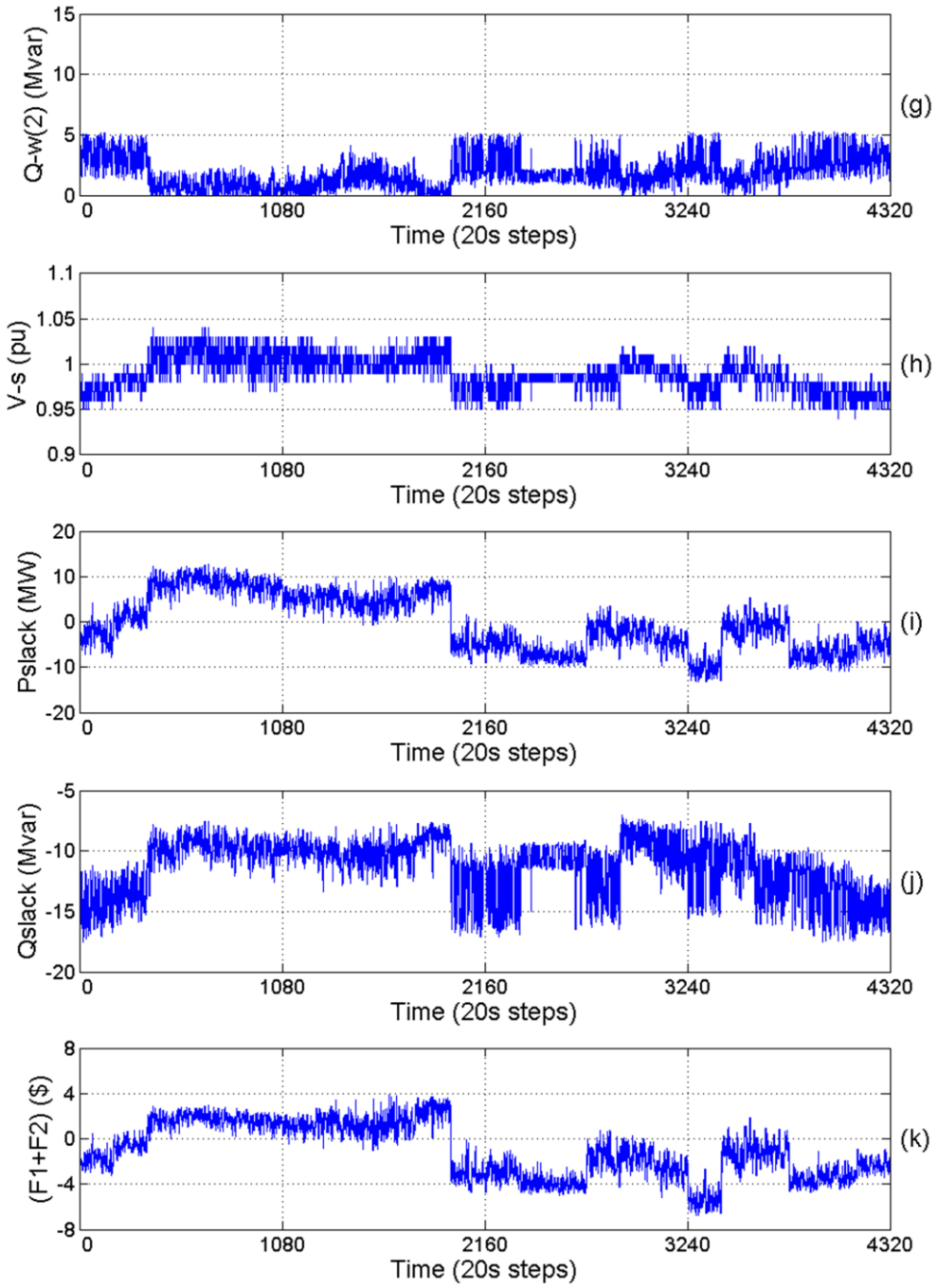

Figure 4.4. (Continued). (g) Capacitive reactive power dispatch of the second WF; (h) Slack bus voltage; (i) Active power at the slack bus; (j) Reactive power at the slack bus; (k) Total costs of active and reactive energy at the slack bus.

the slack bus are also decreased slightly in Mode 3. These all together lead to a huge reduction in the total costs obtained by using Mode 3.

Table 4.2. Comparison of the RT-DAR-OPF with the proposed flexible operation strategy to the results obtained by Modes 1 and 2 for one day.

Mode	$N_{cyc}(1)$ $N_{cyc}(2)$	T_{D-OPF} (s)	$DoD_{avg}(1)$ (MWh) $DoD_{avg}(2)$ (MWh)	$ELC(1)$ ($) $ELC(2)$ ($)	F_1 ($)	F_2 ($)	F_3 ($)	F ($)
1	4 4	135.32	2.41 2.611	667.73 679.86	-1166.41	-3184.85	1347.59	-3003.67
2	4 4	212.96	2.368 2.516	665.25 674.06	-1210.2	-3244.31	1339.31	-3115.2
3	1 1	241.15	2.742 3.052	172 177.01	-1230.4	-3279.67	349.01	-4158.06

4.5 Conclusions

In this chapter, a novel multi-time-scale RT-DAR-OPF framework is introduced to deal with fast changing wind power in the presence of BSSs. The framework consists of three phases: in the first phase, a dynamic MINLP problem is solved to simultaneously determine the optimal operation strategies of the BSSs for the upcoming day. In the second phase, wind power scenarios are generated based on the forecasted wind power values for short prediction horizons (e.g., 2min) and then the AR-OPF problems corresponding to the scenarios are solved in parallel. The results are saved as a lookup table from which one solution is selected based on the actual values of wind power in a very short sampling time (e.g., 20s) in the third phase. The solution is then modified to ensure satisfaction of the constraints. Thus the framework safeguards the feasibility and optimality of the operations in real-time.

5 Conclusions and Future Challenges

The dramatic increase of renewable energy penetration represents a significant challenge in the operation of energy DNs. In particular, wind power generation is intermittent, i.e., the DN operator has to correspondingly update the operation strategy. Therefore, it is highly desired to carry out this task by an online optimization framework. However, the optimization problem to be solved is usually high-dimensional and complicated when a large network with a detailed nonlinear model as well as mixed-integer variables is considered. Thus the computation time can be much higher than required for reacting to the fast changes of the wind power generation. Even by using advanced optimization algorithms combined with modern computation facilities, the computation time can still be too high to achieve this target. Furthermore, the feasibility of the solution should be ensured within a specified sampling time. Therefore, a computation framework addressing these difficulties needs to be developed for the implementation of RT-OPF under wind energy penetration.

For this, a novel RT-OPF framework was initially developed to address the conflict between the fast changing wind power and the slow optimization computation and consequently to realize an online optimization of energy systems in a very short sampling time. The RT-OPF framework simultaneously optimize discrete reference values of the slack bus voltage, wind power curtailment of WFs, and reverse power flow to an upstream network, leading to a MINLP problem. A scenario generation method was integrated in the RT-OPF framework to represent uncertain wind power for the prediction horizon, which leads to a set of uncoupled MINLP problems solved by parallel computing.

The reactive power of WFs was incorporated into the real-time framework to increase the economic benefit of the network. However, since nodal voltages are very sensitive to reactive power, incorporating reactive power dispatch of WFs in a RT-OPF problem can lead to voltage violations at PQ buses. This is because any discrepancies between the actual and forecasted values of active power dispatch will also influence the reactive power dispatch. In this dissertation, we addressed this problem by using a back-off strategy to ensure the satisfaction of voltage constraints when there is any deviation between the forecasted and actual reactive power dispatch during the real-time operation. From another perspective, for the RT-AR-OPF, the computation should provide a solution within a specified sampling time. However, there can be some (rare) cases that the algorithm takes too much time or even fails

to converge. To address this problem, we propose a reconciliation algorithm which allows for online solving the problem of non-convergence of the MINLP OPF by providing sub-optimal and feasible control strategies to be realized to the network in real-time. Furthermore, based on the operating mode of the WFs, a power factor modification scheme is introduced to ensure a feasible operation in the realization phase of the RT-AR-OPF.

Since a considerable amount of wind energy generation may need to be curtailed due to technical constraints in the network, BSSs can be optimally used to store the energy, decrease the curtailment and consequently increase economic benefits. For this, the framework was further extended to solve real-time 'dynamic' RT-DAR-OPF and optimally deal with spontaneous changes in wind power in DNs with BSSs. The framework offers the possibility of simultaneous optimization of a huge number of mixed-integer decision variables including active power charge/discharge of each BSS, reactive power dispatch of each WF and BSS, length of charge and discharge periods of each BSS, length of charge-discharge cycles of each BSS, number of charge-discharge cycles of each BSS in the prediction horizon, status of charge/discharge of each BSS, active-reactive reverse power flow to an upstream network, etc. In addition, fully flexible optimal operation strategies for BSSs are determined for the dynamic AR-OPF while minimizing the expended life costs of the BSSs. All in all, the developed RT-DAR-OPF framework safeguards, in real-time, the feasibility and optimality of the operations of DNs with BSSs. The future research aspects related to this dissertation can be summarized as follows:

- The developed framework in this work can be effectively extended to incorporate other uncertainties e.g., active-reactive power demand, solar power, prices, etc.
- Security constrained OPF can be considered in the RT-DAR-OPF framework in order to secure the network against equipment failures.
- The computation speed can be further improved by using graphics processing units (GPUs).
- The framework can be further extended to deal with increasing number of plug-in electric vehicles in DNs. This will be more interesting if the electric vehicles can inject active-reactive power to the networks through bidirectional power electronic inverters.
- Considering lifetime of power devices (e.g., batteries, power electronic devices, etc.) in the RT-DAR-OPF is still an open question to be addressed.

References

[1] B. H. Chowdhury and S. Rahman, "A review of recent advances in economic dispatch," *IEEE Transactions on Power Systems*, vol. 5, pp. 1248-1259, 1990.

[2] M. El-Hawary, "Optimal economic operation of large scale electric power systems: A review," in *Athens Power Tech, 1993. APT 93. Proceedings. Joint International Power Conference*, 1993, pp. 206-210.

[3] M. Huneault and F. Galiana, "A survey of the optimal power flow literature," *IEEE Transactions on Power Systems*, vol. 6, pp. 762-770, 1991.

[4] J. A. Momoh, R. Adapa, and M. El-Hawary, "A review of selected optimal power flow literature to 1993. I. Nonlinear and quadratic programming approaches," *IEEE Transactions on Power Systems*, vol. 14, pp. 96-104, 1999.

[5] J. A. Momoh, M. El-Hawary, and R. Adapa, "A review of selected optimal power flow literature to 1993. II. Newton, linear programming and interior point methods," *IEEE Transactions on Power Systems*, vol. 14, pp. 105-111, 1999.

[6] W. Zhang and L. M. Tolbert, "Survey of reactive power planning methods," in *Power Engineering Society General Meeting, 2005. IEEE*, 2005, pp. 1430-1440.

[7] X. Xia and A. Elaiw, "Optimal dynamic economic dispatch of generation: A review," *Electric Power Systems Research*, vol. 80, pp. 975-986, 2010.

[8] K. Pandya and S. Joshi, "A survey of optimal power flow methods," *Journal of Theoretical & Applied Information Technology*, vol. 4, 2008.

[9] Z. Qiu, G. Deconinck, and R. Belmans, "A literature survey of optimal power flow problems in the electricity market context," in *Power Systems Conference and Exposition, 2009. PSCE'09. IEEE/PES*, 2009, pp. 1-6.

[10] S. Frank, I. Steponavice, and S. Rebennack, "Optimal power flow: a bibliographic survey I," *Energy Systems*, vol. 3, pp. 221-258, 2012.

[11] S. Frank, I. Steponavice, and S. Rebennack, "Optimal power flow: a bibliographic survey II," *Energy Systems*, vol. 3, pp. 259-289, 2012.

[12] M. B. Cain, R. P. O'neill, and A. Castillo, "History of optimal power flow and formulations," *Federal Energy Regulatory Commission*, pp. 1-36, 2012.

[13] A. Castillo and R. P. O'Neill, "Survey of approaches to solving the ACOPF (OPF Paper 4)," *US Federal Energy Regulatory Commission, Tech. Rep*, 2013.

[14] A. Castillo and R. P. O'Neill, "Computational performance of solution techniques applied to the ACOPF," *Federal Energy Regulatory Commission, Optimal Power Flow Paper*, vol. 5, 2013.

[15] L. Bird, J. Cochran, and X. Wang, "Wind and solar energy curtailment: experience and practices in the United States," *US National Renewable Energy Laboratory, NREL/TP-6A20-60983,* p. 3, 2014.

[16] S. W. Alnaser and L. F. Ochoa, "Advanced network management systems: A risk-based AC OPF approach," *IEEE Transactions on Power Systems,* vol. 30, pp. 409-418, 2015.

[17] A. Gabash and P. Li, "Active-reactive optimal power flow in distribution networks with embedded generation and battery storage," *IEEE Transactions on Power Systems,* vol. 27, pp. 2026-2035, 2012.

[18] A. Gabash and P. Li, "Flexible optimal operation of battery storage systems for energy supply networks," *IEEE Transactions on Power Systems,* vol. 28, pp. 2788-2797, 2013.

[19] M. J. Dolan, E. M. Davidson, I. Kockar, G. W. Ault, and S. D. McArthur, "Reducing distributed generator curtailment through active power flow management," *IEEE Transactions on Smart Grid,* vol. 5, pp. 149-157, 2014.

[20] J. P. Barton and D. G. Infield, "Energy storage and its use with intermittent renewable energy," *IEEE transactions on energy conversion,* vol. 19, pp. 441-448, 2004.

[21] C. Li, H. Shi, Y. Cao, J. Wang, Y. Kuang, Y. Tan, and J. Wei, "Comprehensive review of renewable energy curtailment and avoidance: a specific example in China," *Renewable and Sustainable Energy Reviews,* vol. 41, pp. 1067-1079, 2015.

[22] H. Hale and J. Ward, "Digital computer solution of power flow problems," *AIEE Transactions, pt. III (Power Apparatus and Systems),* vol. 75, pp. 398-402, 1956.

[23] J. E. Van Ness and J. H. Griffin, "Elimination methods for load-flow studies," *Transactions of the American Institute of Electrical Engineers. Part III: Power Apparatus and Systems,* vol. 80, pp. 299-302, 1961.

[24] A. Glimn and G. Stagg, "Automatic calculation of load flows," *Transactions of the American Institute of Electrical Engineers. Part III: Power Apparatus and Systems,* vol. 76, pp. 817-825, 1957.

[25] R. Burchett, H. H. Happ, D. Vierath, and K. Wirgau, "Developments in optimal power flow," *IEEE Transactions on Power Apparatus and Systems,* pp. 406-414, 1982.

[26] H. W. Dommel and W. F. Tinney, "Optimal power flow solutions," *IEEE Transactions on Power Apparatus and Systems,* pp. 1866-1876, 1968.

[27] E. Mohagheghi, A. Gabash, and P. Li, "A study of uncertain wind power in active-reactive optimal power flow," *Power and Energy Student Summit (PESS) 2015, January 13th-14th, Dortmund Germany,* 2015.

[28] E. Mohagheghi, A. Gabash, and P. Li, "Real-time optimal power flow under wind energy penetration-Part II: Implementation," in *2016 IEEE 16th International Conference on Environment and Electrical Engineering (EEEIC)*, 2016, pp. 1-6.

[29] T. Gomez, I. Perez-Arriaga, J. Lumbreras, and V. Parra, "A security-constrained decomposition approach to optimal reactive power planning," *IEEE Transactions on Power Systems*, vol. 6, pp. 1069-1076, 1991.

[30] Y.-j. Zhang and Z. Ren, "Optimal reactive power dispatch considering costs of adjusting the control devices," *IEEE Transactions on Power Systems*, vol. 20, pp. 1349-1356, 2005.

[31] L. Chen, Y. Taka, H. Okamoto, R. Tanabe, and A. Ono, "Optimal operation solutions of power systems with transient stability constraints," *IEEE Transactions on Circuits and Systems I: Fundamental Theory and Applications*, vol. 48, pp. 327-339, 2001.

[32] Q. Jiang, H.-D. Chiang, C. Guo, and Y. Cao, "Power–current hybrid rectangular formulation for interior-point optimal power flow," *IET generation, transmission & distribution*, vol. 3, pp. 748-756, 2009.

[33] G. L. Torres and V. H. Quintana, "An interior-point method for nonlinear optimal power flow using voltage rectangular coordinates," *IEEE Transactions on Power Systems*, vol. 13, pp. 1211-1218, 1998.

[34] M. Li, W. Tang, W. Tang, Q. Wu, and J. Saunders, "Bacterial foraging algorithm with varying population for optimal power flow," in *Workshops on Applications of Evolutionary Computation*, 2007, pp. 32-41.

[35] E. Mohagheghi, A. Gabash, and P. Li, "A framework for real-time optimal power flow under wind energy penetration," *Energies*, vol. 10, p. 535, 2017.

[36] R. A. Jabr, I. Dzafic, and S. Karaki, "Tracking Transformer Tap Position in Real-Time Distribution Network Power Flow Applications," *IEEE Transactions on Smart Grid*, 2016.

[37] N. M. Peterson and W. S. Meyer, "Automatic adjustment of transformer and phase-shifter taps in the Newton power flow," *IEEE Transactions on power apparatus and systems*, pp. 103-108, 1971.

[38] A. Gomez-Exposito, E. Romero-Ramos, and I. Džafić, "Hybrid real–complex current injection-based load flow formulation," *Electric Power Systems Research*, vol. 119, pp. 237-246, 2015.

[39] H. Zhang and P. Li, "Probabilistic analysis for optimal power flow under uncertainty," *IET Generation, Transmission & Distribution*, vol. 4, pp. 553-561, 2010.

[40] H. Zhang and P. Li, "Chance Constrained Programming for Optimal Power Flow Under Uncertainty," *Power Systems, IEEE Transactions on*, vol. 26, pp. 2417-2424, 2011.

[41] Y. Cao, Y. Tan, C. Li, and C. Rehtanz, "Chance-constrained optimization-based unbalanced optimal power flow for radial distribution networks," *IEEE Transactions on Power Delivery*, vol. 28, pp. 1855-1864, 2013.

[42] N. S. Rau, *Optimization principles: practical applications to the operation and markets of the electric power industry* vol. 16: John Wiley & Sons, 2003.

[43] B. Stott, J. Jardim, and O. Alsaç, "DC power flow revisited," *IEEE Transactions on Power Systems*, vol. 24, pp. 1290-1300, 2009.

[44] J. Carpentier, "Contribution a l'etude du dispatching economique," *Bulletin de la Societe Francaise des Electriciens*, vol. 3, pp. 431-447, 1962.

[45] H. Glavitsch and M. Spoerry, "Quadratic loss formula for reactive dispatch," *IEEE Transactions on Power Apparatus and Systems*, pp. 3850-3858, 1983.

[46] R. Burchett, H. Happ, and K. Wirgau, "Large scale optimal power flow," *IEEE Transactions on Power Apparatus and Systems*, pp. 3722-3732, 1982.

[47] E. Lobato, L. Rouco, M. Navarrete, R. Casanova, and G. Lopez, "An LP-based optimal power flow for transmission losses and generator reactive margins minimization," in *Power Tech Proceedings, 2001 IEEE Porto*, 2001, p. 5 pp. vol. 3.

[48] F. G. Lima, F. D. Galiana, I. Kockar, and J. Munoz, "Phase shifter placement in large-scale systems via mixed integer linear programming," *IEEE Transactions on Power Systems*, vol. 18, pp. 1029-1034, 2003.

[49] X. Bai and H. Wei, "Semi-definite programming-based method for security-constrained unit commitment with operational and optimal power flow constraints," *IET generation, transmission & distribution*, vol. 3, pp. 182-197, 2009.

[50] M. AlRashidi and M. El-Hawary, "Hybrid particle swarm optimization approach for solving the discrete OPF problem considering the valve loading effects," *IEEE Transactions on Power Systems*, vol. 22, pp. 2030-2038, 2007.

[51] P. Subbaraj and P. Rajnarayanan, "Optimal reactive power dispatch using self-adaptive real coded genetic algorithm," *Electric Power Systems Research*, vol. 79, pp. 374-381, 2009.

[52] H. Smith and S.-Y. Tong, "Minimizing power transmission losses by reactive-volt-ampere control," *IEEE Transactions on Power Apparatus and Systems*, vol. 82, pp. 542-544, 1963.

[53] J. Peschon, D. S. Piercy, W. F. Tinney, O. J. Tveit, and M. Cuenod, "Optimum control of reactive power flow," *IEEE Transactions on Power Apparatus and Systems*, pp. 40-48, 1968.

[54] A. M. Sasson, "Nonlinear programming solutions for load-flow, minimum-loss, and economic dispatching problems," *IEEE Transactions on Power Apparatus and Systems*, pp. 399-409, 1969.

[55] F. Capitanescu, J. M. Ramos, P. Panciatici, D. Kirschen, A. M. Marcolini, L. Platbrood, and L. Wehenkel, "State-of-the-art, challenges, and future trends in security constrained optimal power flow," *Electric Power Systems Research*, vol. 81, pp. 1731-1741, 2011.

[56] O. Alsac and B. Stott, "Optimal load flow with steady-state security," *IEEE Transactions on Power Apparatus and Systems*, pp. 745-751, 1974.

[57] F. Palacios-Gomez, L. Lasdon, and M. Engquist, "Nonlinear optimization by successive linear programming," *Management science*, vol. 28, pp. 1106-1120, 1982.

[58] L. S. Vargas, V. H. Quintana, and A. Vannelli, "A tutorial description of an interior point method and its applications to security-constrained economic dispatch," *IEEE Transactions on Power Systems*, vol. 8, pp. 1315-1324, 1993.

[59] C.-N. Lu and M. Unum, "Network constrained security control using an interior point algorithm," *IEEE Transactions on Power Systems*, vol. 8, pp. 1068-1076, 1993.

[60] N. Grudinin, "Combined quadratic-separable programming OPF algorithm for economic dispatch and security control," *IEEE Transactions on Power Systems*, vol. 12, pp. 1682-1688, 1997.

[61] P. E. Gill and E. Wong, "Sequential quadratic programming methods," in *Mixed integer nonlinear programming*, ed: Springer, 2012, pp. 147-224.

[62] P. T. Boggs and J. W. Tolle, "Sequential quadratic programming," *Acta numerica*, vol. 4, pp. 1-51, 1995.

[63] E. Philip and W. Elizabeth, "Sequential quadratic programming methods," *UCSD Department of Mathematics Technical Report NA-10-03 August*, 2010.

[64] G. Granelli and M. Montagna, "Security-constrained economic dispatch using dual quadratic programming," *Electric Power Systems Research*, vol. 56, pp. 71-80, 2000.

[65] R. Fernandes, H. Happ, and K. Wirgau, "Optimal reactive power flow for improved system operations," *International Journal of Electrical Power & Energy Systems*, vol. 2, pp. 133-139, 1980.

[66] R. Mota-Palomino and V. Quintana, "Sparse reactive power scheduling by a penalty function-linear programming technique," *IEEE Transactions on Power Systems*, vol. 1, pp. 31-39, 1986.

[67] A. Santos, S. Deckmann, and S. Soares, "A dual augmented Lagrangian approach for optimal power flow," *IEEE Transactions on Power Systems*, vol. 3, pp. 1020-1025, 1988.

[68] W. Thomas, A. Dixon, D. Cheng, R. Dunnett, G. Schaff, and J. Thorp, "Optimal reactive planning with security constraints," in *Power Industry Computer Application Conference, 1995. Conference Proceedings., 1995 IEEE*, 1995, pp. 79-84.

[69] N. Karmarkar, "A new polynomial-time algorithm for linear programming," in *Proceedings of the sixteenth annual ACM symposium on Theory of computing*, 1984, pp. 302-311.

[70] J. A. Momoh, S. Guo, E. Ogbuobiri, and R. Adapa, "The quadratic interior point method solving power system optimization problems," *IEEE Transactions on Power Systems*, vol. 9, pp. 1327-1336, 1994.

[71] C. Parker, I. Morrison, and D. Sutanto, "Application of an optimisation method for determining the reactive margin from voltage collapse in reactive power planning," *IEEE Transactions on Power Systems*, vol. 11, pp. 1473-1481, 1996.

[72] G. Da Costa, "Optimal reactive dispatch through primal-dual method," *IEEE Transactions on Power Systems*, vol. 12, pp. 669-674, 1997.

[73] M. Yehia, R. Ramadan, Z. El-Tawail, and K. Tarhini, "An integrated technico-economical methodology for solving reactive power compensation problem," *IEEE Transactions on Power Systems*, vol. 13, pp. 54-59, 1998.

[74] J.-Y. Park, J.-M. Sohn, and J.-K. Park, "Optimal capacitor allocation in a distribution system considering operation costs," *IEEE Transactions on Power Systems*, vol. 24, pp. 462-468, 2009.

[75] A. M. Azmy, "Optimal power flow to manage voltage profiles in interconnected networks using expert systems," *IEEE Transactions on Power Systems*, vol. 22, pp. 1622-1628, 2007.

[76] S.-Y. Lin, "Distributed optimal power flow with discrete control variables of large distributed power systems," *IEEE Transactions on Power Systems*, vol. 23, pp. 1383-1392, 2008.

[77] F. Capitanescu and L. Wehenkel, "Sensitivity-based approaches for handling discrete variables in optimal power flow computations," *IEEE Transactions on Power Systems*, vol. 25, pp. 1780-1789, 2010.

[78] A. G. Bakirtzis, P. N. Biskas, C. E. Zoumas, and V. Petridis, "Optimal power flow by enhanced genetic algorithm," *IEEE Transactions on Power Systems*, vol. 17, pp. 229-236, 2002.

[79] J. H. Holland, "Adaptation in natural and artificial systems. An introductory analysis with application to biology, control, and artificial intelligence," *Ann Arbor, MI: University of Michigan Press*, pp. 439-444, 1975.

[80] D. Goldberg, "Genetic algorithms: search and optimization algorithms," ed: Addison-Wesley Publishing, Massachusetts, 1989.

[81] B. Stott and E. Hobson, "Power system security control calculations using linear programming, Part I," *IEEE Transactions on Power Apparatus and Systems*, pp. 1713-1720, 1978.

[82] B. Stott and E. Hobson, "Power system security control calculations using linear programming, Part II," *IEEE Transactions on Power Apparatus and Systems*, pp. 1721-1731, 1978.

[83] B. Stott and J. Marinho, "Linear programming for power-system network security applications," *IEEE Transactions on Power Apparatus and Systems*, pp. 837-848, 1979.

[84] D. S. Kirschen and H. P. Van Meeteren, "MW/voltage control in a linear programming based optimal power flow," *IEEE Transactions on Power Systems*, vol. 3, pp. 481-489, 1988.

[85] K. Iba, H. Suzuki, K.-I. Suzuki, and K. Suzuki, "Practical reactive power allocation/operation planning using successive linear programming," *IEEE Transactions on Power Systems*, vol. 3, pp. 558-566, 1988.

[86] J. Peschon, D. W. Bree, and L. P. Hajdu, "Optimal power-flow solutions for power system planning," *Proceedings of the IEEE*, vol. 60, pp. 64-70, 1972.

[87] P. Wolfe, "Methods of nonlinear programming," *Nonlinear programming*, 1967.

[88] A. Sasson, F. Viloria, and F. Aboytes, "Optimal load flow solution using the Hessian matrix," *IEEE Transactions on Power Apparatus and Systems*, pp. 31-41, 1973.

[89] O. Crisan and M. Mohtadi, "Efficient identification of binding inequality constraints in the optimal power flow Newton approach," in *IEE Proceedings C (Generation, Transmission and Distribution)*, 1992, pp. 365-370.

[90] G. Irisarri, X. Wang, J. Tong, and S. Mokhtari, "Maximum loadability of power systems using interior point nonlinear optimization method," *IEEE Transactions on Power Systems*, vol. 12, pp. 162-172, 1997.

[91] A. J. Conejo and J. A. Aguado, "Multi-area coordinated decentralized DC optimal power flow," *IEEE Transactions on Power Systems*, vol. 13, pp. 1272-1278, 1998.

[92] Y. Xia and K. W. Chan, "Dynamic constrained optimal power flow using semi-infinite programming," *IEEE Transactions on Power Systems*, vol. 21, pp. 1455-1457, 2006.

[93] J. Lavaei and S. H. Low, "Zero duality gap in optimal power flow problem," *IEEE Transactions on Power Systems*, vol. 27, pp. 92-107, 2012.

[94] N. S. Rau and Y.-h. Wan, "Optimum location of resources in distributed planning," *IEEE Transactions on Power Systems*, vol. 9, pp. 2014-2020, 1994.

[95] S. Liew and G. Strbac, "Maximising penetration of wind generation in existing distribution networks," *IEE Proceedings-Generation, Transmission and Distribution,* vol. 149, pp. 256-262, 2002.

[96] G. Harrison and A. Wallace, "Optimal power flow evaluation of distribution network capacity for the connection of distributed generation," *IEE Proceedings-Generation, Transmission and Distribution,* vol. 152, pp. 115-122, 2005.

[97] Y. M. Atwa and E. El-Saadany, "Optimal allocation of ESS in distribution systems with a high penetration of wind energy," *IEEE Transactions on Power Systems,* vol. 25, pp. 1815-1822, 2010.

[98] Y. Atwa, "Distribution system planning and reliability assessment under high DG penetration," 2010.

[99] F. Geth, J. Tant, E. Haesen, J. Driesen, and R. Belmans, "Integration of energy storage in distribution grids," in *Power and Energy Society General Meeting, 2010 IEEE*, 2010, pp. 1-6.

[100] C. Chen, S. Duan, T. Cai, B. Liu, and G. Hu, "Optimal allocation and economic analysis of energy storage system in microgrids," *IEEE Transactions on Power Electronics,* vol. 26, pp. 2762-2773, 2011.

[101] T. K. Brekken, A. Yokochi, A. Von Jouanne, Z. Z. Yen, H. M. Hapke, and D. A. Halamay, "Optimal energy storage sizing and control for wind power applications," *IEEE Transactions on Sustainable Energy,* vol. 2, pp. 69-77, 2011.

[102] J. Tant, F. Geth, D. Six, P. Tant, and J. Driesen, "Multiobjective battery storage to improve PV integration in residential distribution grids," *IEEE Transactions on Sustainable Energy,* vol. 4, pp. 182-191, 2013.

[103] Y. Levron, J. M. Guerrero, and Y. Beck, "Optimal power flow in microgrids with energy storage," *IEEE Transactions on Power Systems,* vol. 28, pp. 3226-3234, 2013.

[104] D. Gayme and U. Topcu, "Optimal power flow with large-scale storage integration," *IEEE Transactions on Power Systems,* vol. 28, pp. 709-717, 2013.

[105] S. Gill, I. Kockar, and G. W. Ault, "Dynamic optimal power flow for active distribution networks," *IEEE Transactions on Power Systems,* vol. 29, pp. 121-131, 2014.

[106] H. Oh, "Optimal planning to include storage devices in power systems," *IEEE Transactions on Power Systems,* vol. 26, pp. 1118-1128, 2011.

[107] P. C. Loh and F. Blaabjerg, "Autonomous control of distributed storages in microgrids," in *Power Electronics and ECCE Asia (ICPE & ECCE), 2011 IEEE 8th International Conference on*, 2011, pp. 536-542.

[108] P. C. Loh, Y. K. Chai, D. Li, and F. Blaabjerg, "Autonomous operation of distributed storages in microgrids," *IET Power Electronics,* vol. 7, pp. 23-30, 2014.

[109] E. Mohagheghi, A. Gabash, M. Alramlawi, and P. Li, "Real-time optimal power flow with reactive power dispatch of wind stations using a reconciliation algorithm," *Renewable Energy*, 2018.

[110] T. J. E. Miller, *Reactive power control in electric systems*: Wiley, 1982.

[111] O. Gandhi, C. D. Rodríguez-Gallegos, W. Zhang, D. Srinivasan, and T. Reindl, "Economic and technical analysis of reactive power provision from distributed energy resources in microgrids," *Applied Energy*, 2017.

[112] M. Sedghi, A. Ahmadian, and M. Aliakbar-Golkar, "Optimal storage planning in active distribution network considering uncertainty of wind power distributed generation," *IEEE Transactions on Power Systems*, vol. 31, pp. 304-316, 2016.

[113] A. Ahmadian, M. Sedghi, M. Aliakbar-Golkar, A. Elkamel, and M. Fowler, "Optimal probabilistic based storage planning in tap-changer equipped distribution network including PEVs, capacitor banks and WDGs: a case study for Iran," *Energy*, vol. 112, pp. 984-997, 2016.

[114] H. Sangrody, M. Sarailoo, N. Zhou, N. Tran, M. Motalleb, and E. Foruzan, "Weather forecasting error in solar energy forecasting," *IET Renewable Power Generation*, vol. 11, pp. 1274-1280, 2017.

[115] H. Sangrody, M. Sarailoo, N. Zhou, A. Shokrollahi, and E. Foruzan, "On the performance of forecasting models in the presence of input uncertainty," *arXiv preprint arXiv:1707.04692*, 2017.

[116] M. H. Athari and Z. Wang, "Modeling the uncertainties in renewable generation and smart grid loads for the study of the grid vulnerability," in *Innovative Smart Grid Technologies Conference (ISGT), 2016 IEEE Power & Energy Society*, 2016, pp. 1-5.

[117] M. H. Athari and Z. Wang, "Impacts of Wind Power Uncertainty on Grid Vulnerability to Cascading Overload Failures," *IEEE Transactions on Sustainable Energy*, vol. 9, pp. 128-137, 2018.

[118] R. Jabr and B. C. Pal, "Intermittent wind generation in optimal power flow dispatching," *IET generation, transmission & distribution*, vol. 3, pp. 66-74, 2009.

[119] A. Gabash, M. Alhallak, M. Alramlawi, E. Mohagheghi, and P. Li, "A Wireless-Web-Framework for Real-Time Optimal Power Flow in Sustainable Power Supply Systems," in *2018 IEEE International Conference on Environment and Electrical Engineering and 2018 IEEE Industrial and Commercial Power Systems Europe (EEEIC/I&CPS Europe)*, 2018, pp. 1-6.

[120] S. Huang and V. Dinavahi, "Fast Batched Solution for Real-Time Optimal Power Flow with Penetration of Renewable Energy," *IEEE Access*, pp. 13898-13910, 2018.

[121] B. Borkowska, "Probabilistic load flow," *IEEE Transactions on Power Apparatus and Systems*, pp. 752-759, 1974.

[122] L. Wu, M. Shahidehpour, and Y. Fu, "Security-constrained generation and transmission outage scheduling with uncertainties," *IEEE Transactions on Power Systems,* vol. 25, pp. 1674-1685, 2010.

[123] F. Capitanescu, S. Fliscounakis, P. Panciatici, and L. Wehenkel, "Cautious operation planning under uncertainties," *IEEE Transactions on Power Systems,* vol. 27, pp. 1859-1869, 2012.

[124] F. Capitanescu and L. Wehenkel, "A new iterative approach to the corrective security-constrained optimal power flow problem," *IEEE Transactions on Power Systems,* vol. 23, pp. 1342-1351, 2008.

[125] M. Sedghi, A. Ahmadian, E. Pashajavid, and M. Aliakbar-Golkar, "Storage scheduling for optimal energy management in active distribution network considering load, wind, and plug-in electric vehicles uncertainties," *Journal of Renewable and Sustainable Energy,* vol. 7, p. 033120, 2015.

[126] A. Ahmadian, M. Sedghi, M. Aliakbar-Golkar, M. Fowler, and A. Elkamel, "Two-layer optimization methodology for wind distributed generation planning considering plug-in electric vehicles uncertainty: A flexible active-reactive power approach," *Energy Conversion and Management,* vol. 124, pp. 231-246, 2016.

[127] L. Wu, M. Shahidehpour, and T. Li, "Stochastic security-constrained unit commitment," *IEEE Transactions on Power Systems,* vol. 22, pp. 800-811, 2007.

[128] L. Wu, M. Shahidehpour, and Z. Li, "GENCO's risk-constrained hydrothermal scheduling," *IEEE Transactions on Power Systems,* vol. 23, pp. 1847-1858, 2008.

[129] M. Alramlawi, A. Gabash, and P. Li, "Optimal operation strategy of a hybrid PV-battery system under grid scheduled blackouts," in *Environment and Electrical Engineering and 2017 IEEE Industrial and Commercial Power Systems Europe (EEEIC/I&CPS Europe), 2017 IEEE International Conference on*, 2017, pp. 1-5.

[130] M. Alramlawi, A. Gabash, E. Mohagheghi, and P. Li, "Optimal operation of hybrid PV-battery system considering grid scheduled blackouts and battery lifetime," *Solar Energy,* vol. 161, pp. 125-137, 2018.

[131] M. Alramlawi, A. F. Timothy, A. Gabash, E. Mohagheghi, and P. Li, "Optimal Operation of PV-Diesel MicroGrid with Multiple Diesel Generators under Grid Blackouts," *arXiv preprint arXiv:1806.10034,* 2018.

[132] M. Alramlawi, A. Gabash, E. Mohagheghi, and P. Li, "Optimal Operation of PV-Battery-Diesel MicroGrid for Industrial Loads Under Grid Blackouts," *arXiv preprint arXiv:1807.05753,* 2018.

[133] A. Prékopa, *Stochastic programming* vol. 324: Springer Science & Business Media, 2013.

[134] A. Ben-Tal, L. El Ghaoui, and A. Nemirovski, *Robust optimization*: Princeton University Press, 2009.

[135] A. Soroudi and M. Ehsan, "IGDT based robust decision making tool for DNOs in load procurement under severe uncertainty," *IEEE Transactions on Smart Grid*, vol. 4, pp. 886-895, 2013.

[136] D. Bertsimas, E. Litvinov, X. A. Sun, J. Zhao, and T. Zheng, "Adaptive robust optimization for the security constrained unit commitment problem," *IEEE Transactions on Power Systems*, vol. 28, pp. 52-63, 2013.

[137] A. Lorca and X. A. Sun, "Adaptive robust optimization with dynamic uncertainty sets for multi-period economic dispatch under significant wind," *IEEE Transactions on Power Systems*, vol. 30, pp. 1702-1713, 2015.

[138] R. Jabr, "Robust transmission network expansion planning with uncertain renewable generation and loads," *IEEE Transactions on Power Systems*, vol. 28, pp. 4558-4567, 2013.

[139] A. H. Hajimiragha, C. A. Canizares, M. W. Fowler, S. Moazeni, and A. Elkamel, "A robust optimization approach for planning the transition to plug-in hybrid electric vehicles," *IEEE Transactions on Power Systems*, vol. 26, pp. 2264-2274, 2011.

[140] T. Ding, S. Liu, W. Yuan, Z. Bie, and B. Zeng, "A two-stage robust reactive power optimization considering uncertain wind power integration in active distribution networks," *IEEE Transactions on Sustainable Energy*, vol. 7, pp. 301-311, 2016.

[141] A. Martinez-Mares and C. R. Fuerte-Esquivel, "A robust optimization approach for the interdependency analysis of integrated energy systems considering wind power uncertainty," *IEEE Transactions on Power Systems*, vol. 28, pp. 3964-3976, 2013.

[142] H. Yu and W. Rosehart, "An optimal power flow algorithm to achieve robust operation considering load and renewable generation uncertainties," *IEEE Transactions on Power Systems*, vol. 27, pp. 1808-1817, 2012.

[143] A. Charnes and W. W. Cooper, "Chance-constrained programming," *Management science*, vol. 6, pp. 73-79, 1959.

[144] P. Li, H. Arellano-Garcia, and G. Wozny, "Chance constrained programming approach to process optimization under uncertainty," *Computers & chemical engineering*, vol. 32, pp. 25-45, 2008.

[145] A. Geletu, M. Klöppel, H. Zhang, and P. Li, "Advances and applications of chance-constrained approaches to systems optimisation under uncertainty," *International Journal of Systems Science*, vol. 44, pp. 1209-1232, 2013.

[146] A. Geletu, A. Hoffmann, M. Klöppel, and P. Li, "Monotony analysis and sparse-grid integration for nonlinear chance constrained process optimization," *Engineering Optimization*, vol. 43, pp. 1019-1041, 2011.

[147] D. Bienstock, M. Chertkov, and S. Harnett, "Chance-constrained optimal power flow: Risk-aware network control under uncertainty," *Siam Review*, vol. 56, pp. 461-495, 2014.

[148] Y. Zhang, S. Shen, and J. L. Mathieu, "Distributionally robust chance-constrained optimal power flow with uncertain renewables and uncertain reserves provided by loads," *IEEE Transactions on Power Systems*, vol. 32, pp. 1378-1388, 2017.

[149] S. Bofinger, A. Luig, and H. Beyer, "Qualification of wind power forecasts," presented at the 2002 Global Windpower Conference, Paris, 2002.

[150] A. Fabbri, T. G. S. Roman, J. R. Abbad, and V. M. Quezada, "Assessment of the cost associated with wind generation prediction errors in a liberalized electricity market," *IEEE Transactions on Power Systems*, vol. 20, pp. 1440-1446, 2005.

[151] H. Bludszuweit, J. A. Domínguez-Navarro, and A. Llombart, "Statistical analysis of wind power forecast error," *IEEE Transactions on Power Systems*, vol. 23, pp. 983-991, 2008.

[152] T. Mühlpfordt, V. Hagenmeyer, and T. Faulwasser, "The Price of Uncertainty: Chance-constrained OPF vs. In-hindsight OPF," *arXiv preprint arXiv:1803.08711*, 2018.

[153] T. Mühlpfordt, T. Faulwasser, and V. Hagenmeyer, "A Generalized Framework for Chance-constrained Optimal Power Flow," *arXiv preprint arXiv:1803.08299*, 2018.

[154] M. Lubin, Y. Dvorkin, and S. Backhaus, "A robust approach to chance constrained optimal power flow with renewable generation," *IEEE Transactions on Power Systems*, vol. 31, pp. 3840-3849, 2016.

[155] B. Pagnoncelli, S. Ahmed, and A. Shapiro, "Sample average approximation method for chance constrained programming: theory and applications," *Journal of optimization theory and applications*, vol. 142, pp. 399-416, 2009.

[156] M. Wendt, P. Li, and G. Wozny, "Nonlinear chance-constrained process optimization under uncertainty," *Industrial & engineering chemistry research*, vol. 41, pp. 3621-3629, 2002.

[157] A. Geletu, A. Hoffmann, M. Klöppel, and P. Li, "An inner-outer approximation approach to chance constrained optimization," *SIAM Journal on Optimization*, vol. 27, pp. 1834-1857, 2017.

[158] E. Mohagheghi, A. Geletu, N. Bremser, M. Alramlawi, A. Gabash, and P. Li, "Chance Constrained Optimal Power Flow Using the Inner-Outer Approximation Approach," *arXiv preprint arXiv:1805.00669*, 2018.

[159] J. W. Taylor, "An evaluation of methods for very short-term load forecasting using minute-by-minute British data," *International Journal of Forecasting*, vol. 24, pp. 645-658, 2008.

[160] M. Alamaniotis, A. Ikonomopoulos, and L. H. Tsoukalas, "Evolutionary multiobjective optimization of kernel-based very-short-term load forecasting," *IEEE Transactions on Power Systems*, vol. 27, pp. 1477-1484, 2012.

[161] C. Guan, P. B. Luh, L. D. Michel, and Z. Chi, "Hybrid Kalman filters for very short-term load forecasting and prediction interval estimation," *IEEE Transactions on Power Systems*, vol. 28, pp. 3806-3817, 2013.

[162] Y.-H. Hsiao, "Household electricity demand forecast based on context information and user daily schedule analysis from meter data," *IEEE Transactions on Industrial Informatics*, vol. 11, pp. 33-43, 2015.

[163] A. Mohamed, V. Salehi, and O. Mohammed, "Real-time energy management algorithm for mitigation of pulse loads in hybrid microgrids," *IEEE Transactions on Smart Grid*, vol. 3, pp. 1911-1922, 2012.

[164] A. Mohamed, V. Salehi, T. Ma, and O. Mohammed, "Real-time energy management algorithm for plug-in hybrid electric vehicle charging parks involving sustainable energy," *IEEE Transactions on Sustainable Energy*, vol. 5, pp. 577-586, 2014.

[165] A. Di Giorgio, F. Liberati, and A. Lanna, "Electric energy storage systems integration in distribution grids," presented at the IEEE 15th International Conference on Environment and Electrical Engineering (EEEIC), 2015.

[166] J. M. Maciejowski, *Predictive control: with constraints*: Pearson education, 2002.

[167] M. Morari, C. Garcia, J. Lee, and D. Prett, *Model predictive control*: Prentice Hall Englewood Cliffs, NJ, 1993.

[168] E. F. Camacho and C. B. Alba, *Model predictive control*: Springer Science & Business Media, 2013.

[169] B. Kouvaritakis and M. Cannon, *Model predictive control*: Springer, 2016.

[170] A. Di Giorgio, F. Liberati, A. Lanna, A. Pietrabissa, and F. D. Priscoli, "Model predictive control of energy storage systems for power tracking and shaving in distribution grids," *IEEE Transactions on Sustainable Energy*, vol. 8, pp. 496-504, 2017.

[171] E. M. Davidson, S. D. McArthur, M. J. Dolan, and J. R. McDonald, "Exploiting intelligent systems techniques within an autonomous regional active network management system," in *Power & Energy Society General Meeting, 2009. PES'09. IEEE*, 2009, pp. 1-8.

[172] E. Davidson, M. Dolan, S. McArthur, and G. Ault, "The use of constraint programming for the autonomous management of power flows," in *Intelligent System Applications to Power Systems, 2009. ISAP'09. 15th International Conference on*, 2009, pp. 1-7.

[173] R. Bacher and H. P. Van Meeteren, "Real-time optimal power flow in automatic generation control," *IEEE Transactions on Power Systems,* vol. 3, pp. 1518-1529, 1988.

[174] S. S. Sharif, J. H. Taylor, E. F. Hill, B. Scott, and D. Daley, "Real-time implementation of optimal reactive power flow," *IEEE Power Engineering Review,* vol. 20, pp. 47-51, 2000.

[175] P. Siano, C. Cecati, H. Yu, and J. Kolbusz, "Real time operation of smart grids via FCN networks and optimal power flow," *IEEE Transactions on Industrial Informatics,* vol. 8, pp. 944-952, 2012.

[176] L. Gan and S. H. Low, "An online gradient algorithm for optimal power flow on radial networks," *IEEE Journal on Selected Areas in Communications,* vol. 34, pp. 625-638, 2016.

[177] W. Hong, S. Wang, P. Li, G. Wozny, and L. T. Biegler, "A quasi-sequential approach to large-scale dynamic optimization problems," *AIChE Journal,* vol. 52, pp. 255-268, 2006.

[178] M. Bartl, P. Li, and L. T. Biegler, "Improvement of state profile accuracy in nonlinear dynamic optimization with the quasi-sequential approach," *AIChE Journal,* vol. 57, pp. 2185-2197, 2011.

[179] M. J. Dolan, E. M. Davidson, I. Kockar, G. W. Ault, and S. D. McArthur, "Distribution power flow management utilizing an online optimal power flow technique," *IEEE Transactions on Power Systems,* vol. 27, pp. 790-799, 2012.

[180] Z. Li, F. Qiu, and J. Wang, "Data-driven real-time power dispatch for maximizing variable renewable generation," *Applied Energy,* vol. 170, pp. 304-313, 2016.

[181] L. F. Ochoa, C. J. Dent, and G. P. Harrison, "Distribution network capacity assessment: Variable DG and active networks," *IEEE Transactions on Power Systems,* vol. 25, pp. 87-95, 2010.

[182] L. F. Ochoa, C. J. Dent, and G. P. Harrison, "Maximisation of intermittent distributed generation in active networks," 2008.

[183] L. F. Ochoa, A. Keane, C. Dent, and G. P. Harrison, "Applying active network management schemes to an Irish distribution network for wind power maximisation," in *Proc. 2009 International Conference on Electricity Distribution (CIRED)*, 2009, pp. 1-4.

[184] L. F. Ochoa and G. P. Harrison, "Minimizing energy losses: Optimal accommodation and smart operation of renewable distributed generation," *IEEE Transactions on Power Systems,* vol. 26, pp. 198-205, 2011.

[185] A. Di Giorgio, F. Liberati, and A. Lanna, "Real time optimal power flow integrating large scale storage devices and wind generation," presented at the 23th Mediterranean Conference on Control and Automation (MED), 2015.

[186] N. Mazzi, B. Zhang, and D. S. Kirschen, "An Online Optimization Algorithm for Alleviating Contingencies in Transmission Networks," *IEEE Transactions on Power Systems*, 2018.

[187] A. Papavasiliou, Y. Mou, L. Cambier, and D. Scieur, "Application of stochastic dual dynamic programming to the real-time dispatch of storage under renewable supply uncertainty," *IEEE Transactions on Sustainable Energy*, vol. 9, pp. 547-558, 2018.

[188] Y. Zhang, E. Dall'Anese, and M. Hong, "Dynamic ADMM for real-time optimal power flow," in *Signal and Information Processing (GlobalSIP), 2017 IEEE Global Conference on*, 2017, pp. 1085-1089.

[189] K. Utkarsh, D. Srinivasan, A. Trivedi, W. Zhang, and T. Reindl, "Distributed Model-predictive Real-time Optimal Operation of a Network of Smart Microgrids," *IEEE Transactions on Smart Grid*, 2018.

[190] S. S. Reddy and P. Bijwe, "Day-Ahead and Real Time Optimal Power Flow considering Renewable Energy Resources," *International Journal of Electrical Power & Energy Systems*, vol. 82, pp. 400-408, 2016.

[191] S. S. Reddy, P. Bijwe, and A. R. Abhyankar, "Real-time economic dispatch considering renewable power generation variability and uncertainty over scheduling period," *IEEE Systems Journal*, vol. 9, pp. 1440-1451, 2015.

[192] S. S. Reddy and P. Bijwe, "Real time economic dispatch considering renewable energy resources," *Renewable Energy*, vol. 83, pp. 1215-1226, 2015.

[193] S. S. Reddy and J. A. Momoh, "Realistic and transparent optimum scheduling strategy for hybrid power system," *IEEE Transactions on Smart Grid*, vol. 6, pp. 3114-3125, 2015.

[194] S. S. Reddy, "Optimal scheduling of thermal-wind-solar power system with storage," *Renewable Energy*, vol. 101, pp. 1357-1368, 2017.

[195] Y. Liu, Z. Qu, H. Xin, and D. Gan, "Distributed real-time optimal power flow control in smart grid," *IEEE Transactions on Power Systems*, vol. 32, pp. 3403-3414, 2017.

[196] S. Bolognani, G. Cavraro, and S. Zampieri, "A distributed feedback control approach to the optimal reactive power flow problem," in *Control of Cyber-Physical Systems*, ed: Springer, 2013, pp. 259-277.

[197] E. Dall'Anese, S. V. Dhople, and G. B. Giannakis, "Photovoltaic inverter controllers seeking AC optimal power flow solutions," *IEEE Transactions on Power Systems*, vol. 31, pp. 2809-2823, 2016.

[198] E. Dall'Anese and A. Simonetto, "Optimal power flow pursuit," *IEEE Transactions on Smart Grid*, vol. 9, pp. 942-952, 2018.

[199] V. Salehi, A. Mohamed, and O. A. Mohammed, "Implementation of real-time optimal power flow management system on hybrid AC/DC smart microgrid," presented at the IEEE Industry Applications Society (IAS) Annual Meeting, 2012.

[200] H. Zhu and H. J. Liu, "Fast local voltage control under limited reactive power: Optimality and stability analysis," *IEEE Transactions on Power Systems*, vol. 31, pp. 3794-3803, 2016.

[201] E. Mohagheghi, M. Alramlawi, A. Gabash, and P. Li, "A survey of real-time optimal power flow " *(under review in Energies)*.

[202] N. Menemenlis, M. Huneault, and A. Robitaille, "Computation of dynamic operating balancing reserve for wind power integration for the time-horizon 1–48 hours," *IEEE Transactions on Sustainable Energy*, vol. 3, pp. 692-702, 2012.

[203] X. Wu, X. Wang, and C. Qu, "A hierarchical framework for generation scheduling of microgrids," *IEEE Transactions on Power Delivery*, vol. 29, pp. 2448-2457, 2014.

[204] Z. Wang, B. Chen, J. Wang, M. M. Begovic, and C. Chen, "Coordinated energy management of networked microgrids in distribution systems," *IEEE Transactions on Smart Grid*, vol. 6, pp. 45-53, 2015.

[205] P. Li, X. Guan, J. Wu, and X. Zhou, "Modeling dynamic spatial correlations of geographically distributed wind farms and constructing ellipsoidal uncertainty sets for optimization-based generation scheduling," *IEEE Transactions on Sustainable Energy*, vol. 6, pp. 1594-1605, 2015.

[206] M. D. McKay, R. J. Beckman, and W. J. Conover, "Comparison of three methods for selecting values of input variables in the analysis of output from a computer code," *Technometrics*, vol. 21, pp. 239-245, 1979.

[207] E. Mohagheghi, A. Gabash, and P. Li, "Real-time optimal power flow under wind energy penetration-Part I: Approach," in *2016 IEEE 16th International Conference on Environment and Electrical Engineering (EEEIC)*, 2016, pp. 1-6.

[208] A. Gabash and P. Li, "On variable reverse power flow-part I: Active-Reactive optimal power flow with reactive power of wind stations," *Energies*, vol. 9, p. 121, 2016.

[209] I. Van der Hoven, "Power spectrum of horizontal wind speed in the frequency range from 0.0007 to 900 cycles per hour," *Journal of meteorology*, vol. 14, pp. 160-164, 1957.

[210] E. Kaya, B. Barutcu, and Ş. S. MENTEŞ, "A method based on the van der Hoven spectrum for performance evaluation in prediction of wind speed," *Turkish Journal of Earth Sciences*, vol. 22, pp. 681-689, 2013.

[211] Y. Tao and H. Chen, "A hybrid wind power prediction method," presented at the Power and Energy Society General Meeting (PESGM), 2016.

[212] A. Gabash, *Flexible optimal operations of energy supply networks: with renewable energy generation and battery storage*: Südwestdeutscher Verlag für Hochschulschriften, 2014.

[213] Y. M. Atwa and E. F. El-Saadany, "Probabilistic approach for optimal allocation of wind-based distributed generation in distribution systems," *IET Renewable Power Generation*, vol. 5, pp. 79-88, 2011.

[214] (2018). *General algebraic modeling system (GAMS)*. Available: https://www.gams.com/

[215] P. Bonami and J. Lee, "BONMIN user's manual," *Numer Math*, vol. 4, pp. 1-32, 2007.

[216] P. Hallberg, "Active distribution system management a key tool for the smooth integration of distributed generation," *Eurelectric TF Active System Management*, vol. 2, 2013.

[217] "NIE Briefing on Connecting Renewable Generation to the Electricity Network," Northern Ireland Electricity2015.

[218] (2015). *Distributed Generation Technical Interconnection Requirements: Interconnections at Voltages 50 kV and Below*.

[219] A. Gabash, M. Alkal, and P. Li, "Impact of allowed reverse active power flow on planning PVs and BSSs in distribution networks considering demand and EVs growth," *Power & Energy Student Summit (PESS) 2013, IEEE Student Branch Bielefeld*, pp. 11-16, 2013.

[220] S. A. Arefifar, Y. A.-R. I. Mohamed, and T. H. El-Fouly, "Supply-adequacy-based optimal construction of microgrids in smart distribution systems," *IEEE Transactions on Smart Grid*, vol. 3, pp. 1491-1502, 2012.

[221] M. F. Shaaban, Y. M. Atwa, and E. F. El-Saadany, "DG allocation for benefit maximization in distribution networks," *IEEE Transactions on Power Systems*, vol. 28, pp. 639-649, 2013.

[222] A. Gabash, R. Murad, M. Alramlawi, E. Mohagheghi, and P. Li, "Optimal Configuration of Sustainable Power Supply Networks with Export Power," in *2018 IEEE International Conference on Environment and Electrical Engineering and 2018 IEEE Industrial and Commercial Power Systems Europe (EEEIC/I&CPS Europe)*, 2018, pp. 1-6.

[223] "ENTSO-E overview of transmission tariffs in Europe: synthesis 2015," 2015.

[224] H. Gerard, E. Rivero, and D. Six. (2016). *Basic schemes for TSO-DSO coordination and ancillary services provision*. Available: https://pdfs.semanticscholar.org/fc1a/c4c8e95bb213ad623addf2ff966cfb14edd4.pdf

[225] P. Bahri, J. Bandoni, G. Barton, and J. Romagnoli, "Back-off calculations in optimising control: a dynamic approach," *Computers & chemical engineering,* vol. 19, pp. 699-708, 1995.

[226] H. Arellano-Garcia, "Chance constrained optimization of process systems under uncertainty," Doctoral Thesis Doctoral Thesis, Technische Universität Berlin, 2006.

[227] Y. Atwa, E. El-Saadany, M. Salama, and R. Seethapathy, "Optimal renewable resources mix for distribution system energy loss minimization," *IEEE Transactions on Power Systems,* vol. 25, pp. 360-370, 2010.

[228] R. Eberhart and J. Kennedy, "A new optimizer using particle swarm theory," in *Micro Machine and Human Science, 1995. MHS'95., Proceedings of the Sixth International Symposium on*, 1995, pp. 39-43.

[229] H. Yoshida, K. Kawata, Y. Fukuyama, S. Takayama, and Y. Nakanishi, "A particle swarm optimization for reactive power and voltage control considering voltage security assessment," *IEEE Transactions on Power Systems,* vol. 15, pp. 1232-1239, 2000.

[230] J. Soares, T. Sousa, H. Morais, Z. Vale, B. Canizes, and A. Silva, "Application-Specific Modified Particle Swarm Optimization for energy resource scheduling considering vehicle-to-grid," *Applied Soft Computing,* vol. 13, pp. 4264-4280, 2013.

[231] T. Prakash, V. Singh, S. P. Singh, and S. Mohanty, "Economic load dispatch problem: quasi-oppositional self-learning TLBO algorithm," *Energy Systems,* pp. 1-24, 2017.

[232] A. Attarha and N. Amjady, "Solution of security constrained optimal power flow for large-scale power systems by convex transformation techniques and Taylor series," *IET generation, transmission & distribution,* vol. 10, pp. 889-896, 2016.

[233] H. Zeineldin, E. El-Saadany, and M. Salama, "Optimal coordination of overcurrent relays using a modified particle swarm optimization," *Electric Power Systems Research,* vol. 76, pp. 988-995, 2006.

[234] L. Yiqing, Y. Xigang, and L. Yongjian, "An improved PSO algorithm for solving non-convex NLP/MINLP problems with equality constraints," *Computers & chemical engineering,* vol. 31, pp. 153-162, 2007.

[235] M. R. Bussieck and S. Vigerske, "MINLP solver software," *Wiley encyclopedia of operations research and management science,* 2010.

[236] P. Q. A. Guide, "Voltage Disturbances," *Standard EN,* vol. 50160, 2004.

[237] A. Klajn and M. Bątkiewicz-Pantuła, "Standard EN 50160: Voltage characteristics of electricity supplied by public electricity networks," *European Copper Institute*, 2013.

[238] J. R. Birge, "The value of the stochastic solution in stochastic linear programs with fixed recourse," *Mathematical programming*, vol. 24, pp. 314-325, 1982.

[239] C. Valente, G. Mitra, M. Sadki, and R. Fourer, "Extending algebraic modelling languages for stochastic programming," *INFORMS Journal on Computing*, vol. 21, pp. 107-122, 2009.

[240] A. J. Conejo, M. Carrión, and J. M. Morales, *Decision making under uncertainty in electricity markets* vol. 1: Springer, 2010.

[241] B. Zhao, A. J. Conejo, and R. Sioshansi, "Coordinated Expansion Planning of Natural Gas and Electric Power Systems," *IEEE Transactions on Power Systems*, 2017.

[242] M. Carrión and J. M. Arroyo, "A computationally efficient mixed-integer linear formulation for the thermal unit commitment problem," *IEEE Transactions on Power Systems*, vol. 21, pp. 1371-1378, 2006.

[243] E. Mohagheghi, M. Alramlawi, A. Gabash, F. Blaabjerg, and P. Li, "Real-time active-reactive optimal power flow with flexible operation of battery storage systems," *(under review in Renewable Energy)*.

[244] F. Dong, B. H. Chowdhury, M. L. Crow, and L. Acar, "Improving voltage stability by reactive power reserve management," *IEEE Transactions on Power Systems*, vol. 20, pp. 338-345, 2005.

[245] B. Venkatesh, G. Sadasivam, and M. A. Khan, "A new optimal reactive power scheduling method for loss minimization and voltage stability margin maximization using successive multi-objective fuzzy LP technique," *IEEE Transactions on Power Systems*, vol. 15, pp. 844-851, 2000.

[246] H. H. Abdeltawab and Y. A.-R. I. Mohamed, "Market-oriented energy management of a hybrid wind-battery energy storage system via model predictive control with constraint optimizer," *IEEE Transactions on Industrial Electronics*, vol. 62, pp. 6658-6670, 2015.